Surface Engineering of Organic Conductors

by

Jonathan Edwin Cook

A dissertation submitted to the Graduate Faculty of
Auburn University
in partial fulfillment of the
requirements for the Degree of
Doctor of Philosophy

Auburn, Alabama
December 15, 2018

Keywords: Polyaniline, Conducting Polymers, Organic Conductors, Carbon Nanotubes, Microwave

Approved by

Dr. Xinyu Zhang, Chair, Associate Professor Department of Chemical Engineering
Dr. Maria Auad, Professor Department of Chemical Engineering
Dr. Russell Mailen, Assistant Professor Department of Aerospace Engineering
Dr. Bryan Beckingham, Assistant Professor Department of Chemical Engineering

Abstract

Surfaces represent a rich area for research and scientific exploration, as they often govern how a material interacts with its environment. Control over the properties of a surface allows materials to be used in new ways and can improve their performance in existing applications. Organic conductors are rapidly developing as cutting edge materials in a variety of applications, replacing traditional metallic components. By investigating the modification of these materials and developing methods to alter or improve their surface characteristics organic conductors can continue to expand their application in new technologies. This work covers the surface engineering of two prominent organic conducting materials: polyaniline through chemical modification and carbon materials through microwave processing.

The first portion of this work looks to develop new polyaniline derivatives through the reductive-addition of amine nucleophiles to the fully oxidized pernigraniline. This reaction allows for the introduction of substituents post-polymerization, offering a route to new derivatives without forfeiting the advantages of previously developed polyaniline syntheses such as low cost reagents and nanoscale morphological control. Reaction solvents, temperature, and amine concentration were explored to determine suitable conditions for functionalization without compromising pre-established morphological features. The reaction was found to proceed in low to moderate yields with aliphatic and aromatic amines covering various structural features. Conducting the reaction in water at room temperature with one half molar equivalent of amine

produced substituted polyanilines with minimal erosion of pre-established nanoscale morphology.

The kinetics of the reductive addition reaction was examined through UV-Visible spectroscopy. It was found that increasing steric bulk around the amine nitrogen significantly slowed the reaction. A Hammett study of the reaction showed a linear response to changes in the electronic characteristics of the amine, with electron donating substituents increasing the reaction rate. The observed reaction constant indicates a slight sensitivity to substituent effects and a build up of positive charge during the rate determining step, thought to be the addition of the amine to the quinoid ring.

The applicability of the reductive addition of amines was demonstrated by producing polyamine functionalized polyaniline for use in the curing of epoxy resins, and in self cross-linking of the polymer. While no clear trends were observed in the effect of cross-linker structure, the functionalized polymers did display improved thermal stability compared to samples prepared with the parent polymer.

The second portion of this work focuses on the modification of carbon structures with carbon nanotubes based on a microwave promoted carbonization. These nanocomposite materials have the potential for significantly improved electrochemical, catalytic, and mechanical properties over traditional materials, while the microwave processing approach offers a rapid, low cost and easily accessible means of production. Nanostructure decorated hollow carbon nanospheres were successfully produced through the templated synthesis of polypyrrole nanospheres followed by microwave carbonization in the presence of various organometallic precursors. Both carbon nanotubes and metal oxide nanowires were successfully produced using this approach, demonstrating the utility of microwave processing for the production of

nanocomposite materials. The growth of carbon nanotubes on carbon fiber fabrics was also explored, investigating various treatment methods and parameters. Nanotubes were successfully formed from the microwave treatment of ferrocene suspensions in ethylene glycol and diethylene glycol, although the nanostructures did not appear to be anchored to the surface of the fabrics. Further investigation of various parameters and additives failed to yield the desired growth but demonstrated that the interaction of solvent, ferrocene concentration and ferrocene dispersion appeared to have the most dramatic effect on the growth of nanostructures during microwave processing. Continued development of this process will yield a rapid and low cost production route to nanocomposite reinforcing materials for high performance engineering applications.

Acknowledgments

To Becca, Mom, and Dad: I really couldn't have made it this far without you. Your support, patience (so much patience), and love helped carry me through. My success is yours as much as it is mine.

To my friends: You made the tough times fun, and made the life of a graduate student bearable.

To Amit: you've been a real paaji. Your advice, questions, critiques and support made a lot of this work possible.

Table of Contents

List of Figures

List of Tables

List of Abbreviations

APS	ammonium peroxydisulfate
BDA	1,4 butanediamine
B.P.	boiling point
CFF	carbon fiber fabric
CNT	carbon nanotube
C_p	specific heat capacity
CVD	chemical vapor deposition
DDA	1,12 dodecanediamine
DEA	diethylamine
DEG	diethylene glycol
DETA	diethylenetriamine
DMSO	dimethylsulfoxide
DSC	dynamic scanning calorimetry
EB	emeraldine base
EDA	1,2 ethylenediamine
EDX	electron diffraction X-ray
EG	ethylene glycol
ε	dielectric permittivity
Et	ethyl
F.P.	flash point
FT-IR	Fourier transform infrared spectroscopy
FT-IR-ATR	attenuated total reflection Fourier transform infrared
HCNS	hollow carbon nanostructures
HCS	hollow carbon sphere
HDA	1,6 hexanediamine
Hex	hexylamine
HOMO	highest occupied molecular orbital
ICP	intrinsically conducting polymers
iPr	isopropyl
LUMO	lowest unoccupied molecular orbital
Me	methyl
MONW	metal oxide nanowire
μ	dipole moment
MWNT	multi-wall nanotube

nBu	neobutyl
NMP	N-methylpyrrolidone
NMR	nuclear magnetic resonance
NS	nanospheres
nPr	neopropyl
PAn	polyaniline
PB	pernigraniline base
PDA	p-phenylenediamine
PEG	poly(ethylene glycol)
Ph	phenyl
PNVP	poly(N-vinyl pyrrolidone)
PPy	polypyrrole
PS	polystyrene
PTFE	poly(tetrafluoroethylene)
PVA	poly(vinyl alcohol)
Pyd	pyrrolidine
SDS	sodium dodecylsulfate
SEM	scanning electron microscopy
SWNT	single wall nanotube
tBu	tertbutyl
TEA	triethylamine
TETA	triethylenetetramine
TGA	thermogravimetric analysis
THF	tetrahydrofuran
TRIS	tris(2-aminoethyl)amine
UV-Vis	UV-Visible

Introduction

This dissertation focuses on the surface engineering of organic conductors through derivatization or modification and is divided into two sections based upon the substrate and modification method. The first section details the chemical modification of polyaniline nanofibers, investigating reaction parameters, steric and electronic influences on reaction kinetics, and the use of amine functionalized polyanilines for cross-linking applications.

The second section focuses on the microwave-assisted modification of carbon based substrates. Carbon nanotube and metal oxide nanowire decorated hollow carbon nanospheres achieved through the carbonization of polypyrrole in the presence of organometallic precursors, while the surface decoration of carbon fiber fabrics with carbon nanotubes was explored through a similar approach.

While these two sections may seem disparate, they are linked by an underlying theme: the derivatization of carbon based conducting materials and the exploration of the mechanisms through which they can be modified. Both polyaniline and pure carbon materials represent prominent materials in the field of organic conductors, and the introduction of surface modifications serves to expand their utility and offer new materials better suited for advanced technological applications.

Section 1: Exploration of Amine Functionalized Polyaniline through Reductive-Addition

1. Introduction

Conducting polymers present an interesting class of materials combining the properties of metals and organic polymers. These materials stand apart from traditional polymeric materials and offer advantages, such as lighter weight and better environmental stability, over metals in a variety of applications. Due in part to their unique properties conducting polymers present a rich field of research with many benefits stemming from the exploration of their properties and application to traditional systems.

1.1. Conducting Polymers

Most traditional organic polymeric materials are considered insulating materials, as the electrons in the polymer bonds are highly localized and unable to carry an electric charge. In recent decades however, a new class of organic polymers have been discovered, exhibiting electrical conductivity in the near metallic range as well as other metallic properties. These intrinsically conducting polymers (ICPs) have gained significant research interest and found use in a diverse array of applications. In addition to intrinsically conducting polymers, several other types of conductive polymeric systems exist. They are differentiated by their mechanism of conduction and exhibit a wide range of achievable electrical conductivity. The four main types are conductive filler composites, ionically conducting polymers, redox active polymers and intrinsically conducting polymers[1].

Conductive filler composites are widely used due to ease of manufacturing and generally good conductivity. In these systems, a conductive filler material such as metal or carbon is suspended within an insulating polymer matrix, and conductivity arises from pathways of connected filler through the matrix. Although the polymer element itself is insulating, the system presents an initial starting point for the preparation and application of polymer based conducting materials[2,3]. The conductive filler must be present at a certain concentration, known as the percolation threshold, to achieve conductivity and is influenced by the geometry of the added filler. High aspect ratio fillers, such as fibers, are able to achieve conductivity at a lower threshold, as they are able to span greater distances through the matrix for the same weight compared to particulates of the same material[4,5]. These composite materials find use in a wide array of applications including aerospace manufacturing, conducting adhesives, and printed circuit boards. Although easy to produce, conductive filler composites suffer from several drawbacks, mainly poor environmental stability and being quite heavy[1,6].

Ionically conducting polymers derive their conductivity from the transport of ions along and between polymer chains[7]. Chain motion in the amorphous phase allows for additional coordination between ions followed by transfer of one ionic species to a new site[8]. The movement of ions through the polymer creates a current, and ionically conducting polymers are often referred to as polymer electrolytes. Polyethylene oxide is a commonly used polymer electrolyte for the transport of lithium ions. The electron rich oxygen atoms in the polymer backbone attract the electron deficient lithium cation, forming a temporary electrostatic bond between the two atoms. With a multitude of oxygen atoms present, the lithium ion can hop from one site to another, effectively shuttling along the length of the polymer chain[9].

Redox active polymers are comprised of redox active centers in fixed locations throughout the polymer, and conduction occurs as electrons move from one center to another. The redox centers must be close enough for electrons to traverse the insulating sections connecting them, and present in great enough number to promote long range electron transport. Ferrocene containing polymers are one such example, where the redox stable ferrocene moiety can be included as a pendant group in vinyl polymers or as part of the backbone[10].

The last main class of conducting polymer systems is known as intrinsically conducting polymers. These materials derive their conductivity from extended networks of π-conjugated orbitals created by alternating single and double bonds. While electrons are able to move freely through the conjugated network, the observed conductivity is quite low without the introduction of a dopant[11]. Oxidation or reduction of the π network and stabilization by an ionic species increases the conductivity of the polymer by several orders of magnitude[11]. The conjugated structure of the polymer provides the pathway for electron transport and the introduction of a dopant generates electron holes that promote conduction. The main families of intrinsically conducting polymers are polyacetylene, polyparaphenylene, polyparaphenylene vinylene, polyaniline, polypyrrole, and polythiophene[12].

Doped polyacetylene and polyparaphenylene display conductivity comparable to metals such as copper but at the expense of poor processability and low environmental stability. Polyaniline, polypyrrole and polythiophene are less conducting, 10^0-10^2 S/cm, but are significantly more stable compounds, and in some instances exhibit high processability[13].

Intrinsically conducting polymers, and polyaniline in particular, are excellent materials for many applications due to their unique blend of optical and electrical properties. Of the many potential uses in electronics, sensors, and membranes, intrinsically conducting polymers have yet

to be employed broadly and effectively in these areas as a result of a few major hurdles. Although considered "synthetic metals" their conductivity is still substantially lower than that of copper and other pure metals outside a few specific cases. Additionally, these polymers tend to thermally decompose rather than melt which makes many traditional polymer-processing methods unusable. As a result conducting polymers are often used as an additive to a matrix or carrier such as resin or paint, or deposited as thin films through casting or electrochemical deposition[14]. Low solubility in common solvents is also a major factor limiting their utility. Solubility can be improved by using specific dopants or modification of the polymer structure, but these changes often adversely impact the conductivity[15,16].

1.2. Polyaniline

Of the intrinsically conducting polymers, polyaniline stands out as a particularly attractive research subject. The low cost of reagents and ease of synthesis are complimented by good environmental stability of the produced polymer and its moderate conductivity. Of particular interest is the reversible doping and dedoping mechanism not displayed by other conducting polymers[17].

1.2.1. Structure

While polyaniline was discovered in the early 1900s as the material aniline black, it wasn't until the elucidation of the structure by MacDiarmid and coworkers that polyaniline and its properties could be properly studied[18]. Understanding the structure of polyaniline and the transformations that occur during doping and oxidation is critical to predicting its behavior and properties. The structure and subsequent changes under varying conditions is discussed further in this section.

1.2.1.i. Oxidation States

Polyaniline is comprised of repeating N, 4 linked aniline units. Two key substructures, the benzoid unit and the quinoid unit, are used to describe the overall structure and oxidation state of the polymer based on their relative abundance in the polymer sample[19,20]. The benzoid structure is N-phenyl 1,4-diaminobenzene representing the reduced state of the backbone. On a molecular level polyaniline occupies one of three oxidation states, described by the number of benzoid and quinoid units, and can shift between these states upon oxidation or reduction (Figure 1). Leucoemeraldine is the fully reduced form of polyaniline, comprised entirely of benzoid units. The quinoid structure is N-phenyl 1,4-diiminoquinoid, and represents the oxidized state of the polymer. Pernigraniline is the fully oxidized form of polyaniline, comprised of repeating quinoid units. The emeraldine state is the most stable of the polyaniline oxidation states and is comprised of alternating benzoid and quinoid units. The oxidation state of emeraldine polyaniline is considered to be one half[19].

The predominant oxidation state is the emeraldine state, halfway between the fully reduced leucoemeraldine and the fully oxidized pernigraniline. Transitioning between oxidation states requires treatment with an oxidant such as ammonium persulfate or a reducing agent such as hydrazine. While these transitions are generally reversible, repeated treatments with oxidizing or reducing agents does pose the risk of introducing irreversible defects into the polymer structure[21]. It has been shown that on a molecular level polyaniline occupies one the of three discreet oxidation states mentioned above[22]. Transitions between these states occur in a single step with no observed intermediates. The average oxidation state of polyaniline can exist on a continuum however, depending on the ratio of molecular oxidation states present.

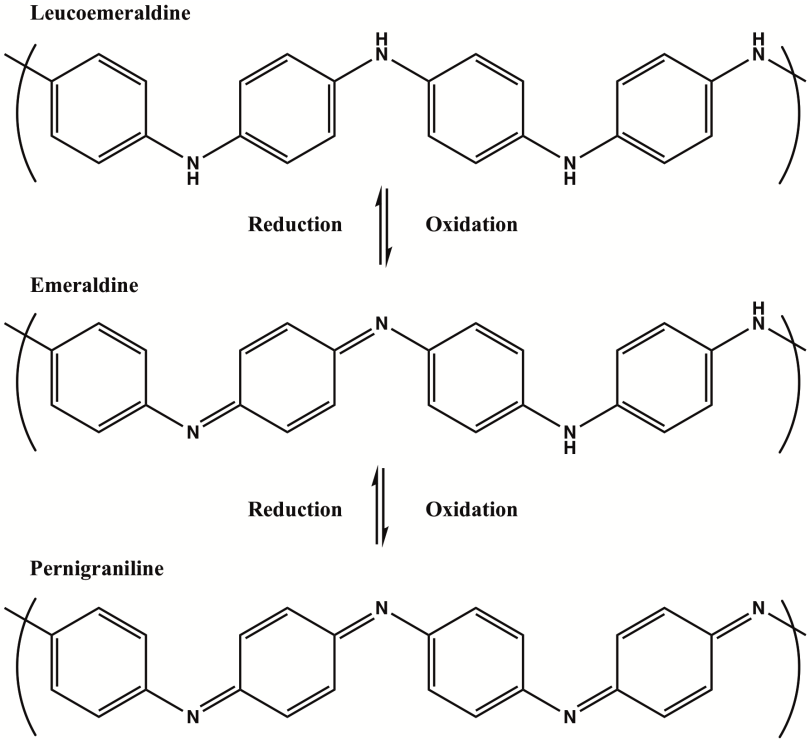

Figure 1. The three distinct oxidation states of polyaniline: leucoemeraldine, emeraldine, and pernigraniline.

1.2.1.ii. Doping

Doping is the key factor to achieving conductivity in conducting polymers as it generates electron holes that promote the flow of electrons. Typically, doping is an oxidative process removing electrons from the backbone and stabilizing the generated radical cation with an anionic species[11,23]. This type of process produces p-type doping as electron holes are introduced into the previously neutral backbone[17]. The process of doping polyaniline is unique however, in that it undergoes p-type doping through an acidic protonation mechanism coupled with an internal redox process[17,24]. During the doping process the imine nitrogen atoms are protonated and facilitate the formation of a diradical cation (Figure 2). This process is fully reversible and the doped emeraldine salt can be converted to the corresponding base via treatment with an

alkaline solution[25]. This allows for the facile exchange of dopant anions, which can alter the conductivity, solubility and other properties of the polymer. A similar doping process has been achieved in poly(heteroaromatic vinylene)s designed with structural similarities to poly(aniline)[26].

The leucoemeraldine and pernigraniline oxidation states can also undergo this protonic doping process. As the leucoemeraldine state does not contain any imine units, the amine nitrogen atoms are protonated and no structural changes are observed[27]. In the case of pernigraniline and emeraldine, the transition from the base to the salt is accompanied by a visible shift in color: the deep blue of the emeraldine base becomes the vibrant green emeraldine salt, and the violet pernigraniline base transitions to the teal pernigraniline salt[19-22].

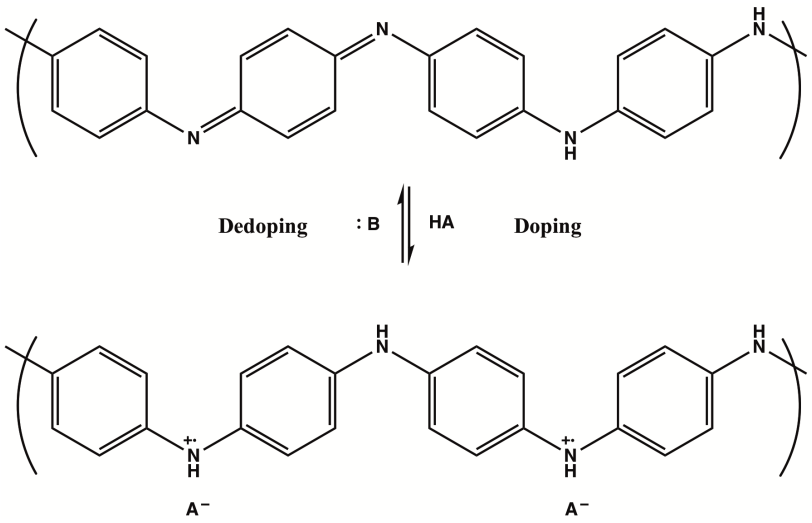

Figure 2. The reversible doping of polyaniline with protonic acid results in conversion of the diiminoquinoid unit into a diradical cation species.

1.2.2. Synthesis

Polyaniline can be synthesized by a variety of methods that fall into two broad methods: chemical synthesis and electrochemical synthesis. Each has advantages and the method employed is often dependent on the final application.

1.2.2.i. Chemical oxidative polymerization

The most common chemical synthesis of polyaniline derives from the work of MacDiarmid and is the oxidative addition of aniline monomer in acidic aqueous media to produce the polyaniline emeraldine salt (Figure 3), which can be easily isolated by filtration[19-22]. The acidic media is typically aqueous hydrochloric acid and the oxidant is ammonium persulfate. Other oxidants have been successfully employed, such as ferric chloride and potassium dichromate, and studies have been undertaken to examine the influence of oxidant choice on the final properties of the polymer[28]. The use of other mineral and organic acids have also been reported, such as sulfuric acid, perchloric acid, camphor sulfonic acid, and many others[19,29,30]. The use of different acids can improve the solubility of the final product, as well as shape the nanoscale morphological features.

Chemical synthesis is not limited to this simple procedure however, and numerous publications have covered the interfacial, emulsion, dispersion, solution, sonochemical, metathesis, template, and seeding polymerization methodologies[31]. Many of these methods are used to produce specific morphological features such as nanofibers, nanotubes or spherical structures instead of the amorphous granular structure formed using MacDiarmid's synthesis[32].

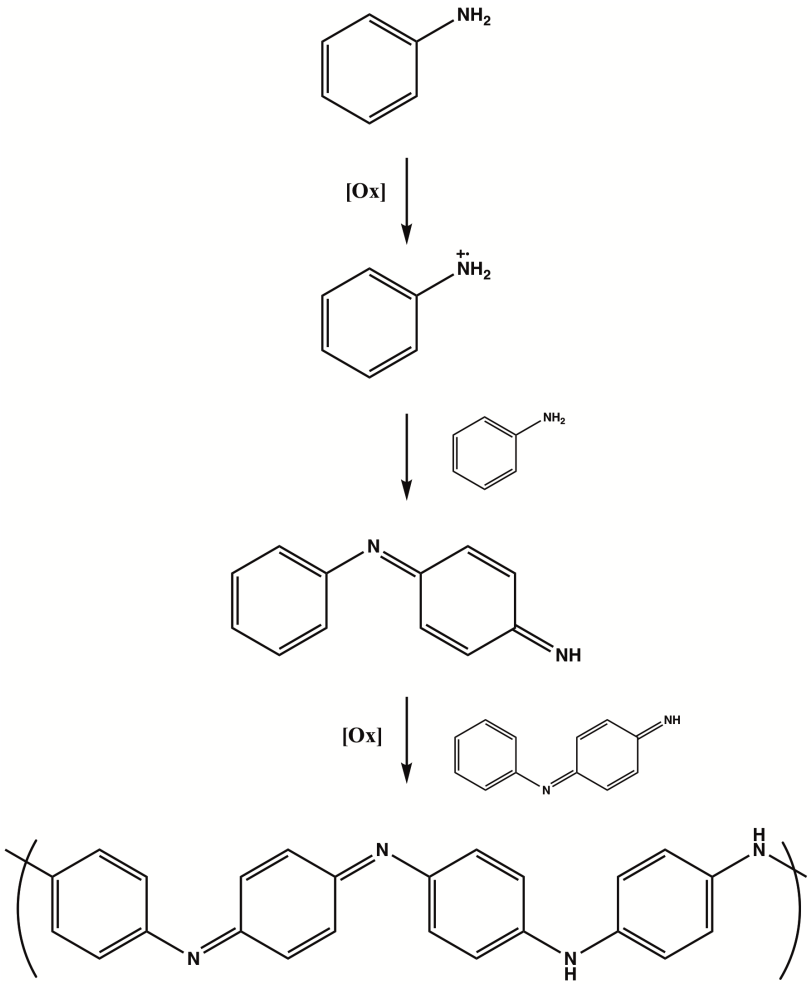

Figure 3. The synthesis of polyaniline occurs through the oxidative coupling of the aniline monomer forming dimers and trimers that eventually form larger oligomers and the final polymer.

1.2.2.ii. Electrochemical polymerization

Electrochemical synthesis of polyaniline is a versatile method for producing polyaniline films and coatings for precision applications. Polymerization can be achieved through several different types of techniques including galvanostatic, potentiostatic, or cycling methods, each with unique advantages[31]. The main advantage of electrochemical synthesis is the control over monomer oxidation and the ability to fine-tune the polymerization reaction[31]. By limiting or controlling the rate and degree of monomer oxidation the purity of the final product is greatly

enhanced while reducing the number of waste products. This purity comes at the expense of sample quantity, as large volumes of polyaniline and other conducting polymers cannot be produced this way.

Electrochemical polymerization can also be used to produce various nanoscale morphological features such as wires, tubes and belts[33-36]. In addition to the polymer morphology, the thickness and adhesion of deposited films can also be controlled[37-39]. This fine control over polymer formation and deposition has made electrochemical synthesis an essential tool for producing polyaniline based devices and sensors.

1.2.3. Morphology

Nanoscale control of polyaniline morphology has been a subject of great interest due to the influence of morphology on the bulk properties as well as the unique properties that can arise with new nanoscale features[40,41]. These nanostructures range from "zero"-dimensional granules to three-dimensional self assembled microstructures, with many unique configurations in between (Figure 4).

One dimensional nanofibers can be generated using a variety of methods to control both fiber length as well as diameter, and in some cases produce hollow tube-like structures[41]. Nanofibrillar polyaniline has a significantly larger specific surface area compared to granular morphologies. This is advantageous for many applications of polyanilines including chemical sensing, energy storage and catalysis[42,43]. Two-dimensional nanostructures are also possible through the use of templates and polymeric directing agents[41]. Polyaniline nanoplatelets and leaf like structures have been produced[44]. These structures are often building blocks for larger three-dimensional self-assembled architectures. The self-assembly of polyaniline nanostructures has gained significant interest as a route to developing nanoscale devices as well as exploring the

intermolecular interactions between nanostructures[45,46]. While the exact mechanism is not fully understood, the self assembly of nanostructures arises primarily from hydrogen bonding interactions and π-π stacking between polyaniline chains[45,47].

Three-dimensional nanostructures require more care to produce but come in a variety of shapes and configurations, often leading to new properties[48]. Of the 3D architectures, nanospheres are perhaps the most basic and easily synthesized. Hollow polyaniline nanospheres can be easily produced using hard templates like polystyrene or surfactant based soft templates[49,50]. More unique rambutan or urchin like structures result from the self-assembly of smaller polyaniline units under controlled conditions[41,51]. These high surface area materials also exhibit super-hydrophobic properties[51,52].

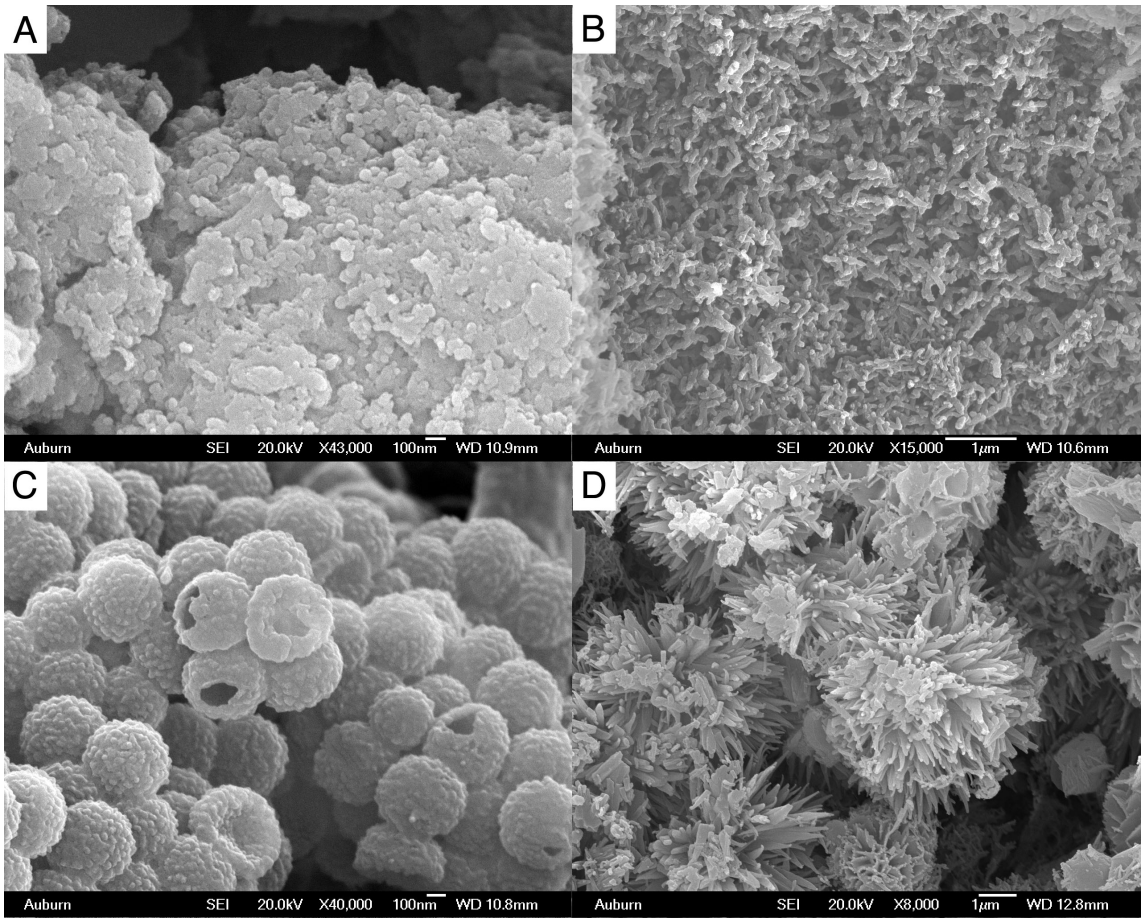

Figure 4. Polyaniline can be synthesized from a variety of procedures to produce micro and nanoscale structures such as granules (A), nanofibers (B), hollow spheres (C), and urchins (D).

1.2.4. Mechanism of Conduction

Intrinsically conducting polymers achieve conductivity through the movement of electrons filling electron "holes" along the length of the polymer chain. These electron holes are typically created through oxidation of the polymer and stabilized by the presence of an anionic dopant species. Electrons flow towards these holes creating a movement of charge carriers, giving rise to conductivity. Polyaniline differs from other conducting polymers in the way the electron holes are formed. Rather than generating electron holes through direct oxidation, polyaniline undergoes a unique internal redox reaction upon treatment with protonic acids[19,20].

Protonation of the imine nitrogen atoms in the diiminoquinoid moiety leads to an internal redox process (Figure 5) in which the quinoid rearranges to a benzoid configuration and leaves both imine nitrogens as radical cationic amines[53]. This state is known as a bipolaron, and the radical cationic nitrogen atoms act as the electron holes in the polymer system. In the pernigraniline salt most of the nitrogen atoms are in the bipolaron state, creating an abundance of electron holes with few electrons available to fill them[54]. The presence of so many adjacent electrons holes also severely limits the distance an electron can travel along the polymer[55]. These two factors, an overabundance of charge carriers and a limited conductive pathway, account for the generally insulating nature of the pernigraniline salt. The lack of conductivity in the leucoemeraldine salt can be explained similarly. Since the leucoemeraldine state possesses no imine nitrogens, it cannot form the bipolaron radical cations despite protonation. Without any electrons holes to promote the movement of electrons along the polymer backbone, conduction does not occur[54].

As mentioned previously, the emeraldine state is able to generate a radical cation species upon protonation due to the presence of the diiminoquinoid unit. Through the same internal redox process that occurs in the pernigraniline salt, the diiminoquinoid is converted into a bipolaron radical species[53]. The critical difference is that only half of the nitrogen atoms in the polymer are in this state while the other half remain neutral. The emeraldine salt undergoes an electron transfer in which a neutral nitrogen adjacent to the bipolaron transfers an electron to one of the charged radicals to create an alternating charged-neutral configuration. This process converts the bipolaron structure to a polaron structure that is better suited for conduction[56,57].

Conduction occurs as electrons move from neutral nitrogen atoms to electron holes on adjacent cationic nitrogen atoms. Several key factors influence the conductivity in polyaniline: the degree of oxidation, the extent of doping and the nature of the dopants, the degree of crystallinity and packing of the crystal structure, and the molecular weight of the polymer.

The role that the oxidation state plays in the conductivity of the polymer has already been discussed, and control of the oxidation state is the most critical component to achieving a highly conducting polymer. Without the repeating emeraldine structure, charge transport and electron flow along the polymer chain will be limited and electrical conduction will decrease significantly as the overall oxidation state of the polymer trends away from the ideal emeraldine state.

The second most influential factor in achieving good conductivity is the level of doping and the type of dopant used[31]. Protonation of the imine nitrogen atoms leads to the formation of the bipolaron structure, which is then able to form the essential polaron structure. In the emeraldine state, protonation of the imine nitrogen atoms occurs rather than protonation of the amine nitrogens, facilitating the internal redox process[58]. A doping level of 50% results in complete protonation of all imine units and the subsequent conversion of the polymer into a

completely polaron state. Any remaining unprotonated imines will not form the polaron structure, disrupting the flow of charge carriers and lowering conductivity. A doping level greater than 50% indicates that the neutral amines have been protonated and can no longer transfer electrons to form the polaron state with adjacent radical cations. The small islands of bipolarons are unable to conduct electrons and also generate insulating regions, lowering the overall conductivity.

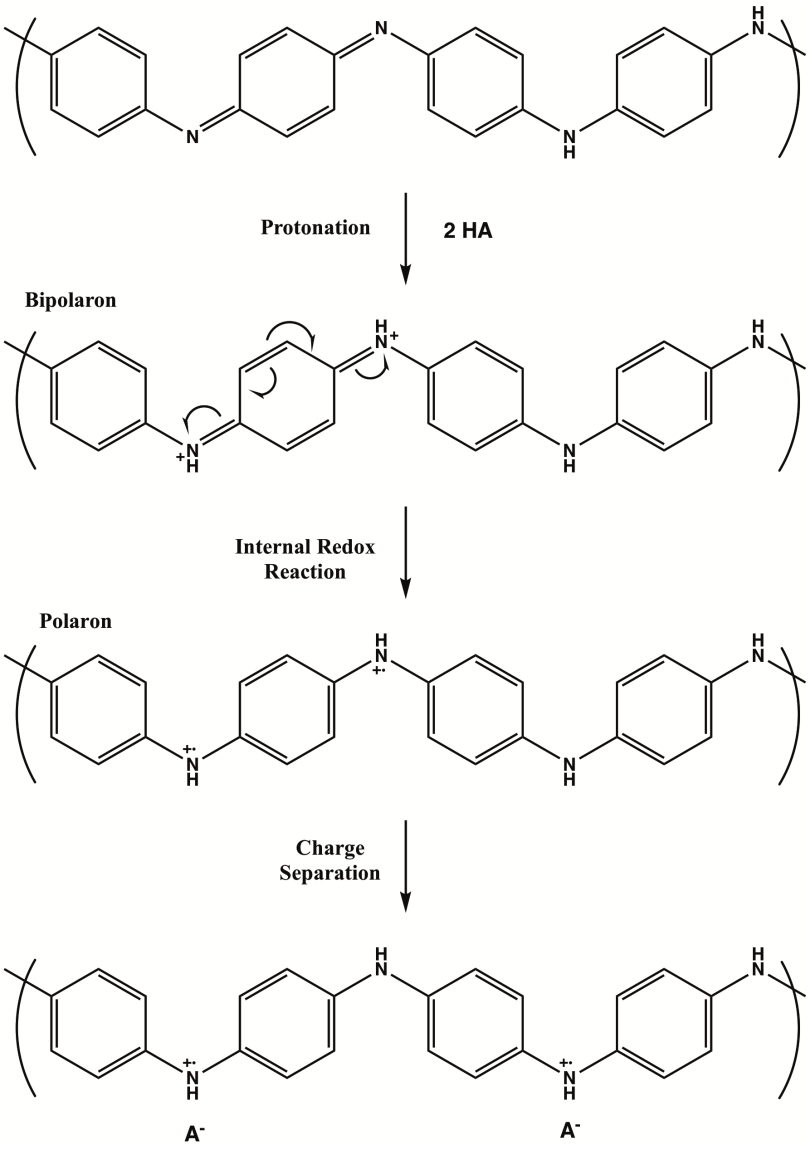

Figure 5. Mechanism for the conversion of the emeraldine base to the emeraldine salt upon treatment with protonic acid.

1.2.5. Functionalization

While pure polyaniline, sometimes referred to as parent polyaniline, has found use in a variety of applications, it is still limited by its poor solubility and low processability[31,59]. The synthesis of polyaniline derivatives has been investigated by a number of different researchers to address these issues. The introduction of substituents provides the opportunity to modify the electronic properties of the polymer, introduce new groups for acid-base interactions, and induce new conformational behaviors[60-63]. These changes can promote chain mobility and create favorable interactions with solvents and other materials leading to the desired improvements in solubility and processability thus expanding the potential applications of polyaniline.

The synthesis of polyaniline derivatives can be achieved by two main synthetic strategies: polymerizing substituted aniline monomers or introducing substituents to parent polyaniline. Each method has unique challenges and limits to the scope of possible derivatives.

1.2.5.i. Monomers

The use of aniline derivatives for the synthesis of pure substituted polyaniline or copolymers with aniline is the most direct approach to producing substituted polyaniline (Figure 6). Substituents can be located on the amine nitrogen to produce N-substituted polyaniline or on the phenyl ring in the ortho or meta positions to produce ring substituted polyanilines[64].

N-substituents are typically limited to smaller alkyl groups such as methyl and ethyl, as these monomers are commercially available and polymerize with relative ease[65-68]. Ring

substituted anilines have much greater variety ranging from alkyl and alkoxy groups to carboxylic acids, sulfonic acids, halogens, nitro groups, and others[59,69,70].

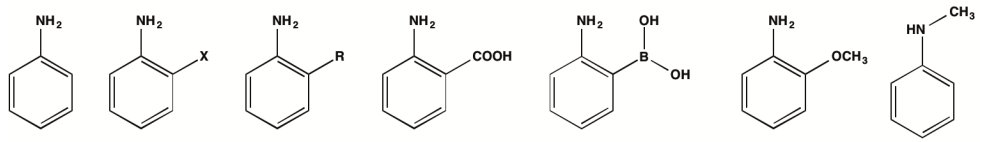

Figure 6. Various substituted aniline monomers used for the synthesis of substituted polyanilines and copolymers. A variety of groups can be incorporated at the nitrogen or on the ring, including halogens, alkyl groups, and ethers.

Introduction of N-substituents typically lower the conductivity of the polymer through stabilization of the positive radical cation and disrupting the acid-base doping mechanism[71]. The added steric bulk of larger groups also induce conformational changes in the backbone, which break the extended conjugation necessary for conduction. N-substitution has been noted to promote unique changes in the polymer such as solvatochromism and improved solubility in organic solvents[72]. The introduction of removable substituents to the nitrogen atom such as nitrosyl or amine protecting groups can allow for improved processing followed by removal to restore the original properties[73,74].

A greater variety of ring-substituted anilines have been employed for the synthesis of pure substituted polyanilines as well as copolymers with aniline to control the degree of substitution in the final product[75]. Depending on the nature of the substituent, ring substituted polyanilines exhibit improved solubility in organic solvents, self-doping capabilities, as well as changes in conductivity, molecular weight, and thermal stability[63-73]. More sterically imposing substituents result in lowered conductivity due to induced conformational changes resulting in a loss of planarity and thus conjugation along the backbone. These conformational defects also

reduce the overall crystallinity of the polymer, which further contributes to a drop in conductivity[67].

Groups such as alkyl sulfonic acids and carboxylic acids are able to provide inter- and intra-molecular doping without the need for an additional protonic acid source[76,77]. These interactions enhance the conductivity of the polymer as well as improve the solubility in aqueous solutions due to the greater number of hydrogen bonding interactions. Electron donating substituents can improve the conductivity by increasing electron density in the conjugated system.

While the use of substituted monomers provides a direct route to polyaniline derivatives, several main drawbacks exist. The introduction of substituents to the monomer alters the reactivity towards oxidative polymerization, slowing the polymerization rate compared to unsubstituted aniline. This drop in reactivity results in lowered yields for both homopolymers of substituted aniline, and copolymers[68,78,79]. In the case of copolymers with aniline, the substituted monomers are often found to have lower inclusion rates despite high feed ratios as well as poor distribution throughout the copolymer[80-82]. Another significant drawback is the inclusion of substituted monomers alters the polymerization rate and can lead to unintended morphological features[83-85].

1.2.5.ii. Post-polymerization Substitution

The post-polymerization synthesis of polyaniline derivatives offers a slightly more complicated path but possesses some inherent benefits over the use of substituted monomers. Ring substituents are introduced through nucleophilic addition or aromatic substitution mechanisms, while N-substituents can be introduced through reactions of amine nitrogens with alkylhalides or other activated substrates such as acylchlorides[63,70,86-88]. The main advantage to

introducing substituents post-polymerization is the extensive methodologies for the synthesis of polyaniline can be employed. Both bulk chemical polymerization and electrochemical synthesis methods can be used to produce the parent polymer in good yields with the desired molecular weight and nanoscale morphology. Depending on the reaction conditions used to generate the polyaniline derivative, it is possible to retain these features.

The N-substitution of polyaniline can be accomplished quite easily using chemistry designed for secondary aromatic amines. A greater variety of substituents can be introduced in this way compared to the polymerization of N-substituted anilines, since the functional groups aren't present to interfere with the oxidation of the monomer. Longer aliphatic chains, acyl groups, nitrosyl, and some sulfonates have been successfully introduced in this manner[63,71,72,89].

Ring substitution of the polymer is more limited post polymerization. The main focus has been on the introduction of sulfur based acids to produce self-doped, water-soluble polyanilines[90-93]. By introducing these groups post-polymerization, larger molecular weight polymers can be converted into soluble derivatives that are able to maintain their doped state at higher pH values than the parent polyaniline. Other works have been presented demonstrating the introduction of alkylthiols, halogens, nitrates and diazo groups to the backbone, although the examples are limited compared to reports utilizing substituted monomers[94-98].

Amine based nucleophiles

While sulfur based nucleophiles have received considerable attention, there is very little evidence in the literature of a comprehensive effort to produce amine-substituted polyanilines. Amines present a promising substrate scope for potential nucleophiles due to their low cost, commercial availability, and diverse structures. Additionally, amines are a common functional group in a variety of other research fields including biology, materials and composites, and

organic chemistry. A better understanding of the scope and limitations of the reductive addition of amines would allow polyaniline to gain further use in new applications and fields of study.

The first portion of this work is devoted to the exploration of amine functionalized polyaniline in three phases: preparation and refinement of synthetic conditions; exploration of the underlying reaction kinetics to determine mechanistic features; and finally, the formation of cross-linked polyanilines to demonstrate the potential application of the amine functionalization reaction.

2. Development and Optimization of the Amine Functionalization of Polyaniline

The key strengths of polyaniline are its unique doping process and the wide array of achievable morphologies that can be achieved and allow for tuning of its inherent properties. Additionally, the aromatic rings that form the core of the polymer backbone are rich sites for chemical modification through a variety of means. However, there have been no previous reports of the synthesis of amine-functionalized polyanilines on the bulk scale. Additionally, there has been little focus on the preservation of nanoscale morphological features in the post-polymerization functionalization of polyaniline. The following work describes the conditions for the bulk synthesis of amine-functionalized polyanilines optimized for the retention of nanoscale morphology.

2.1. Introduction

Many polyaniline derivatives are achieved through nucleophilic attack by the polyaniline nitrogens on electrophilic sites. The utilization of nucleophilic reagents leads to their addition to the quinoid moieties with concurrent reduction of the ring system to produce a reduced but substituted polyaniline. This method offers a powerful method for introducing unique functional groups to the polymer backbone while leaving the nitrogens unaffected.

2.1.1. Reductive Addition of Nucleophiles to Polyaniline

The majority of reactions producing ring-substituted polyanilines post-polymerization follow a common mechanistic pathway[95-98]. Nucleophilic addition of the substituent group takes

place at the quinoid moiety of the backbone, converting the diiminoquinoid to a substituted diaminobenzoid structure. This conversion results in the overall reduction of the polymer oxidation state, thus the reactions are labeled as concurrent reduction-substitution reactions or reductive-addition reactions. The final product of these reactions is typically highly substituted leucoemeraldine polyaniline.

Nucleophilic addition to the quinoid ring structure was observed early on in the study of polyaniline. MacDiarmid noted that attempts to protonate the pernigraniline base with hydrochloric acid resulted in the formation of chlorine substituted emeraldine base structure[99]. The use of I_2 as an oxidant to synthesize the pernigraniline base yielded an oxidized form of the polymer containing a significant percentage of iodine, even when dedoped[99]. The nucleophilic I^- anion produced during oxidation undergoes addition to the polyaniline rings, resulting in the substituted polymer. Solutions of emeraldine base in slightly nucleophilic solvents like pyrrolidone were observed to undergo an aging process resulting in a loss of conductivity and a color change in the polymer solution[100]. These processes were seen not so much as a method for producing polyaniline derivatives, but as an unwanted byproduct of trying to accomplish other reactions.

As polyaniline continued to be studied, the reductive addition of nucleophiles began to take shape as a viable method for the introduction of substituents. An initial kinetic study by Han and coworkers found that amine, oxygen, and sulfur nucleophiles could all undergo addition to the polyaniline backbone[100]. Sulfur was shown to be an extremely effective nucleophile, undergoing substitution at a rate several orders of magnitude faster than oxygen, both of which reacted more readily than amines. Han continued to investigate the addition of alkylthiols to electrochemically synthesized films of polyaniline, as well as developing a unique fluoride

mediated Michael addition to small molecule analogues of polyaniline[97,98,101]. Barbero, Morales, and Salavagione also pursued the synthesis of substituted polyanilines via reductive addition, focusing on sulfonic and sulfinic acid. They also demonstrated the addition of diazo salts and nitro groups to polyaniline samples[94,102].

Most of the literature on the reductive addition of polyaniline focuses on the conversion of the emeraldine base to the fully reduced leucoemeraldine state, although it has been noted that starting from fully oxidized pernigraniline results in a greater degree of substitution[93,100]. Reoxidation of the polymer is necessary to return the derivative to the emeraldine state where it can be doped to the conducting salt, or subjected to additional substitution. One drawback to oxidation of the polymer after substitution is the potential for degradation of the substituent during this process.

Polyaniline is a material with unique properties and a rich body of research dedicated to producing unique nanoscale morphologies. This work aims to develop a method for introducing amine-based substituents to polyaniline while maintaining pre-established morphological features. Utilizing a reductive-addition reaction and starting from the pernigraniline state should allow for the introduction of substituents while simultaneously returning to the emeraldine oxidation state, eliminating the need for re-oxidation after the introduction of substituents.

2.1.2. Substrate Scope

Amines were chosen for the initial substrate scope to represent the most common types of amine structures (Figure 7). Primary, secondary, and tertiary aliphatic amines were represented by hexylamine, diethylamine, and triethylamine respectively. Pyrrolidine represented cyclic amines, while aniline represented aromatic amines.

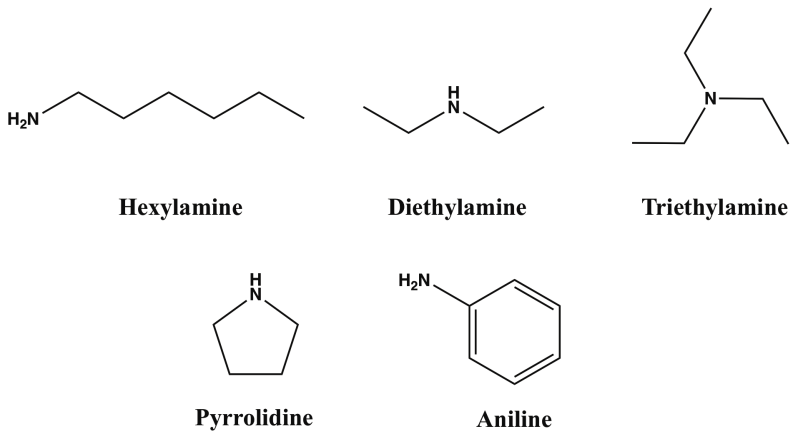

Figure 7. A small scope of amine was chosen to explore the reductive addition to polyaniline. The alkyl amines cove the primary, secondary and tertiary architectures. Aniline is representative of aromatic amines.

2.2. Experimental Methods

All chemicals were obtained from Alpha Aesar, with the exception of hexylamine and triethylamine which were obtained from Acros Organics, and used without further purification. Solvents used were all of reagent grade purity. All water used was deionized to a resistivity of 18 MΩm.

UV-Visible spectroscopy was conducted on a Shimadzu 2450 spectrometer using 1 cm quartz cuvettes. FT-IR spectra were collected using a Thermo Nicolette 6700 FT-IR with SmartOrbit ATR attachment, with a resolution of 2.0 cm^{-1}. Deuterated DMSO was used to prepare samples for NMR spectroscopy, and spectra were collected on a Bruker 400 MHz spectrometer. Scanning electron microscopy was carried out on a JEOL microscope with samples mounted on carbon tape and gold coated for improved image resolution.

2.2.1. Synthesis of Polyaniline Emeraldine Base

Polyaniline emeraldine base was synthesized in two steps following the general procedure developed by MacDiarmid and coworkers[17]. In a 600 mL beaker, aniline monomer

(10.2 g, 0.1095 mol) was dissolved in 300 mL of 1 M aqueous hydrochloric acid. Ammonium peroxydisulfate (11.55 g, 0.0506 mol) was added as a solution in 100 mL 1 M aqueous hydrochloric acid. The reaction was stirred rapidly for 30 seconds to ensure even mixing of the oxidant solution before being left undisturbed for 3 hrs. Shortly following removal from stirring, the clear solution took on a vibrant blue hue before rapidly darkening. Within 30 min of adding the oxidant the solution had become completely opaque and taken on a dark green color. The additional reaction time was to ensure that the majority of the monomer had been converted to polyaniline.

The formed polyaniline emeraldine salt was collected via filtration and washed with excess 1 M aqueous hydrochloric acid until the filtrate ran clear. Excess acetone was then used to rinse the collected polymer to remove any residual monomer or reaction byproducts, as well as to aid in the drying of the sample. The washed polymer was dried under vacuum at 60 ºC overnight then ground with mortar and pestle to yield a fine, deep green powder.

The emeraldine salt was converted to emeraldine base by stirring in a 1 M aqueous solution of ammonium hydroxide for several hours. The deep blue polymer was collected by filtration and washed with deionized water and acetone, then dried under vacuum at 60 ºC.

This procedure yields polyaniline with an amorphous, granular nanostructure. However, to investigate the impact of the reaction conditions on the polymer morphology, polyaniline nanofibers were synthesized using a template seeding method[103]. Vanadium pentoxide sol-gel (10 mL) was added to the monomer solution followed by the addition of the oxidant, all other steps remained the same.

2.2.2. Oxidation to the Pernigraniline Base

Polyaniline emeraldine base (1.0 g) was dispersed in 150 mL deionized water under heavy magnetic stirring, followed by the addition of ammonium peroxydisulfate (1.5 g, 0.0044 mol). The oxidation took place over the course of 30 minutes, during which the solution changed from deep blue to purple, indicating the conversion to pernigraniline base. The product was collected via filtration and washed with 1 M aqueous ammonium hydroxide to ensure that the polymer was in the base state, and followed by acetone to remove any residual water or byproducts of the oxidation. The resulting bronze-purple powder was dried under vacuum at 60 ºC for 15 min to remove any residual solvent.

2.2.3. Functionalization with Amines

Polyaniline pernigraniline base (100.00 mg, 0.277 mmol) was measured into a 20 mL glass vial followed by 2.0 mL of solvent and a small magnetic stir bar. The mixture was placed under medium magnetic stirring, followed by addition of the amine. The vial was capped and left to stir at room temperature. Reactions were allowed to proceed for 24 hrs.

The reaction was quenched by the addition of 10 mL of cold deionized water and products were collected by filtration, rinsing with copious deionized water to remove excess amines. The collected powders were dried under vacuum at 40 ºC.

Reaction yields were determined by the mass of the recovered polymer. A theoretical 100% yield was calculated based on conversion of the pernigraniline repeat unit to the amine-substituted product. The pernigraniline repeat unit was defined as the N-phenyl diiminoquinoid subunit with a molecular weight of 182.23 g/mol. The difference in mass of the obtained product and the initial mass of pernigraniline base used was divided by the difference in mass between the theoretical 100% yield and the initial mass of pernigraniline.

$$Reaction\ yield = \frac{m_{obtained} - m_i}{\left(m_i \frac{MW_{product}}{MW_{PB}}\right) - m_i} \times 100\%$$

Using this definition, a 100% yield would result in a product where each of the quinoid moieties has undergone reductive addition to the amino-substituted benzoid structure. This affords a substituted polyaniline in the leucoemeraldine oxidation state while a yield of 50% would produce a substituted polyaniline in the emeraldine oxidation state.

2.3. Results and Discussion

Analysis and discussion of the experimental results is detailed below. Solvent, reaction temperature, amine structure and concentration were investigated to evaluate their impact on reaction yields as well as polymer morphology. Ideal conditions would allow introduction of substituents to the polymer backbone without erosion of pre-established morphological features to yield nanostructured polyaniline derivatives through a facile synthetic route.

2.3.1. Oxidation of Emeraldine to Pernigraniline

The synthesis of the pernigraniline state, base or salt, is a process that lacks consistency across the literature[99,104]. The initial synthesis of the pernigraniline base by MacDiarmid is often cited, and is accomplished through the oxidation by chloroperbenzoic acid in a mixture of NMP and glacial acetic acid, yielding a material that is approximately 97% oxidized as determined by titration[99]. The largest drawback to this procedure is the dissolution of polyaniline, eliminating any preformed morphology. The UV-Vis spectroscopy peak absorbances for the pernigraniline base synthesized in this way are 298, 318 and 530 nm[99]. Other works report the λmax for the Peierls gap transition at 536, 550 and 570 nm[105-107].

The oxidation of emeraldine base can also be achieved through treatment with an aqueous solution of ammonium persulfate, from the emeraldine salt or the emeraldine base[95,104]. The oxidized product can then be easily collected via filtration, although reports differ on the solvents used to rinse the collected pernigraniline[104,106,107]. It has also been reported that if collected in air or treated with ammonium hydroxide, the polymer is immediately reduced back to the emeraldine state[108].

For the purposes of this work, the pernigraniline base was reliably produced by the oxidation of the emeraldine base by aqueous ammonium persulfate, followed by filtration and rinsing with a dilute solution of ammonium hydroxide followed by a brief rinsing with acetone to facilitate drying. The isolated polymer sample is stable and displayed characteristic absorbances at 298, 320, and 535 nm. Increasing the concentration of oxidant or extending the reaction time did not shift this value any further. This procedure offers many advantages including fewer reagents, shorter reaction times and preservation of the polymer morphology.

2.3.2. Solvents

Solvent choice in a reaction involves more than simply providing a reaction medium that can suitably mix the reagents. The nature of a solvent can have a large impact on the reaction due to hydrogen bonding with the reagents or intermediates, ordering of transition states through dipole interactions, or serving as proton donors/acceptors[109]. These interactions can greatly enhance the rate of reaction, such as SN2 type substitutions in polar aprotic solvents, or the selectivity for one product over another[110,111].

Several common laboratory solvents were chosen to explore the effect of solvent on reaction rate and polymer morphology (Table 1). Deionized water, ethanol, acetone, tetrahydrofuran and N-methylpyrrolidone were chosen as they were able to solubilize the

amines, and represented a range of polarities, proton availability, hydrogen bonding capability, and ability to solubilize polyaniline. Hexylamine was used as the amine for initial solvent trials, and all reactions were stopped after 24 hrs to assess yields and changes in polymer morphology.

Table 1. Reaction yields of polyaniline functionalized by hexylamine at room temperature in various solvents.

Reaction conditions: Hexylamine 0.5 equivalent, 23 ºC, 24 hrs					
Solvent	H_2O	Ethanol	Acetone	THF	NMP
Yield (%)	19	17	19	16	27

NMP was the only solvent to have a significant effect on the yield of the reaction, most likely due to its excellent ability to solubilize the polymer. This allows the nucleophile greater access to the polymer but at the cost of any pre-established morphological features. Surprisingly, the reaction proceeded reasonably well in water, on par with the other organic solvents, with minimal erosion of morphology observed (Figure 8). Based on the ease of separation, retention of morphology and comparable yield water was chosen as the primary reaction solvent

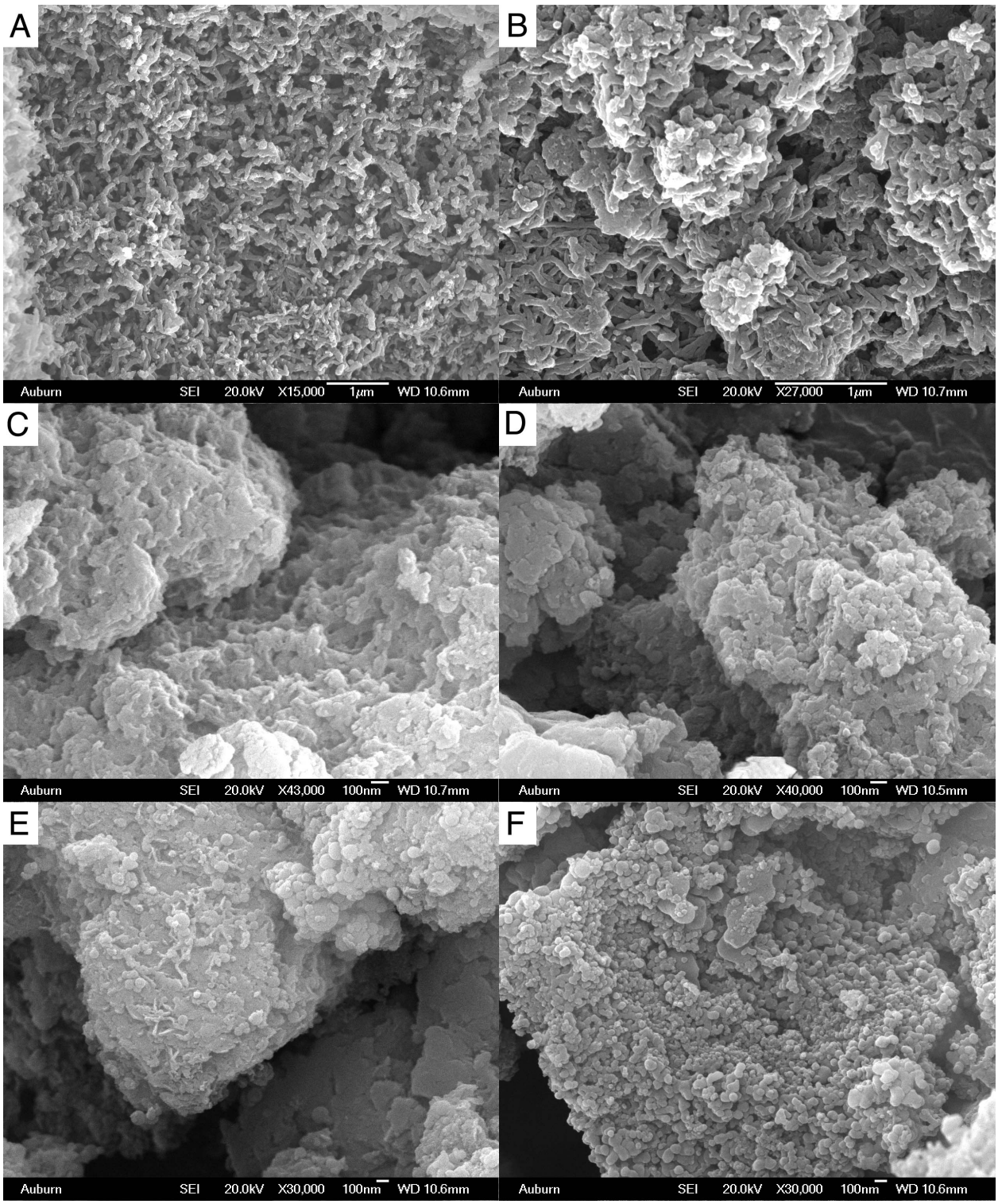

Figure 8. SEM images of polyaniline nanofibers before reaction (A), and after reaction with hexylamine in water (B), ethanol (C), acetone (D), THF (E) and NMP (F) at room temperature.

2.3.3. Temperature

The temperature dependence of reactions has been a subject of much study due to its fundamental impact on chemistry, physics and biology. Fundamental equations developed by Arrhenius, Eyring, Kramer, Van't Hoff and other demonstrate the relationships between temperature, reaction rates, equilibrium and activation energies[112-114]. Possibly the most well known of these equations is the Arrhenius equation:

$$k(T) = Ae^{(-E_a/RT)}$$

where k(T) is the reaction rate as a function of temperature (T), A is a pre-exponential factor often referred to as the Arrhenius factor. The activation energy, E_a, of the reaction describes the energetic barrier to reach an active state, now commonly referred to as the transition state, of the reaction and R is the universal gas constant. The exponential $e^{(-E_a/RT)}$ describes the probability of a collision between molecules resulting in a reaction, and increases as the temperature increases, in turn increasing the reaction rate. Thus, the Arrhenius equation at its most basic demonstrates that increasing reaction temperature leads to an increase in reaction rate.

Controlling the energy available to the reactants can help or hinder their ability to overcome the energy barriers present for a specific transformation. Higher temperatures often lead to faster conversion of the reactants, but it is not always conversion to the desired product. More energy available to the reactants means that more reactive pathways are now available, and what might have previously been a minor product at low temperatures becomes the major product at higher temperatures[115].

In the case of the reductive addition of amines to polyaniline, a temperature dependence on the reaction yield was observed (Table 2). Increasing the reaction temperature from room temperature to 60 ºC resulted in an approximately two-fold increase in yield. The modest

increase in temperature to 40 ºC resulted in a slight increase in yield, although not as significant as the increase observed at 60 ºC. While heating the reaction did improve yields, some of the nanofibrillar structure was eroded (Figure 10). Since a major aim of the project was the retention of polymer morphology, further reactions were carried out at room temperature regardless of solvent.

Table 2. Reaction yields for the polyaniline functionalized by hexylamine at various temperatures in water.

Reaction conditions: Hexylamine 0.5 equivalent, H_2O, 24hrs				
Temp (ºC)	4	23	40	60
Yield (%)	8	19	22	37

2.3.4. Yields

With the reaction solvent and temperature decided, the reaction was expanded to include the rest of the amines in the substrate scope (Table 3). It was observed that the reaction of diethylamine with the pernigraniline base produced a much lower yield compared to the reaction with hexylamine. The yield for the reaction with triethylamine was also significantly reduced compared to hexylamine indicating that steric bulk around the amine nitrogen may inhibit the reaction.

All reactions showed a significant improvement with an increase in amine concentration, with hexylamine, pyrrolidine and aniline providing low to moderate yields from 19-40%. While still an unfavorable substrate for the reaction, diethylamine was able to achieve a four-fold increase in yield with the increase from 0.5 to 1 equivalent. Aside from diethylamine's dramatic increase the other amines showed roughly a two-fold increase in yield when the concentration was doubled. This indicated a strong relationship between amine concentration and reaction rate.

Table 3. Reaction yields of polyaniline functionalized by various amines at different concentrations.

Reaction conditions: H_2O, 23 ºC, 24 hrs		
Amine	Equivalent	Yield (%)
Hexylamine	0.5	19
	1	41
Diethylamine	0.5	3
	1	13
Triethylamine	0.5	2
	1	4
Pyrrolidine	0.5	19
	1	30
Aniline	0.5	14
	1	32

An additional factor is that many of the amines used are able to act as a base or hydrogen-bonding partner and increasing their presence in solution may facilitate the addition to the ring. It would appear that steric bulk around the nitrogen is also a key influence on the reaction rate as the more hindered diethyl- and triethylamine produced low yields despite improved nucleophilic character over aniline and hexylamine.

2.3.5. Impact on Morphology

Polyaniline nanofibers produced using a vanadium pentoxide seeding approach[103] were approximately 50-75 nm in diameter and ranged from 500 to 700 nm long, as measured during

SEM characterization. The fibers also aggregated into larger mats of partially connected fibers. This is a phenomenon described in the literature, primarily resulting from the collection of fibers via filtration[116]. Neither the dedoping process nor oxidation to the pernigraniline state had any significant impact on the dimensions of the fibers as seen in Figure 9. Thus any resulting change in the polymer morphology was a result of the experimental conditions employed during substitution reaction.

Retention of polymer morphology during the oxidation process is a major advantage of the aqueous oxidation method over the pernigraniline synthesis in NMP. This substantially more mild process affords good retention of the polymer morphology, making the substitution of more complex polyaniline structures a feasible task.

The choice of solvent for the reaction had the greatest impact of any reaction parameter on the overall morphological change in the polymer samples. Water had little observable effect on the quality of the nanofibers, but all of the organic solvents caused noticeable erosion increasing in severity as the efficacy of the solvent increased (Figure 8). In addition to the erosion of the nanofibrillar morphology to a more amorphous granular structure, spherical structures were produced, especially for the samples prepared in THF and NMP.

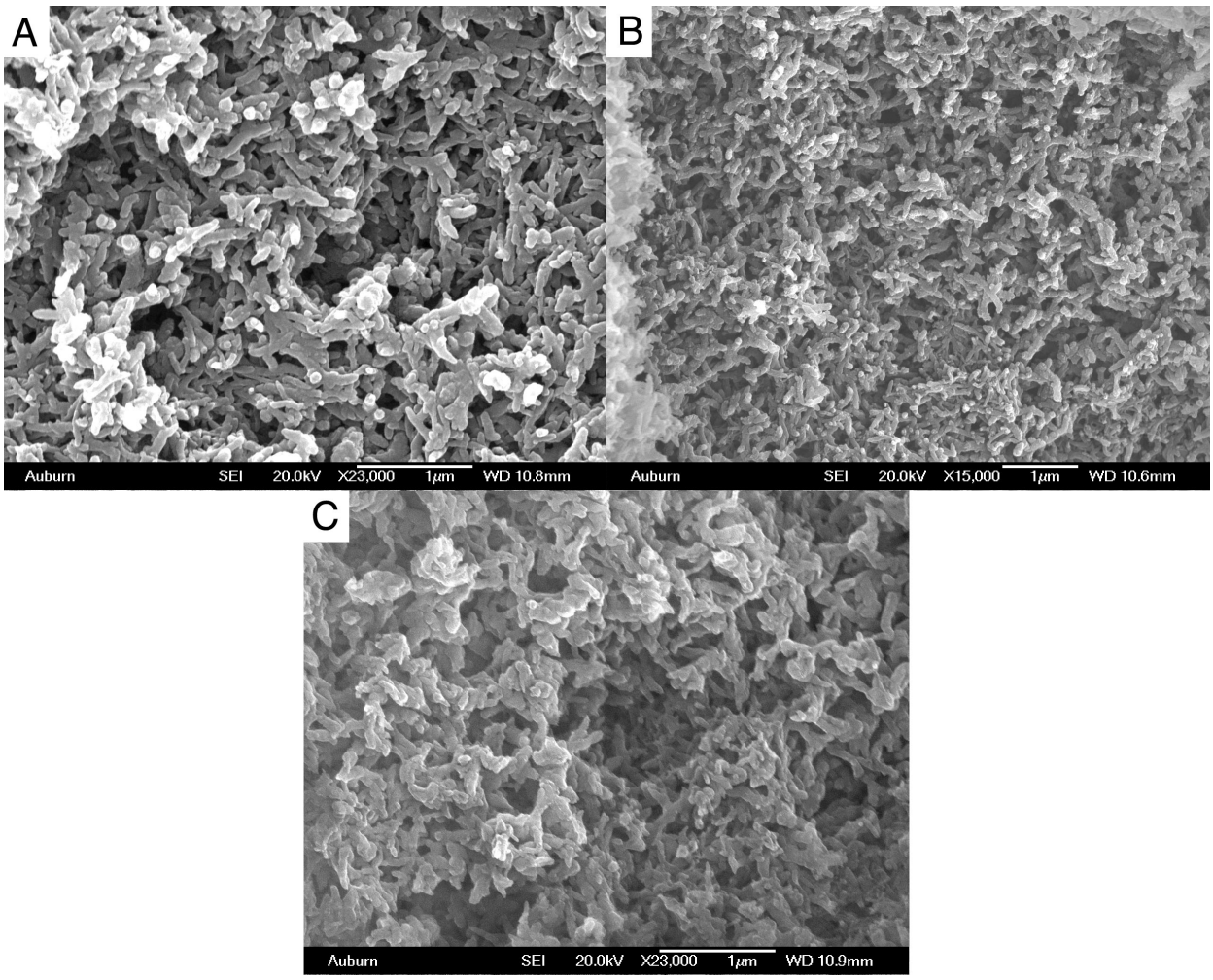

Figure 9. Polyaniline nanofibers converted from the emeraldine salt (A) to the emeraldine base (B) followed by oxidation to the pernigraniline base (C).

The presence of amorphous and spherical structures can be explained by increased solvation of the polymer chains followed by the rapid precipitation induced by the addition of water. No longer soluble in the predominantly aqueous mixture, the solvated chains collapse into a random orientation and aggregate with other surrounding chains.

While insoluble in water and many organic solvents, carrying the reaction out at 60 ºC in water led to erosion of the nanofibrillar morphology. This erosion at higher temperature has two

probable sources. The first is solubilization by the added amine, which has been noted in the literature[117]. While the resulting solubilization and erosion is minimal at room temperature, the solvating capacity increases with increasing temperature[118], becoming more noticeable (Figure 10). The second factor is the increased temperature provides additional energy, promoting chain mobility and allowing some restructuring on the nanoscale level.

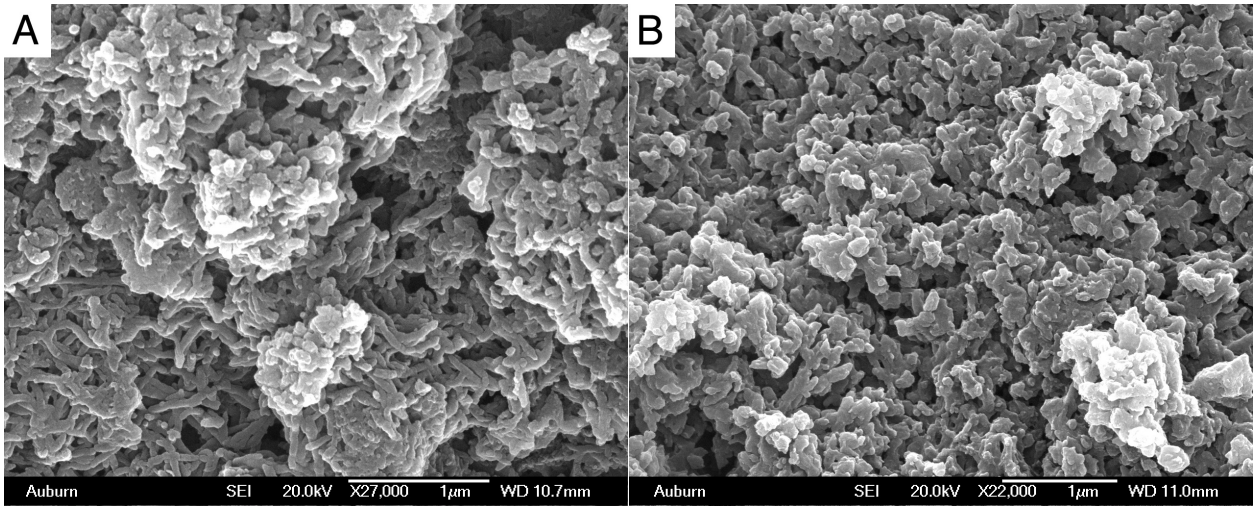

Figure 10. Polyaniline nanofibers substituted with hexylamine in water at 23 ºC (A) and 60 ºC (B). The increased reaction temperature led to substantial degradation of the polymer morphology.

2.3.6. Spectroscopy

Spectroscopic analysis of the reaction products was carried out to evaluate the structural changes in the polymer and confirm attachment of the amine nucleophiles to the polymer backbone. Of the many spectroscopic techniques available, infrared spectroscopy and nuclear magnetic resonance spectroscopy were chosen for their ability to provide information on the types of bonds and atomic environments present in the structures.

The field of spectroscopy covers a wide array of different analytical instruments designed to investigate the interactions of electrons, atoms, and molecules with electromagnetic energy.

The electromagnetic spectrum covers a huge number of energy sources such as radio waves, microwaves, visible light, infrared and x-rays, each of which interact with materials differently and provide unique spectral characteristics. Spectroscopic methods like UV-Visible (UV-Vis) spectroscopy measure the absorption of photons in the visible and near UV portion of the electromagnetic spectrum providing information on the types of electronic transitions in a compound as well as the structure of molecular orbitals[119]. Infrared spectroscopy utilizes the portion of the electromagnetic spectrum adjacent to that of UV-Vis spectroscopy, but rather than interrogating the energetic transitions of a molecule, infrared spectroscopy measures the resonant frequencies of bond stretching and bending which is useful in determining functional groups and atom connectivity[120]. Nuclear magnetic resonance (NMR) spectroscopy utilizes radio waves to influence the magnetic fields of atoms and describes the local electronic environment around atoms; an extremely useful tool for determining chemical structures and bonding interactions[121]. X-rays can be used to probe crystal structures and the arrangement of atoms in a lattice, identify elemental compositions and even the electronic configuration of atoms[122].

The diversity of spectroscopic techniques is also a product of the various ways materials interact with the electromagnetic spectrum. Some of the primary interactions are absorption, emission and scattering. Absorption spectroscopy produces a spectrum describing the wavelength and intensity of energy absorbed by a sample. Various types of absorption spectroscopy are commonly used and operate on the same principle but utilize a specific portion of the electromagnetic spectrum, such as UV-visible spectroscopy or Infrared spectroscopy. In these techniques, an energy beam is passed through the sample and the amount of light collected by the detector is used to determine the energy absorbed by the sample. Energy absorption by the sample indicates some type of excitation or resonance of a particular functional group or moiety

at that particular wavelength. For UV-Vis spectroscopy, this generally indicates an electronic transition where the absorption of a photon promotes an electron to a higher energy state. Quantitatively this can be used to measure the energy associated with a particular transition, as well as the difference in energy between the highest occupied molecular orbital (HOMO) and the lowest unoccupied molecular orbital (LUMO). The HOMO-LUMO gap is of significant interest for determining chemical reactivity, quantum mechanical behaviors and other physical properties[123]. In infrared spectroscopy the absorbed energy creates vibrations in the bonds of the molecule that can be used to determine the presence of specific functional groups and their concentration.

Emission spectroscopy measures the photons emitted by an atom as it decays from an excited state to a lower energy state. Excitations can be induced by thermal energy, used in techniques like flame emission spectroscopy or astronomical spectroscopy, or by the absorption of electromagnetic radiation, used in various types of fluorescence spectrometers. Each element displays a unique emission spectrum dictated by the various available atomic energy levels and the energy gap between them[120,124,125]. Molecules also demonstrate specific energy levels and their emission spectra are often concentrated into bands and result from the rotational, vibrational and electronic states of the atoms.

Spectroscopic techniques based on the scattering of electromagnetic waves provide unique information typically related to the spatial arrangements of atoms and molecules. X-ray crystallography can be used to determine the arrangement of atoms or molecules in a solid as well as the types of lattice structures in crystalline materials. This technique is especially useful for large macromolecules like proteins whose physical structure would be otherwise difficult to

ascertain. Raman spectroscopy also utilizes light scattering to investigate chemical bonds and vibrational energy states, similar to infrared spectroscopy but through a different mechanism.

Infrared Spectroscopy

Infrared (IR) spectroscopy is one of the most popular and common spectroscopic techniques for investigating chemical structures. The technique uses light in the infrared range, typically 2500 nm to 20,000 nm wavelength, to promote various vibrational modes in the chemical bonds present. The resulting signal undergoes a Fourier transform as part of the signal processing to generate a spectrum with clearly defined peaks. The vast majority of IR spectroscopy is processed using this method and is thus described as Fourier Transform Infrared spectroscopy, or more simply FT-IR spectroscopy.

Chemical bonds can experience different types of vibrational modes such as bending, stretching, and wagging; and these modes can be further described as symmetrical or asymmetrical, and in regards to the plane of the molecule such as in-plane and out-of-plane vibrations. These vibrational modes occur when stimulated by a specific wavelength of light, much like the absorbance and electronic transitions observed in optical spectroscopy methods like UV-Vis spectroscopy. Unlike UV-Vis spectroscopy where peaks are expressed in terms of wavelength, FT-IR spectroscopy expresses the peak position as wavenumbers, having units of cm^{-1}. Not only do certain vibrational modes occur at specific wavenumbers, but the nature of the atoms comprising the bond also influences the peak wavenumber[126]. This means that peaks observed in an FT-IR spectrum can be assigned to specific atom pairs, like carbon-oxygen and carbon-hydrogen, but also to specific types of bonds between those atoms. The stretching mode of a carbon-oxygen single bond is very different from the stretching mode of a carbon oxygen double bond (occurring around 1100 cm^{-1} and 1700 cm^{-1}, respectively), and the bending of

hydrogen at an unsaturated bond can be distinguished from the bending of a hydrogen at a saturated bond[127]. The ability to differentiate different types of bonds and vibrational modes creates a powerful spectroscopic tool for identifying functional groups, elucidating structural features and even investigating intermolecular interactions like hydrogen bonding.

Infrared spectroscopy is one of the most common methods of investigating changes in the structure of polyaniline. The vibrational modes of the benzoid ring structure, 1500 cm^{-1}, and the quinoid ring structure, 1590 cm^{-1}, present strong and characteristic peaks. These peaks can be used to qualitatively assess the oxidation state of the polymer based upon their relative intensities. The broad band around 3300 cm^{-1} is attributed to N-H stretching.

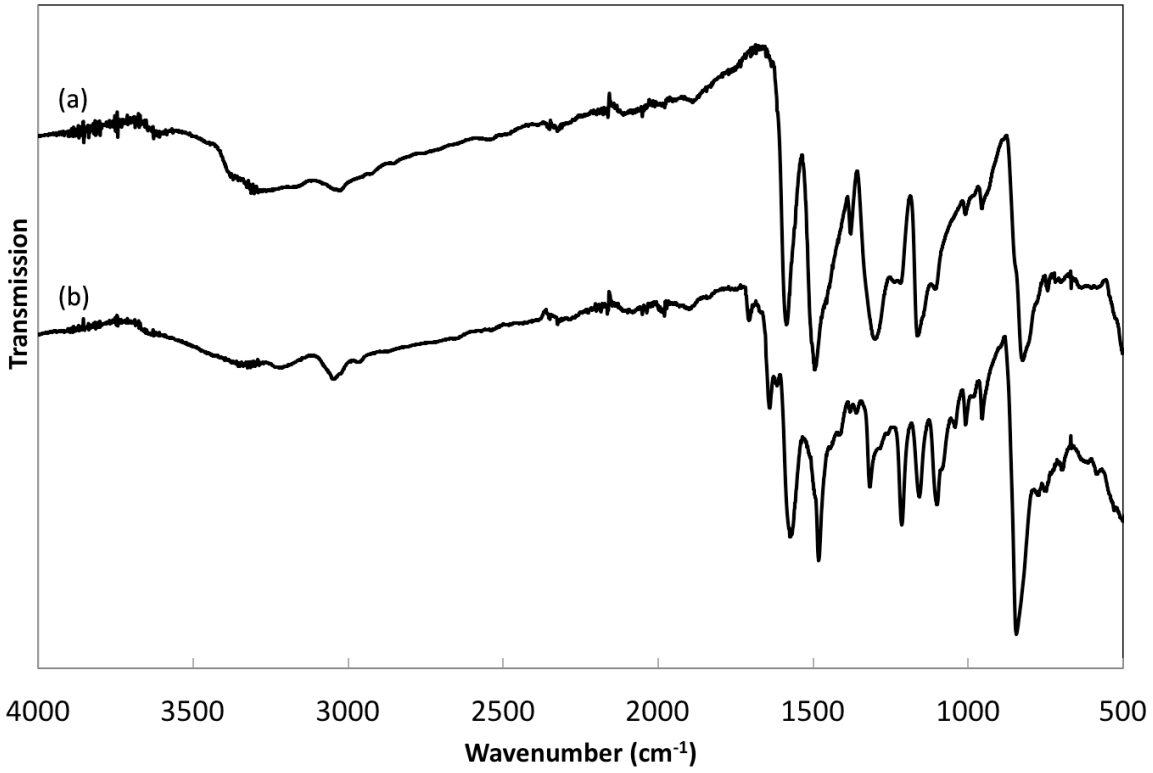

Figure 11. FT-IR-ATR spectra of polyaniline emeraldine base (a) and pernigraniline base (b). The increase in intensity of the peak at 1600 cm^{-1} indicates a greater number of quinoid units present in the polymer, corresponding to an increase in the oxidation state.

Comparison of the emeraldine base and synthesized pernigraniline base displays the expected increase in quinoid stretching as the benzoid units are oxidized (Figure 11). Spectra of both compounds match well with reported values for the benzoid and quinoid peaks as well as various C-N and C-C vibrational modes and ring deformations[127].

It should be noted that the spectrum of the as synthesized emeraldine base displays a stronger quinoid peak than would be expected of true emeraldine base. The increased intensity of this peak indicates a higher degree of oxidation than 0.5, a result that has been addressed in the literature[19]. It has been shown that deprotonation of polyaniline emeraldine salt with ammonium hydroxide solutions in air produces a polymer with an oxidation state of approximately 0.6, while those deprotonated under inert atmosphere are closer to 0.4[20].

While the addition of excess amines facilitates the reductive addition of polyaniline, care should be taken to prevent the reaction proceeding past the emeraldine state and forming the insulating leucoemeraldine. If this process was occurring, the intensity of the quinoid peak would continue to decrease before disappearing altogether.

The characteristic benzoid and quinoid peaks can also be used to qualitatively assess the oxidation state of the polymer, and in this case provide an initial indication of the extent of substitution[126]. This can be accomplished by comparison of the quinoid/benzoid intensity ratio, and examining the values of the substituted products along with the values for the pernigraniline and emeraldine states. In the ideal, fully oxidized pernigraniline state the ratio of peak intensities is equal to one since the pernigraniline state is comprised of alternating quinoid and benzoid rings. As the quinoid rings are converted to the benzoid state by the addition of the amine nucleophile the intensity of the quinoid peak decreases, lowering the quinoid/benzoid ratio. Complete reduction to the leucoemeraldine state would drop the quinoid/benzoid ratio to zero, as

the quinoid peak completely disappears. Table 4 lists the quinoid/benzoid ratios obtained for the parent polymers and the substituted derivatives. The Q/B ratio for the substituted products does show a decrease that corresponds well to the observed yields for the reaction, but the relatively high ratio observed in the emeraldine base makes a quantitative comparison between Q/B ratio and reaction rate difficult.

Table 4. Q/B ratio of FT-IR spectroscopy peak intensities for polyaniline and its derivatives.

Sample	Q/B Ratio	Reaction yields (%)
PAn emeraldine base	0.877	
PAn pernigraniline base	0.943	
PAn hexylamine	0.813	41
PAn diethylamine	0.917	13
PAn triethylamine	0.935	4
PAn pyrrolidine	0.855	30
PAn aniline	0.877	32

FT-IR spectroscopy also provides an effective means for confirming the presence of the aliphatic amine substituents as polyaniline does not possess any sp^3 hybridized C-H stretching that is characteristic of the aliphatic amines. As seen in Figure 12, the long carbon chain of hexylamine is easily distinguished, with the aliphatic peaks from the pyrrolidine ring visible but significantly less prominent. The lower yields for the reactions of diethylamine and triethylamine make distinguishing the aliphatic peaks more difficult due to the large N-H stretching bands adjacent.

The presence of aniline is more difficult to discern as it is the monomeric unit of the polymer and thus shares many of the same peaks. It has been shown that the C-H out-of-plane deformations in aromatic systems are strong, characteristic peaks that shift in response to the degree of ring substitution, while being independent of the substituent nature[128]. 1,4-disubstituted benzenes show a strong peak in the range of 860-780 cm^{-1}, which is observed in the polyaniline spectrum at 840 cm^{-1}. Addition of a substituent to form 1,2,4-trisubstituted benzenes produces weak to medium peaks at 940-920 cm^{-1} and 900-885 cm^{-1}, and a stronger peak at 780-760 cm^{-1}.

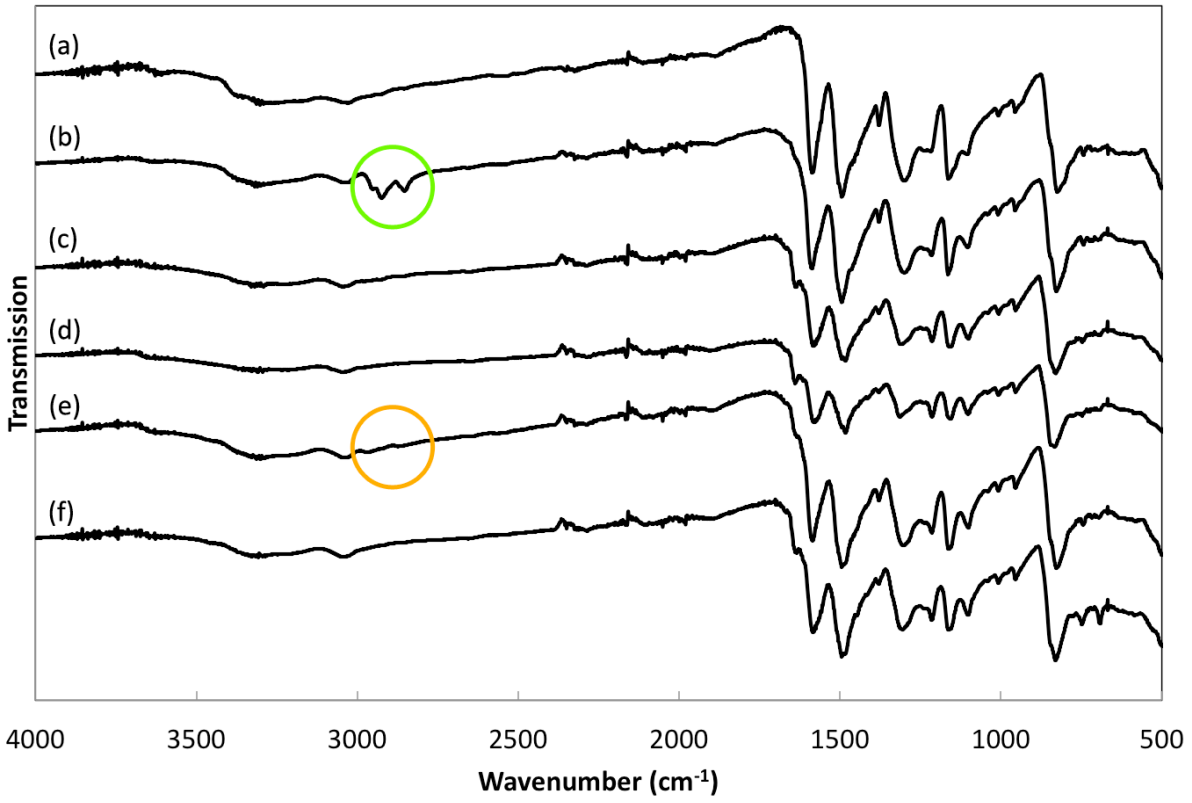

Figure 12. FT-IR-ATR spectra of polyaniline emeraldine base (a) polyaniline functionalized with hexylamine (b), diethylamine (c), triethylamine (d), pyrrolidine (e) and aniline (f). Green highlight for aliphatic peaks of hexylamine chain. Orange highlight for aliphatic peaks of pyrrolidine ring.

These peaks are not observed in the functionalized polyaniline samples, likely due to the low concentration of tri-substituted rings in comparison to the number of disubstituted rings in the

polyaniline structure. Work by Stejskal on brominated polyanilines demonstrate that even in highly substituted polyanilines, the corresponding 1,2,4-trisubstituted peak is still relatively weak in comparison to the main polyaniline peaks[98]. In the case of the aniline substituted derivative, weak signals are observed at 750 cm^{-1} and 690 cm^{-1} which are characteristic of monosubstituted aromatic rings, which would result from the addition of aniline to the backbone.

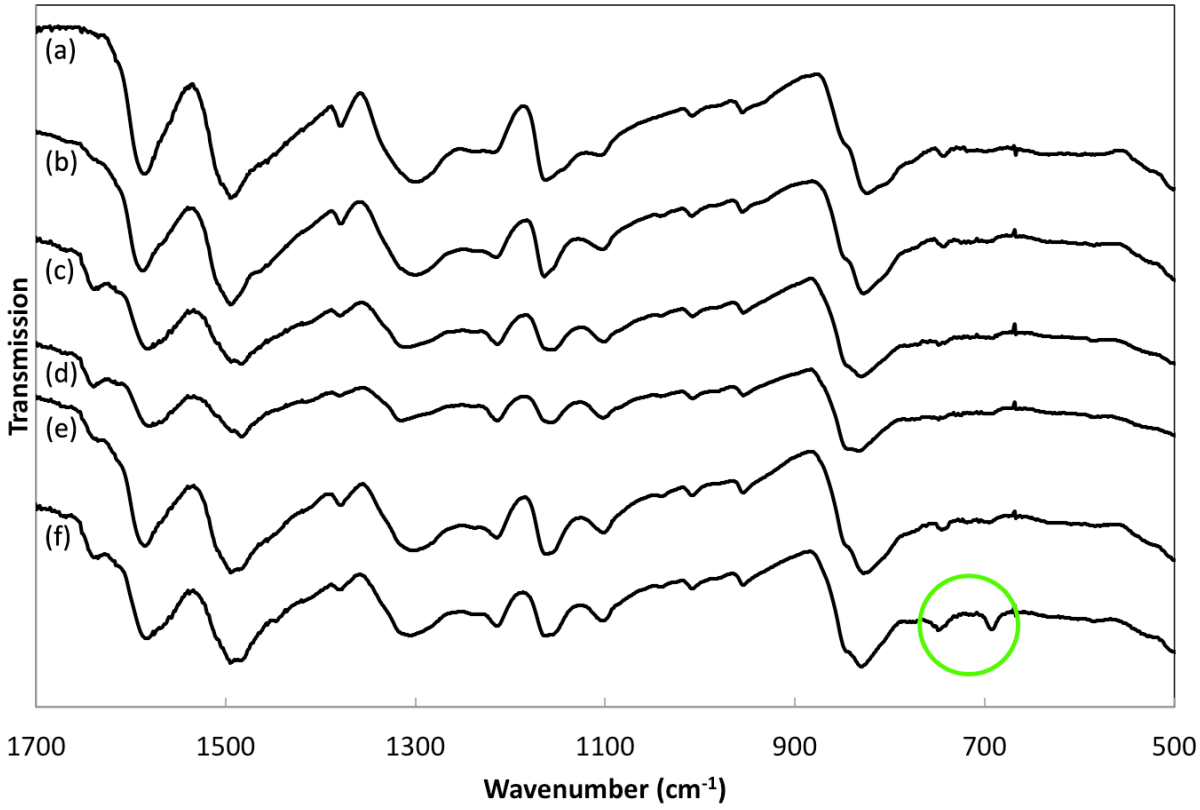

Figure 13. FT-IR-ATR spectra of polyaniline emeraldine base (a) polyaniline functionalized with hexylamine (b), diethylamine (c), triethylamine (d), pyrrolidine (e) and aniline (f) from 1700-500 cm^{-1} for clarification of aromatic stretching peaks. Green highlight for monosubstitued aromatic ring stretching in aniline functionalized polyaniline.

NMR Spectroscopy

Nuclear magnetic resonance (NMR) spectroscopy is a powerful tool for chemists looking to elucidate molecular structures and investigate the electronic environments of specific atoms. It can be used to interrogate the structure of small molecules as well as polymers, providing

information on pendant functional groups, monomer linkages and chain end groups[129]. A variety of NMR spectroscopy techniques are available to analyze various materials but all operate on the same principles. NMR spectroscopy utilizes a frequency specific pulsed radio wave to interact with the quantum mechanical magnetic spins of atoms[120]. Atoms or isotopes of atoms that contain unpaired magnetic spins, such as ^{1}H, ^{13}C, ^{15}N and ^{31}P, are influenced by the magnetic portion of the applied electromagnetic radio wave[130]. The frequency of the field is chosen to match the rotational frequency of the atom, leading to resonance and alignment of the atomic spin with applied field.

A broad frequency pulse is applied perpendicular to the original field resulting in a reorientation of the atoms and a shift in the total magnetic moment produced by their rotation, which is picked up by the detector[131]. When this pulse ends the atoms undergo a relaxation process in which they return to alignment with the initial field, thus the signal recorded by the detector diminishes. The recorded signal can be processed using a Fourier transform to produce a spectrum with peaks corresponding to the frequency and intensity of the excited nuclei[120].

The differentiation in chemical environments results from the influence of electrons on the overall magnetic moment of the atom[129]. The orbiting of electrons about the atomic nucleus produces a small magnetic field that affects the overall magnetic moment of the atom, in effect shielding it from the applied field and altering the resonant frequency of the nucleus. These shifts in resonant frequency describe the types of electronic interactions between atoms occurring in the molecule and can be assigned to specific types of functional groups or chemical environments[129]. From this information, a clear picture of a compound's chemical structure can be obtained making NMR spectroscopy a powerful characterization tool.

In the case of the substituted polyanilines, NMR spectroscopy was used to confirm the presence of the added amines through the presence of protons matching the amine substituents. Since the strength of signals in the NMR spectra are related to the concentration of the target nucleus, the low solubility of polyaniline in organics solvents made obtaining solution state NMR spectra difficult, but comparison of the parent polymer and substituted polymer shows the presence of new signals (Figure 14). The aliphatic side chains can be characterized by the presence of peaks in the 0.9-2.0 ppm, indicating that the proton nuclei are well shielded by the adjacent carbon atoms. The protons nearest the amine nitrogen will be slightly more deshielded as the more electronegative nitrogen atom draws some of the electron density away from the proton nucleus.

The NMR signals for the parent polymer appear in the 6.5-7.5 ppm range associated with the deshielded aromatic protons. The slight differences in peak position for each of the distinct aromatic proton environments leads to peak overlap forming a single broader, complex peak. The smaller peaks visible further downfield from this main aromatic signal are likely polymer chain end-groups or small defects created during the oxidation process such as aldehydes, or amides. The sharp singlet peaks appearing at 2.5 ppm and 3.3 ppm belong to the solvent DMSO and water, respectively. Proton transfer between the substrate and the solvent is a common phenomenon leading to the observed solvent signal, and polyaniline has been shown to retain some adsorbed water despite being subjected to oven drying[132,133].

The aniline functionalized sample does not show any of the aliphatic proton peaks, instead displaying a secondary aromatic peak at 6.5 ppm, and a broad singlet at 5.0 ppm that may belong to the now secondary amine proton of the bonded aniline. Amine protons can be quite labile, easily exchanging with the deuterated solvent. In addition to this facile exchange, the

signal of amine protons is sensitive to a variety of factors including solvent, temperature and concentration. The greater degree of substitution of the aniline functionalized polyaniline compared to some of the other aliphatic amine functionalized may be partly responsible for the observation of this peak, but certainly other factors may be at play.

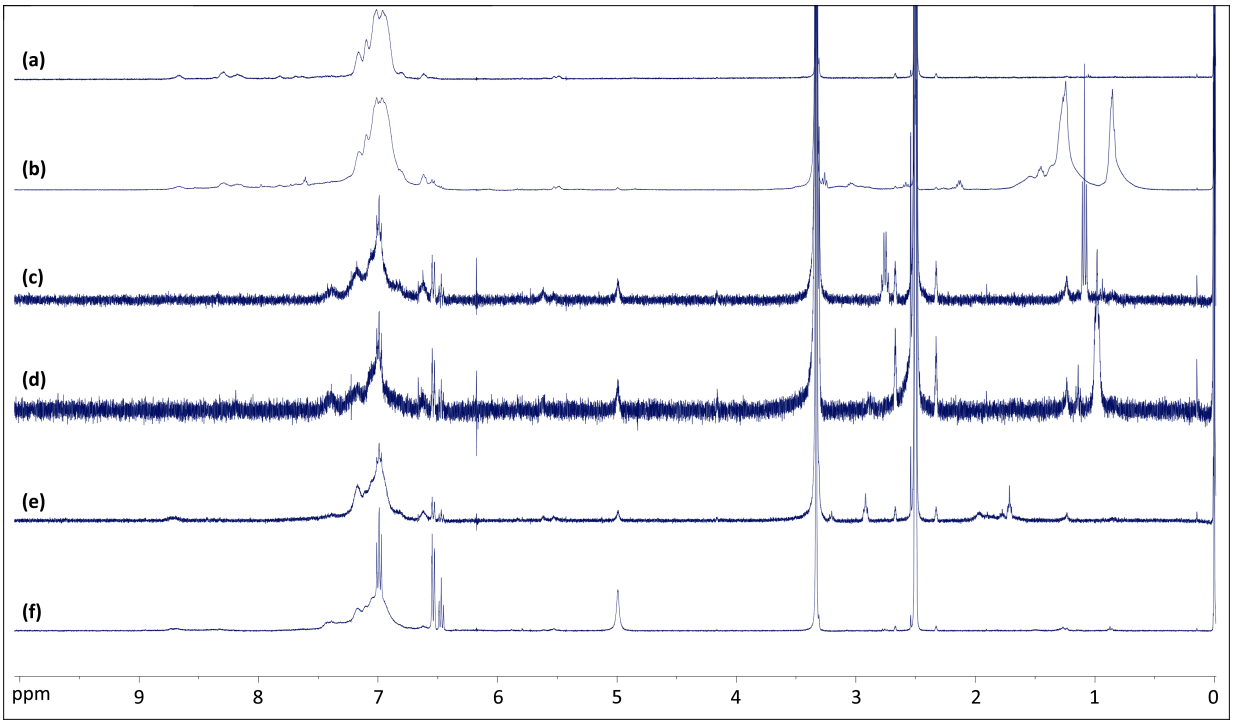

Figure 14. ^{1}H NMR spectra in d_6-DMSO of polyaniline emeraldine base (a), and derivatives prepared with hexylamine (b), diethylamine (c), triethylamine (d), pyrrolidine (e) and aniline (f).

2.4. Summary

The above work describes the first concerted investigation into the production of amine-substituted polyanilines by reductive addition. The pernigraniline base was synthesized by an aqueous oxidation procedure that retained polymer morphology, unlike previously reported methods. Reaction yields ranged from 2-40% depending on the amine being added and the reaction conditions employed. The addition of amines was found to proceed in organic solvents as well as water, although the use of organic solvents led to significant erosion of the morphology. Reaction yields were also increased with increasing temperature, but again at the

expense of the pre-established morphology. The ideal conditions for yield and morphology retention was determined to be one half equivalent of amine in water at room temperature for 24 hrs.

The reaction conditions are easily scalable to produce bulk quantities of amine-functionalized polymer, previously only achieved through electrochemical synthesis. Steric effects appeared to play a significant factor in the formation of the final product, as evidenced by the low yields in the bulky diethylamine and triethylamine. The reaction was also improved by increased concentrations of the amine nucleophile as well as higher reaction temperature but at the expense of preserving the polymer's nanoscale morphology. FT-IR and NMR spectroscopy were useful tools in characterizing the oxidation state of the polymer as well as confirming the presence of the added amines. Overall, the synthesis of amine functionalized polyanilines can be easily achieved post-polymerization through a reductive-addition pathway with minimal degradation of preformed morphological features.

3. Investigation into the Reaction Kinetics of the Reductive Addition of Amines to Polyaniline

From the results of the amine functionalization of bulk polyaniline, it appears that the structure of the amine nucleophile plays a role in the formation of the desired product. In order to further understand the fundamental forces at work, the effect of steric and electronic factors were investigated by examining reaction kinetics.

3.1. Introduction

Chemical thermodynamics is the fundamental starting point for the discussion of how chemical reactions take place, and determining the products formed. The thermodynamics of a reaction describe the relative stabilities of chemical compounds and the energy barriers required to transition from one molecular state to another. The stability of a compound is generally related to the internal energy of the molecule. Compounds with strained bonds, crowded atoms or unfavorable electronic interactions have a higher internal energy[134]. This energy is the driving force for a chemical reaction, as the structure will shift or bonds will break or form to produce a lower energy state. Of two species in a reaction, the one with the lowest energy is said to be thermodynamically stable. Ideally, the desired product of a reaction is more thermodynamically stable than the reactants. This is rarely the case however, and many products are less stable than their reactants. If the energy barrier associated with the reverse reaction is high enough, the conversion of the products back to the reactants is slow enough to be considered negligible[135].

This brings up an important aspect to discussing the thermodynamics of a reaction: time. One of the key assumptions when discussing the stability of products and reactants and the equilibrium between the two is that these transformations occur on an infinite time scale[134]. The principle of microscopic reversibility states that every incremental change along the energy pathway between a reactant and a product is reversible[136]. This concept is important when considering the equilibrium of a reaction, since given enough time some portion of the products may undergo the reverse process to reform the reactants. The height of the energy barrier between the two states influences the ease with which they can interconvert.

Most researchers however, do not have an infinite amount of time with which to conduct a reaction. Here is where the concept of chemical kinetics comes into play. Kinetics describes the rate at which a product is forming, and the kinetic product of a reaction is the product that forms the fastest, even if it is not the most stable[133]. In an efficient and ideal reaction, the kinetic and thermodynamic products are the same. The most stable product is the one that forms the fastest, and the product with the lowest energy has the smallest energy barrier. Sadly, this is rarely the case. The kinetic and thermodynamic products are often in competition with one another, and undesired products result from side reactions that either have a lower energy barrier to form, or are more stable than the desired product.

Examination of the structure of all products formed in a reaction, in conjunction with the ration in which they form can provide important information on the types of reactions occurring and which products are the thermodynamic products and which are the kinetic products. By determining what compounds are forming and how, a mechanism of the reaction process can be devised and the possible rate-determining steps of the reaction can be identified.

Rate-determining, or rate-limiting, steps represent the highest energy transition in a reaction and are responsible for governing the overall rate for the reaction[137]. Investigations of the reaction kinetics ultimately only provide information on this single step, even if other transition states and intermediates are formed. Identifying the rate-determining step of a reaction does provide crucial insight into the pathway of a reaction, and can be used to refine and elucidate the mechanism by which products form.

The rate of a reaction is dependent on the concentration of reactants and is measured by the change in the concentration of reactants over time (1).

$$rate = \frac{-d[R]}{dt} = \frac{d[P]}{dt} \tag{1}$$

The degree of dependence on concentration is described by the order of the reaction with respect to a given substance[136]. If the rate is dependent on multiple reagents, then the overall order is the sum of the individual orders. Here [R] is the concentration of the reactant species, [P] is the concentration of the product expressed as the derivative of that concentration with respect to time *t*. In a first order reaction:

$$A \rightarrow P$$

$$rate = -\frac{d[A]}{dt} = k[A] \tag{2}$$

$$[A] = [A]_o e^{-kt} \tag{3}$$

$$\ln\left(\frac{[A]}{[A]_o}\right) = -kt \tag{4}$$

Reagent A is converted to product P in a single step and the rate of this transformation can be expressed as the change in concentration of A with respect to time, which is equivalent to the product of the rate constant, *k*, and the concentration of A. The concentration of A, [A], at any point in the reaction can be expressed through the integrated rate law (3), where $[A]_o$ is the initial concentration of the reactant[133,136]. This equation can be easily rearranged to (4) and when

graphed, the slope of the line expresses the reaction rate. When a reaction with two reagents, here A and B, which change in concentration over time, is considered in a similar manner the analysis quickly becomes much more complicated. The integrated rate law for this second order reaction (6) cannot be easily visualized and solving for the rate constant requires significant computation[133].

$$A + B \rightarrow P$$

$$rate = -\frac{d[A]}{dt} = k[A][B] \tag{5}$$

$$\ln\left(\frac{[B][A]_o}{[A][B]_o}\right) = k([B]_o - [A]_o)t \tag{6}$$

The challenges of analyzing a second order reaction can be simplified greatly employing a significant excess of one reagent. By increasing the concentration of one reagent, assume reagent B, to large excess it can be assumed that the portion consumed by reaction with A is very small in comparison to the total concentration. This allows the concentration [B] to be approximated as the initial concentration $[B]_o$, and thus treated as independent of time making the reaction only dependent on [A], or 'pseudo' first order[136,138]. With this assumption made the rate law can be expressed as

$$rate = -\frac{d[A]}{dt} = k[A][B]_o = k'[A]$$

$$where\ k' = k[B]_o$$

$$[A] = [A]_o e^{-k[B]_o t} \tag{7}$$

$$\frac{\ln\left(\frac{[A]}{[A]_o}\right)}{[B]_o} = -kt \tag{8}$$

Note the resemblance of (7) to the first order integrated rate law (3). A similar rearrangement to (8) allows a plot of $\frac{\ln\left(\frac{[A]}{[A]_o}\right)}{[B]_o}$ vs time expressing the reaction rate as the slope of the line[137].

3.1.1. Electronic Effects

In the 1930s, researcher Louis Hammett studied the hydrolysis of benzoic esters and the effect substituents on the ring had on the rate of hydrolysis[139-141]. From the data collected, Hammett was able to establish a relationship between the equilibrium constants of a reaction and its substituted analogue through the use of a substituent coefficient. It was also observed that this relationship could be extended to the ratio of reaction rates as well, taking the form of (9)[138]. The reaction rates k_X and k_H represent the substituted and unsubstituted reactions, respectively, are proportional to the product of a substituent constant, σ, and a reaction constant, ρ[139].

$$\log\left(\frac{k_X}{k_H}\right) = \sigma_X \rho \tag{9}$$

The value of the substituent constant, σ, reflects the electronic nature of a given substituent as compared to hydrogen. Positive σ values indicate a substituent is electron withdrawing and describes nitro, cyano, carbonyl and halogen groups. Negative σ values are given to electron donating substituents like amino, alkoxy, hydroxyl and alkyl groups. The magnitude of the σ value indicates the strength of the donating or withdrawing influence. The position of the substituent on the aromatic ring also influences the electronic impact of the substituent due to differences in resonance structures. To account for this, σ values are listed as either σ_p for substituents in the para position, or σ_m for substituents in the meta position. Values for these parameters have been experimentally determined and reported in the literature for a wide variety of functional groups[140].

The reaction constant, ρ, for the reaction being studied provides information on the sensitivity of the reaction to substituents as well as the type of charge built up during the rate-determining step, if any. Plotting the obtained values of log (k_X/k_H) against the σ value of the substituent typically yields a linear relationship. The slope of this line is ρ, and much like σ the both the value and magnitude of ρ provide information on the reaction. A ρ value of zero indicates that the reaction is unaffected by the presence of substituents, while $\rho < 0$ indicates that the reaction is susceptible to electronic influence and that the rate determining step creates a build-up of positive charge. If $\rho > 0$, the rate limiting step is affected by the presence of substituents and a negative charge is developed. Whether ρ is greater or less than one merely describes if the reaction is more or less sensitive than the hydrolysis of benzoic esters.

While Hammett plots typically yield a linear relationship between reaction rates and electronic influence, special cases occur in which the relationship is non-linear. Non-linearity is associated with a change in the rate-determining step of a reaction, due to the electronic influences of a substituent[142]. If a transition state is building a strong positive charge, then an electron-withdrawing group might destabilize that transition state enough that it is no longer favorable, pushing the reaction down a different path[133,142]. While less common than linear free-energy relationships, non-linear Hammett plots present and intriguing case for mechanistic study[143-145].

The construction of a Hammett plot for a given reaction provides a valuable tool for the investigating the kinetics of a reaction beyond the influence of concentrations. Determination of the type and magnitude of charge formed in the rate-determining step allows proposed mechanisms to be evaluated and refined.

3.1.2. Steric Effects

Analogous to the experiments conducted by Hammett on the electronic effects of substituents, R. W. Taft investigated the steric effect of substituents on the acid and base catalyzed hydrolysis and esterification of benzoates[146,147]. Taft designated the steric parameter for substituents E_s, with the reference substituent being the CH_3 methyl group, as opposed to hydrogen, although some tables of values will be shifted to make hydrogen the reference[145,148,149].

Table 5. A comparison of substituent steric parameters defined by Taft (E_S), Dubois (E_S'), Hall (δE_S) and Dienys (E_N).

Substituent	**$-E_s$**	**$-E_s'$**	**$-\delta E_s$**	**$-E_N$**
Me	0.00	0.00	0.02	0.07
Et	0.07	0.06	0.11	0.36
nPr	0.36	0.31		0.37
iPr	0.47	0.48	0.28	0.93
nBu	0.39	0.31	0.12	0.40
tBu	1.54	1.48		1.74
$(Et)_2$	1.98	2.00	0.72	1.98
n-C_5H_{11}	0.40	0.31		
$(CH_2)_4$			0.14	0.51
Ph		2.31		
$(Et)_3$		5.29	1.93	

While the substituent constants derived by Taft provided a starting place for quantifying the steric effect, his methodology left room for improvement. The work of Shorter and Charton aimed to separate the steric effects of substituents from the polar and resonance effects that were

unaccounted for in Taft's work, providing new sets of corrected steric constants[149-151]. Dubois and coworkers performed an overhaul on the determination of steric parameters to present a new set of constants, E_s', determined through a more rigorous approach[152].

The consideration of Taft and Dubois steric parameters gives a good estimation of steric presence in the case of substituents about carbon. Work by Charton and DeTar, among others extended the use of Taft's parameters to oxygen and nitrogen based systems[153-157]. A comparison of various steric parameters are listed in Table 5**,** While the Taft and Dubois parameters are fairly close in value, they are defined for substituents bonded to carbon. The parameters calculated by Hall and Dienys are for aliphatic amines, the former showing much less resemblance to Dubois' values than the latter[151,155,158].

3.1.3. Substrate Scope

To adequately probe the influence of steric factors and electronics on the reductive-addition reaction, a variety of amines architectures were chosen to represent a balanced range of steric or inductive contributions. The structures of the amines can be seen in Figure 15, and the corresponding E_s and σ in Table 6. The aliphatic amines were chosen to provide steric differentiation amongst primary amines (hexylamine vs isopropylamine vs tert-butylamine), as well as differentiation between primary, secondary, and tertiary amines (hexylamine vs diethylamine vs triethylamine). The aromatic amines cover an even spread of electron withdrawing (4-bromo, 4-cyano) and electron donating (4-amino, 4-methoxy) groups, while aniline serves as the unsubstituted comparison. Steric parameters for the aromatic substituents are not included due to the para-position on the ring. This position allows for electron influence through the conjugated pi bonds but is far enough from the reaction center that the substituents do not provide any steric influence, regardless of size.

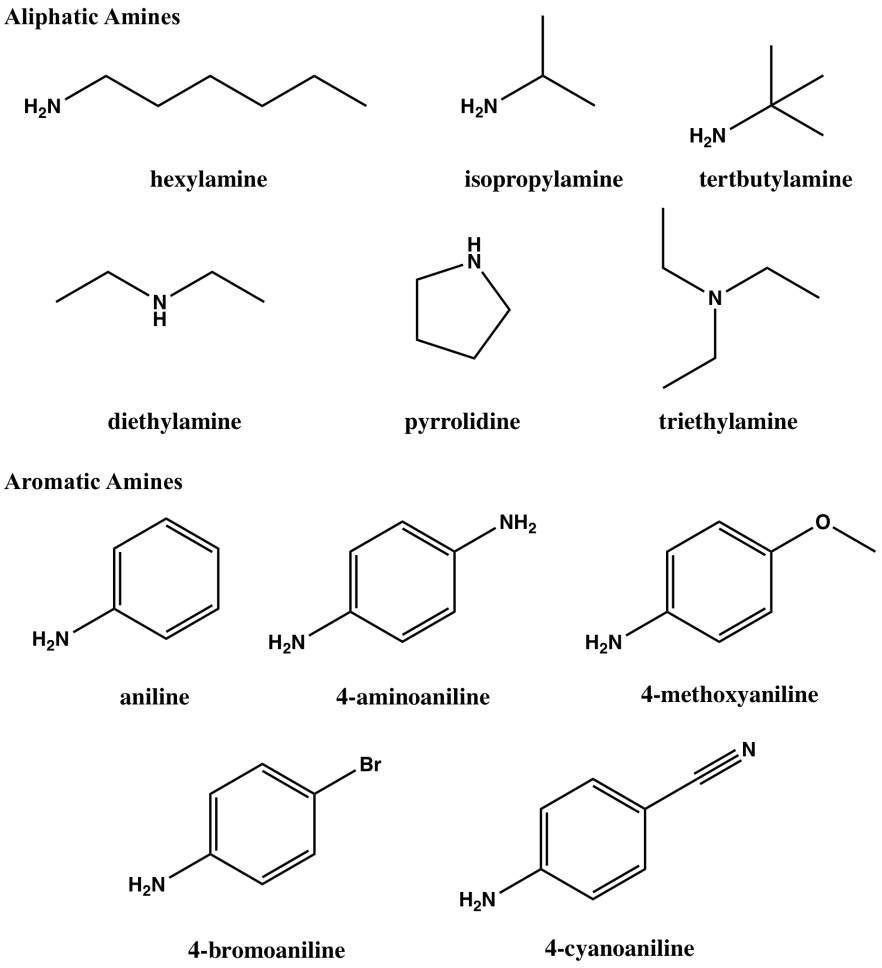

Figure 15. Substrate scope of aliphatic and aromatic amines utilized to investigate the effects of sterics and electronics on reaction rate.

Table 6. Amine nucleophiles and their associated steric or electronic parameters.

Amine	$-E_N$	Amine	σ
Hexylamine	0.40	4-aminoaniline	-0.66
Isopropylamine	0.93	4-methoxyaniline	-0.27
Tert-butylamine	1.74	Aniline	0.00
Diethylamine	1.98	4-bromoaniline	0.23
Pyrrolidine	0.51	4-cyanoaniline	0.66
Triethylamine	5.29		

3.2. Experimental Methods

All chemicals were obtained from Alpha Aesar, with the exception of hexylamine and triethylamine which were obtained from Acros Organics, and used without further purification. Solvents used were all of reagent grade purity. All water used was deionized to a resistivity of 18 MΩm.

Polyaniline pernigraniline base was synthesized using the methods previously described. UV-Visible spectroscopy was conducted on a Shimadzu 2450 spectrometer using 1 cm quartz cuvettes and NMP as the solvent for both samples and reference due to it's strong solvating ability and it's use as a spectroscopic solvent for other polyaniline studies in the literature. Kinetic data was obtained by measuring the absorbance at 535 nm in one second intervals for 30 min. Full spectrum data was collected from 200-1100 nm. Three dimensional structures were produced using MolView software.

3.2.1. Determining Pernigraniline Extinction Coefficient

A stock solution of polyaniline emeraldine base was prepared by dissolving approximately 5.00 mg of the emeraldine base 10.0 mL of NMP, which was vigorously stirred for 30 min to ensure dissolution. The sample was then filtered through a PTFE syringe filter with a pore size of 0.45 μm to remove any undissolved polymer.

The final concentration of the solution was determined from the Beer-Lambert equation using the molar extinction coefficient of 2.2×10^4 reported in the literature[159]. The emeraldine stock solution was converted to the pernigraniline base by the addition of one equivalent of ammonium persulfate, and allowed to equilibrate. This stock solution was then diluted to various concentrations with neat NMP, and UV-visible spectra recorded over 1100-200 nm. Absorbance

values at 535 nm were also collected. The molar extinction coefficient for the pernigraniline base at 535 nm was obtained using the collected data and applying the Beer-Lambert equation.

3.2.2. Sample Preparation and Determination of Reaction Rates

Solutions of pernigraniline base were prepared similarly to those for calibration. A solution of pernigraniline base, 3.0 mL of approximately 7.85×10^{-5} M, was added to the cuvette and mixed with 0.02 mL of the neat amine if they were a liquid, or a 10.0 mM solution of amine in NMP if it was a solid.

The cuvette was placed in the spectrometer and the absorbance at 535 nm was collected continuously for 30 min. Using the Beer-Lambert Law and the molar absorptivity coefficient obtained for the pernigraniline absorption peak at 535 nm, the obtained absorbance values were converted to concentration. The concentration values were then plotted as a function of time using pseudo-first order kinetics and Equation 8, $\frac{\ln\left(\frac{[A]}{[A]_o}\right)}{[B]_o} = -kt$, so that the slope of the plotted data would provide the reaction rate. Linear trendlines were fit to the plotted data and used to determine the values of k. The rate constant for each reaction was determined as the average of three trials.

3.3. Results and Discussion

Both steric and electronic influences were observed in the reaction of amines with the pernigraniline base. Information gathered from the investigation of electronic effects provided additional insight into the mechanism of reaction.

3.3.1. Determination of Pernigraniline Extinction Coefficient

Work by MacDiarmid and Epstein demonstrated that the conversion of polyaniline emeraldine base to the pernigraniline base occurred in a single step on the molecular level with

no observable intermediates[19]. This is advantageous for the kinetic study of reactions involving the pernigraniline base, as monitoring of the peak absorbance at 535 nm can be used to quantitatively measure the change in concentration of pernigraniline over time. The underlying principle for quantitative UV-Visible spectroscopy is the application of the equations developed by Beer and Lambert relating the transmission of light through a solution to the concentration of the solution and path length of the beam through it. The principles of Beer's Law (10) and Lambert's Law (11) are often used in conjunction and from the initial equation (12), the streamlined Beer-Lambert equation (13) can be derived[160].

$$\ln\frac{I_o}{I_T} = k''c \tag{10}$$

$$\ln\frac{I_o}{I_T} = k'b \tag{11}$$

$$-\ln\frac{I_T}{I_o} = \sigma \times N \times b \tag{12}$$

$$\mathrm{A} = \varepsilon bc \tag{13}$$

In Beer's and Lambert's Laws the ratio of intensities of the incident light (I_o) to the light transmitted through the sample (I_T) is proportional to the concentration (c) of absorbing molecules in solution or the path length (b) of the light through the sample, respectively. The terms k′ and k″ are proportionality constants. Combining these concepts into Equation 12 relates the ratio of intensities to the cross sectional area of the absorbing molecule (σ), the number density of absorbing molecules (N) and the path length. Conversion of the natural logarithm to a base 10 logarithm gives the term $\log(I_o/I_T)$ which is defined as the absorbance (A). The number density of absorbing molecules is easily converted to concentration through Avogadro's number and the remaining numerical terms are combined with σ to form the molar absorptivity coefficient (ε) also known as the molar extinction coefficient[159]. As most UV-Vis spectrometers collect absorbance values as a function of wavelength, the Beer-Lambert equation is extremely

useful for quantitatively determining concentrations of analyte in solution if the molar absorptivity coefficient is known, or determining the molar absorptivity coefficient for unknown compounds.

The molar absorptivity coefficients for polyaniline emeraldine base and leucoemeraldine base in NMP have been reported in the literature, but no values could be found for the pernigraniline base[159,161]. Since the molar absorptivity coefficient is wavelength dependent, the value of the coefficient is typically reported at the peak absorbance wavelength for a compound. Pernigraniline displays three characteristic peaks at 272, 320, and 535 nm. The peak of interest to this work is the 535 nm peak corresponding to the Peierls' gap transition, indicative of the polaron-excited state unique to the pernigraniline form of the polymer.

Samples at five concentrations were prepared to provide adequate data points to fit to the Beer-Lambert equation. Figure 16 displays the spectra of pernigraniline in increasing concentrations, while Figure 17 shows the plot of absorbance vs concentration. The data fits a linear trend quite nicely, giving a slope value of 1.56×10^4 $M^{-1}cm^{-1}$, with an R^2 value of 0.99. The obtained value for the molar extinction coefficient fits well with the observed decrease in peak intensity compared with a sample of emeraldine base at the same concentration.

Based upon the concentrations of the pernigraniline solutions and the difficulty in the addition of equimolar volumes of the amine, a pseudo-first order approach was adopted for the analysis of the reaction kinetics utilizing a large excess of amine

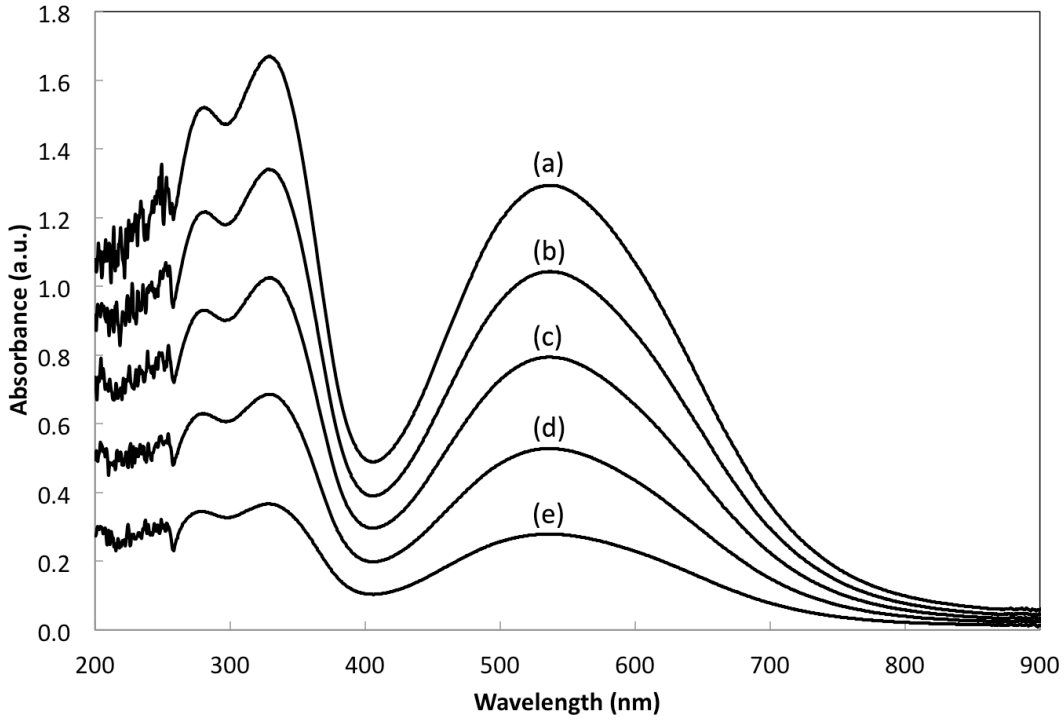

Figure 16. UV-Visible spectra of pernigraniline base decreasing in concentration from 8.30×10^{-5} M (a), to 6.64×10^{-5} M (b), 4.98×10^{-5} M (c), 3.32×10^{-5} M (d), and 1.66×10^{-5} M (e).

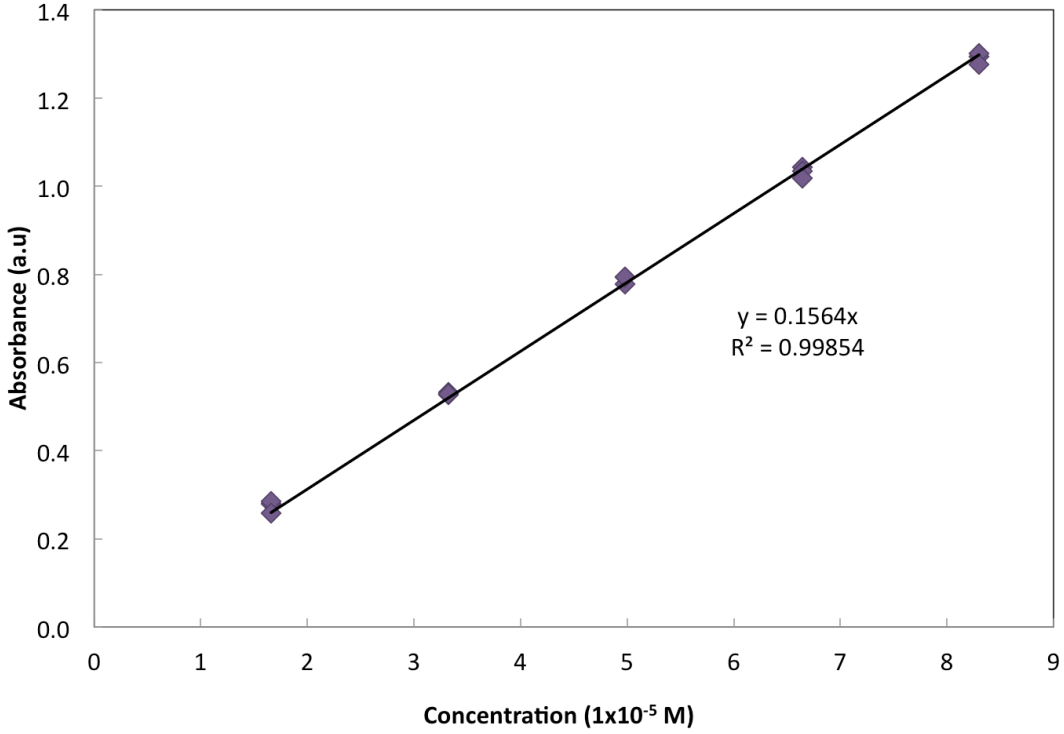

Figure 17. Plot of absorbance at 535 nm vs concentration of pernigraniline base in solution.

3.3.2. Steric Effects

There are several key points to take away from the data aggregated in Table 5. The first is that increasing the linear chain length beyond three carbons appears to have little effect on the steric bulk around the amine. As additional carbons are added, the steric hindrance imposed by the bonded hydrogen atoms is located further and further from the reactive site and thus the impact on steric bulk becomes negligible for the purposes discussed here. From this and for the sake of comparison to other substituents, n-hexylamine can be considered analogous to n-butylamine. The second is that the cyclic pyrrolidine is significantly less hindered than its acyclic counterpart diethylamine. The conformational strain of the ring serves to pin the adjacent hydrogen back and away from the nitrogen center. The third is a general order for increasing steric size: hexylamine < pyrrolidine < isopropylamine < tertbutylamine < diethylamine < triethylamine. From the collected kinetic data, summarized in Table 7, the observed order of reactivity is hexylamine > pyrrolidine > diethylamine > isopropylamine > tertbutylamine ≈ triethylamine. This differs from the expected order based on steric size alone, indicating that additional factors are at work.

Table 7. Rate constants for the reaction of aliphatic amines with pernigraniline base in NMP.

Amine	**Reaction rate constant (10^{-4} M^{-1} s^{-1})**
Hexylamine	3.55 ± 0.07
Isopropylamine	2.12 ± 0.09
Tertbutylamine	1.43 ± 0.08
Diethylamine	2.02 ± 0.04
Pyrrolidine	2.80 ± 0.16
Triethylamine	1.46 ± 0.06

Since the observed results do not strictly follow a trend in increasing steric bulk, it's necessary to consider other factors such as basicity and nucleophilicity. The basicity of amines is a subject of much research interest due to their common usage in a variety of organic reactions[153,162-167]. Measurements of gas phase basicity for aliphatic amines demonstrate that increasing the number and size of alkyl groups increases the basicity affording the following ranking for the substrate scope in this work: triethylamine > diethylamine > tertbutylamine > isopropylamine > hexylamine[166]. Solvation of the amine however changes this order through the influence of the thermodynamic properties of the solvent by interaction with the alkyl groups[167]. In an aqueous system, the observed trend in basicity is secondary > tertiary > primary. The discussion of basicity in non-aqueous solvents becomes more complicated still, and is heavily dependent on the solvent chosen.

Another parameter to discuss is the nucleophilicity of the amines, which can be measured in a variety of solvents and described by the Swain-Scott parameter, *n*. For aliphatic amines in water the order of nucleophilicity is pyrrolidine > diethylamine > hexylamine (approximated by n-butylamine) > triethylamine ≈ isopropylamine > tertbutylamine[157]. Other studies on the nucleophilicity of amines show this order holds true in DMSO and acetonitrile as well[168,169]. Correlations by Hall and coworkers demonstrated a relationship between the nucleophilicity and basicity of various classes of aliphatic amines, with the result that nucleophilicity is more greatly impacted by steric hindrance around the nitrogen than basicty[153].

3.3.3. Electronic Effects

The selected amines underwent reactions with pernigraniline as expected, displaying a gradual decrease in peak intensity at 535 nm over time, with the exception of phenylenediamine (PDA). PDA is readily oxidized to a diiminoquinoid state and exposure to the pernigraniline base

resulted in rapid reduction of the polymer backbone and a swift darkening of the solution to a reddish brown color. Sequential scans of the reaction from 300-700nm reveal the formation of a large additional peak around 430 nm and almost complete disappearance of the polyaniline excitation peak. Neat solutions of PDA also demonstrate the color change from a pale yellow to deep reddish brown upon standing, indicating the formation of by-products as a result of oxidation by oxygen. As the formation of byproducts also interferes with the spectroscopic monitoring of the reaction, PDA was omitted from the study. The other amines were much slower to react but it was observed that the presence of the electron donating methoxy group increased the reaction rate while the electron withdrawing groups slowed it. A good linear fit was observed when the values of $\log(k_X/k_H)$ were plotted against the respective σ_X values (Figure 18).

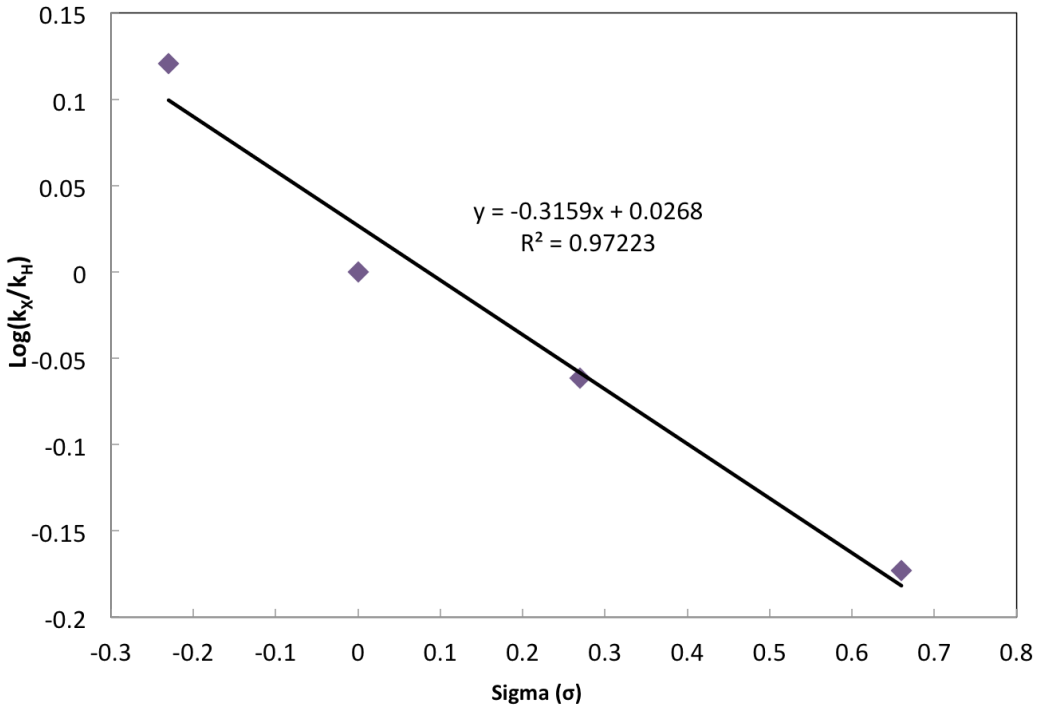

Figure 18. Hammett plot for the reductive-addition of substituted anilines to pernigraniline base.

As mentioned previously, the substituent constant, σ, describes the electronic influence of a substituent independent of the reaction studied while the reaction constant, ρ, is unique to each reaction . The value of ρ indicates the sensitivity of a reaction to substituents and the type of charge, if any, built up during the rate-determining step. From the linear fit of the kinetic data, ρ for the reaction was calculated to be -0.32. This indicates that the reaction is susceptible to the electronic influence of substituents, but more importantly, the reaction builds a positive charge during the rate-determining step.

Previously proposed mechanisms for the reductive addition of nucleophiles to polyaniline are often lacking in detail and generally describe an overall reaction scheme, but are thought to proceed through an aromatic addition/elimination mechanism[93,95]. A more detailed proposal suggests that a hydrogen atom from the incoming amine undergoes hydrogen bonding with the adjacent imine unit of the polymer[170]. This is followed by addition to the 3-position relative to that imine. Electrons are pushed to back towards the imine, which grabs a proton and becomes an amine. The remaining imine removes the proton at the site of addition to restore aromaticity to the ring while being converted to the amine.

The information gained from the investigation of the reaction kinetics serves to further inform the mechanism proposed by Mattes and coworkers[170]. Previous schemes describe the attack of the nucleophile occurring on the quinoid ring after protonation of both imine units[93,95]. Since these nucleophiles are generally sulfuric acids or derivatives, protonation of the imines is likely to occur first and facilitates conversion of the quinoid to the substituted benzoid structure. In the case of amine nucleophiles, there is not a large excess of protons to promote initial protonation of the imine units.

In Mattes' mechanism, hydrogen bonding occurs between the incoming amine and one of the imine units, followed by concerted addition to the 3-position relative to the imine that removes the proton[170]. A preliminary model of this proposed transition state shows significant deformation to the polyaniline ring structure to form the six membered intermediate (Figure 19A,C). The hydrogen bonding between the imine and the incoming amine would, however, facilitate nucleophilic attack at the closer 2-position on the quinoid ring, but without the concerted hydrogen transfer. Modeling of this transition state shows that addition of the amine to the 2-position creates much less strain in the ring systems, which would lower the overall energy of the transition state (Figure 19 B,D). The experimentally determined ρ value points to a build up of positive charge during the rate determining step, something not observed in the previously proposed mechanism[170]. It is rather more likely that hydrogen bonding between the incoming amine and imine leads to addition at the closer 2-position on the ring, pushing electrons to the more distant imine which picks up a proton from solution (Figure 20). This proton could be from an adjacent polyaniline chain or from the solvent. The result of this step is the formation of a quaternary cationic amine species, which would account for the build-up of positive charge and make addition of the nucleophile the rate-determining step. Hydrogen bonding from the imine would additionally stabilize the positively charged intermediate. Following the addition of the nucleophile, the proton at the attack site is removed and the reestablishment of aromaticity converts the imine to an amine as it picks up a proton.

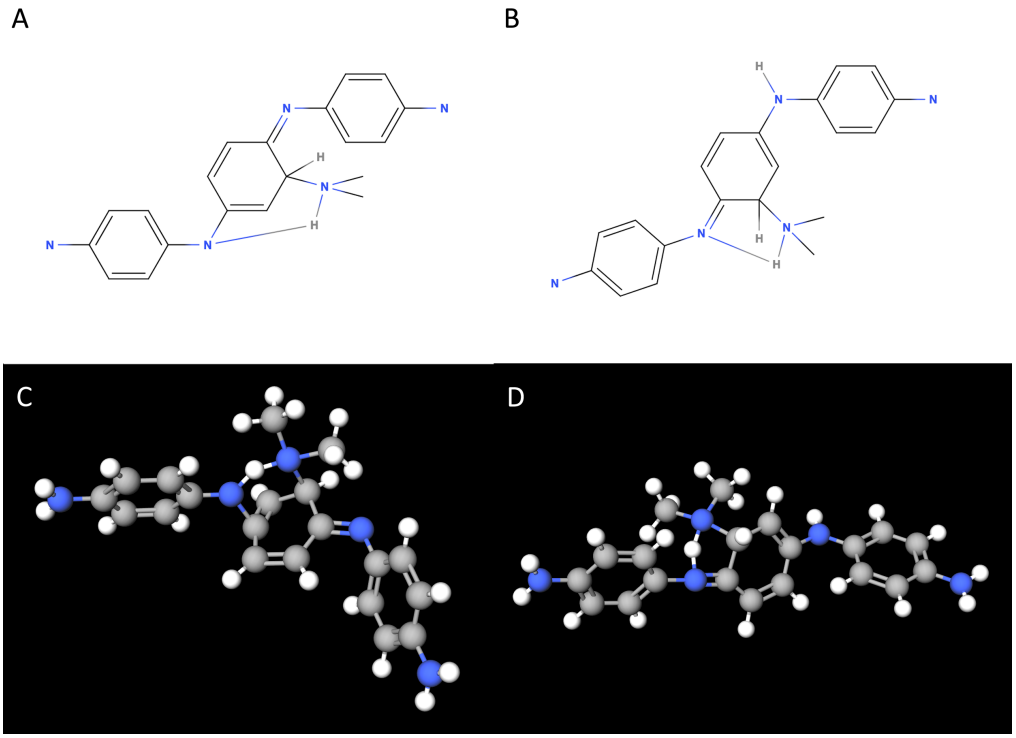

Figure 19. Structures (A,B) and conformational models (C,D) for the transition state of the amine nucleophile addition to the 3-position (A,C) and the 2-position (B,D).

If hydrogen bonding helps stabilize the charged intermediate then it might explain why the more sterically hindered amines, including diethylamine have slower reaction rates. Larger substituents or a more highly substituted nitrogen atom may disrupt or prevent hydrogen bonding from the imine. In the case of triethylamine, there is no hydrogen available for bonding at all. This may lead to a more unstable transition state and reformation of the diiminoquinoid structure could eject the added amine before the ring structure can be reduced.

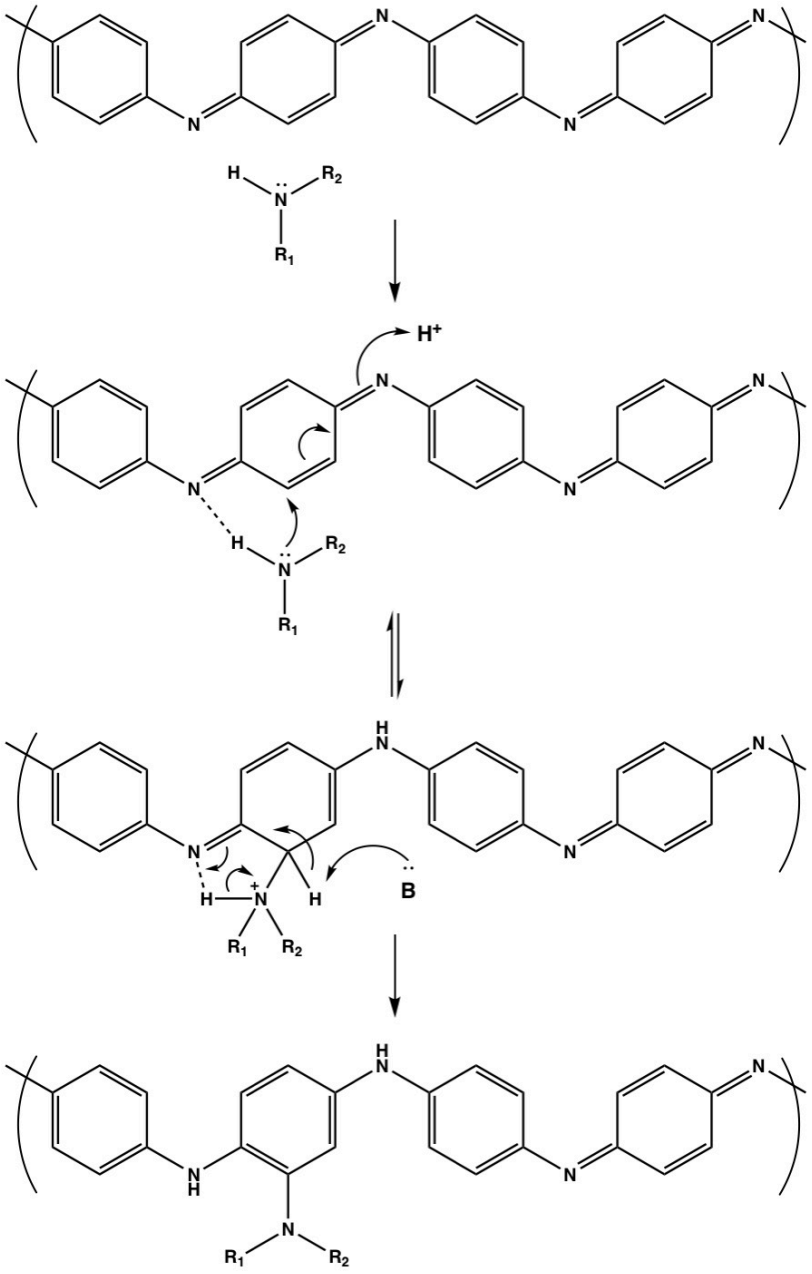

Figure 20. Proposed mechanism for the addition of amines to the quinoid unit of polyaniline.

3.4. Summary

The kinetic investigation of the reductive addition of amines to polyaniline provided excellent insight into the more fundamental aspects of the reaction. An unusual pattern of reactivity was observed in the aliphatic amines, as the more nucleophilic diethylamine exhibited extremely low reaction rates compared to even the sterically hindered primary amines.

The most informative results came from the construction of a Hammett plot for the reaction (Figure 18). The electron donating methoxy substituent increased reaction rate while the electron withdrawing bromo and cyano substituents slowed the reaction. The resulting negative ρ value for the reaction pointed at a build up of positive charge during the rate-determining step. This further elucidates previously proposed mechanisms that indicated a concerted addition and proton transfer, resulting in no net build up of charge. The results obtained here would indicate that addition of the nucleophile and the transfer of protons occur in separate steps which would explain the build up of positive charge indicated by the observed substituent effects.

4. Application of Amine Functionalized Polyanilines for Chemical Crosslinking

Amines are incredibly versatile functional groups, capable of undergoing a variety of transformations and reactions. Additionally, amines are essential components of many materials including amino acids and proteins, polymers such as nylons, and in curing agents for epoxy based resins. Due to their versatility, the addition of amines to polyaniline presents an opportunity for the incorporation of polyaniline into many new applications. In the following chapter, the use of polyamine-functionalized polyanilines will be explored for the chemical crosslinking of polyaniline as well as in conjunction with epoxy resins.

4.1. Introduction

Crosslinking is the joining of polymer chains together to form an extended network and can be accomplished through a variety of methods dependent on the material and the end properties desired. The cross-linking density of a polymer network describes the number of linkages between polymer chains and has some influence over the final properties of the network[171-173]. As the crosslinking density increases, the polymer chains lose their molecular mobility and slowly transform from gel or rubber like materials, to harder, stiffer and more brittle materials. Additionally, the addition of crosslinks to a polymer reduces the solubility to the point that it is no longer soluble but instead swells with the uptake of solvent. Highly cross-linked materials also display improved thermal and mechanical properties, making them ideal materials for composite applications as matrix materials and coatings[174-176].

The crosslinking of polyaniline has received considerable research interest due to the unique redox and doping properties of the polymer and the desire to improve the physical and electrical properties[177,178]. Crosslinking has been investigated as a way to dramatically increase the surface area of the polymer, affording polyaniline based chemical sensors with greater sensitivity and analyte uptake[179-181]. It has also been demonstrated that crosslinking polyaniline can improve the electrochemical performance by improving ordering of the material and facilitating interactions between chains[182-184].

4.1.1. Methods of Crosslinking

There are several main types of cross-linked polymeric materials based on how the polymer chains are joined: covalently cross-linked, ionically cross-linked, and physically cross-linked. In covalently cross-linked polymers, a linker possessing two or more functional groups that can undergo a reaction with a specific functional group on the polymer joins the chains[185]. Possibly the most common example of this type of crosslinking is epoxy resins, where the epoxide groups at the end of the polymer chains are reacted with a curing agent containing multiple amine groups per molecule[186]. The amine adds to the epoxide ring, opening it and forming a covalent bond between the resin polymer and the linker. This process occurs at each amine on the cross linker, attaching to a different polymer chain and converting the liquid epoxy polymers into a rigid network.

Polyaniline can be covalently cross-linked through several approaches including substitution of the amine nitrogens, thermally induced self-crosslinking, and the incorporation of reactive co-monomers that can be further reacted to form crosslinks. The process of forming covalent crosslinks is generally irreversible, providing greater chemical stability to the network.

This stability often comes at the cost of a more involved synthetic procedure, or a loss in conductivity or doping capability.

Ionic crosslinking follows a similar process but rather than forming chemical bonds between the linker and polymer, the network is held together by the electronic pairing of positive and negative charges. Polymers containing anionic groups, like alginate, which has COO^- groups, can be cross-linked by cations like Ca^{2+}, which can coordinate with multiple anions.

Polyaniline is a cationic polymer in the doped state and as such can be ionically cross-linked, and doped, by polyanionic compounds such as phytic acid[180,187]. Ionically crosslinked polyaniline is a common method of producing hydrogels as the charged nature of the linked and doped polymer facilitates the uptake and retention of water. Polyaniline hydrogels can be easily prepared and exhibit good electrical performance. The weakness of these materials is that changes in pH can disrupt the ionic bonds holding the network together, leading to collapse of the three dimensional structure.

Physically cross-linked systems rely on entanglement of the polymer chains to form the network. For this to occur the polymer must exceed a critical molecular weight, M_e, to become entangled and varies with the polymer system[188]. Weaker molecular forces such as van der Walls and hydrogen bonding interactions hold the polymer network together and crosslinking is considered thermally reversible. The addition of heat promotes motion of the polymer chains allowing entanglements to resolve themselves.

The gelation of concentrated polyaniline solutions has been attributed to physical crosslinking of the polymer chains and exhibit viscoelastic behaviors characteristic of polymer networks[189,190]. Hydrogen bonding is thought to play a key role in the physical cross-linking of polyaniline, occurring between the lone pair electrons of the imine units and the amine-bound

hydrogens. A sharp decrease in the gelation of polyaniline solutions was observed when the polymer was reduced to the leucoemeraldine state, as the imine units were converted amines and fewer hydrogen-bonding partners were available[191]. The crystalline regions of the emeraldine base are also considered to be physical crosslink points as multiple chains ordered together readily engage in hydrogen bonding, providing entanglement points between the more disordered amorphous sections[192].

The following work will investigate the reductive addition of amines as a potential tool for the formation of cross-linked polyaniline networks. The use of polyamines should provide the opportunity to form networks of cross-linked polyaniline as well as polyamine derivatives that can act as curing agents for epoxy based resins.

4.2. Experimental Methods

Polyaniline pernigraniline base was prepared following methods described previously. All chemicals were obtained from Alpha Aesar and used without further purification. Solvents used were all of reagent grade purity. All water used was deionized to a resistivity of 18 MΩm.

FT-IR data was collected using a Thermo Nicolette 6700 FT-IR with SmartOrbit ATR attachment, with a resolution of 2.0 cm^{-1}. Scanning electron microscopy was carried out on a JEOL microscope with samples mounted on carbon tape and gold coated for improved image resolution. DSC was carried out on a TA DSC Q2000 using standard aluminum pans; at a heating rate of 10 ºC/min from 20 ºC to 300 ºC. TGA was conducted on a TA TGA Q500 with a platinum pan under a nitrogen atmosphere at a heating rate of 20 ºC/min from 20 ºC to 800 ºC. Analysis of the obtained thermal data was carried out using TA Universal Analysis 2000 software.

4.2.1. Synthesis of Covalently Cross-linked Polyanilines

Polyaniline pernigraniline base (250 mg, 0.6936 mmol) was added to a 20 mL glass vial followed by 1.4 mL NMP . The resulting slurry was mixed vigorously for several minutes to ensure even wetting of the sample and formation of a smooth paste. Ethylenediamine (0.20 mL, 0.3468 mmol) was added, the vial sealed tightly, and the mixture was again mixed vigorously for several minutes to mix the amine crosslinkers into the sample. The mixture was left undisturbed for 72 hrs at which point the surface had taken on a matte finish and residue on the walls of the vial had turned a dark blue. The sample was then soaked in NMP for changing the solvent every hour until no additional polymer was extracted. The NMP was then removed by soaking the sample in deionized water, changing every hour for an additional 6 hours. Samples were then freeze dried for several days to remove residual water while preserving the open structure of the network.

As NMP was removed from the samples a noticeable contraction in the sample size was observed. During drying the reduction in sample size was minimal, and overall the final sample was 60-70% of its original size.

4.2.2. Synthesis of Polyamine Functionalized Polyanilines

Polyaniline pernigraniline base (100.00 mg, 0.277 mmol) was measured into a 20 mL glass vial followed by 5.0 mL of water and a small magnetic stir bar. The mixture was placed under medium magnetic stirring, followed by addition of 4 equivalents of the amine. The vial was capped and left to stir at room temperature for 24 hrs.

The reaction was quenched by the addition of 10 mL of cold deionized water and products were collected by filtration, rinsing with copious amounts of water to remove excess

amines. The collected powders were dried under vacuum at 40 ºC. In the case of dodecylamine, the solubility in water was quite poor and methanol was used as the reaction solvent instead.

4.2.3. Curing of Epoxy Resins by Polyamine Functionalized Polyanilines

The amine functionalized polyanilines were finely ground with a mortar and pestle after drying to improve dispersion in epoxy. The functionalized polyanilines were mixed with neat epoxy in a 10 wt % ratio of polyaniline to epoxy. Curing of the resin was evaluated by dynamic scanning calorimetry (DSC), at a heating rate of 10 ºC/min.

4.2.4. Substrate Scope

Amines were chosen to investigate the effect of chain length in aliphatic diamines, polyamines vs diamines and branched polyamines vs linear. The structures of the amines can be seen in Figure 21. Aliphatic diamines were used to examine the impact of increasing carbon chain length. Aliphatic polyamines were chosen to examine in influence of secondary amines and branching on reactivity.

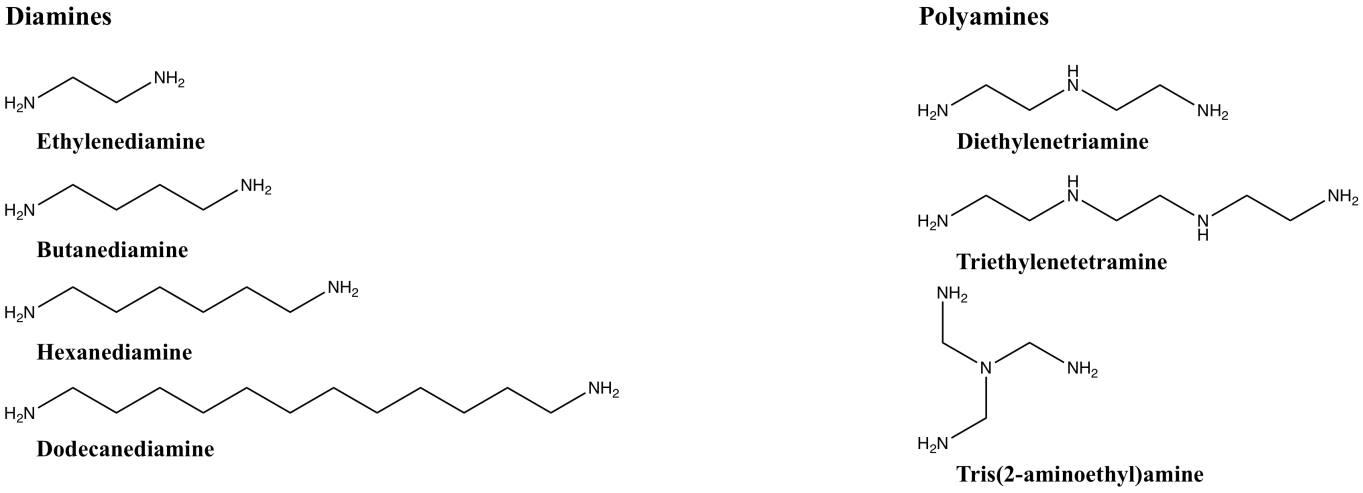

Figure 21. Substrate scope of amines used for the cross-linking of polyanilines.

4.3. Results and Discussion

Polyaniline could be self cross-linked through the use of sub-stoichiometric amounts of diamines and polyamines with concentrated pernigraniline to produce a rigid freestanding material. Treatment of the pernigraniline base with excess diamines and polyamines under more dilute conditions produced derivatized polymers that underwent exothermic curing reactions with epoxy resin. The analysis of these cross-linked materials is discussed below.

4.3.1. FT-IR Characterization of Polyaniline Functionalized or Cross-Linked by Polyamines

Fourier transform infrared spectroscopy is a useful tool for the characterization of polyaniline derivatives and cross-linked polyaniline networks. The presence of aliphatic crosslinking agents can be detected through the characteristic C-H stretching, and the degree of substitution can be evaluated by the ratio of quinoid and benzoid stretching intensities.

4.3.1.i. Polyamine Cross-linked Polyanilines

FT-IR spectra of the cross-linked samples showed a significant and consistent reduction in the quinoid band at 1590 cm^{-1} compared to the parent polyaniline (Figure 22). The ratio of peak intensities for the benzoid and quinoid characteristic bands further confirms the reduction of the quinoid bands by the added amine moieties (Table 8). While the quinoid units of the polymer were successfully reduced the extent of reduction was quite significant, with the overall oxidation state closer to that of the leucoemeraldine state than that of the desired emeraldine. The terminal amine groups present on the polyamines undergo addition to the polymer backbone forming secondary amine moieties. As seen in the initial small molecule studies on the reductive addition of amines to polyaniline, secondary amines are also capable of undergoing the reductive addition reaction. With the high concentration of reactants necessary to form a solid cross-linked

sample, it is possible that after undergoing the initial addition, the newly formed secondary amines could undergo additional reductive additions that would result in the loss of more quinoid units and the observed Q/B ratios.

The presence of the cross-linker can be observed as two peaks around 2900 cm^{-1} corresponding to the sp^3 C-H stretching in the aliphatic chains. These peaks are more distinguishable for the longer chain cross-linkers like hexanediamine and dodecyldiamine as they contain more aliphatic C-H bonds than the smaller cross-linkers. The peaks of ethanediamine and tris(2-aminoethyl)amine are difficult to distinguish clearly, but match up with the frequency of the more intense peaks of butanediamine and hexanediamine.

The extent of reaction seems to be consistent across the various linking agents, indicating that the length or branching of the structure had little impact on the reactivity of the primary amine moieties. While tris(2-aminoethyl)amine does contain the additional tertiary amine group at the core of the structure, the low reactivity observed in the reaction of polyaniline with triethylamine makes it mainly a non-factor in the reaction here.

Table 8. Q/B Ratios of FT-IR Peak Intensities for amine crosslinked polyanilines.

Sample	Q/B Ratio
PAn EB	0.877
PAn PB	0.943
PAn EDA XL	0.594
PAn BDA XL	0.597
PAn HDA XL	0.548
PAn TRIS XL	0.571

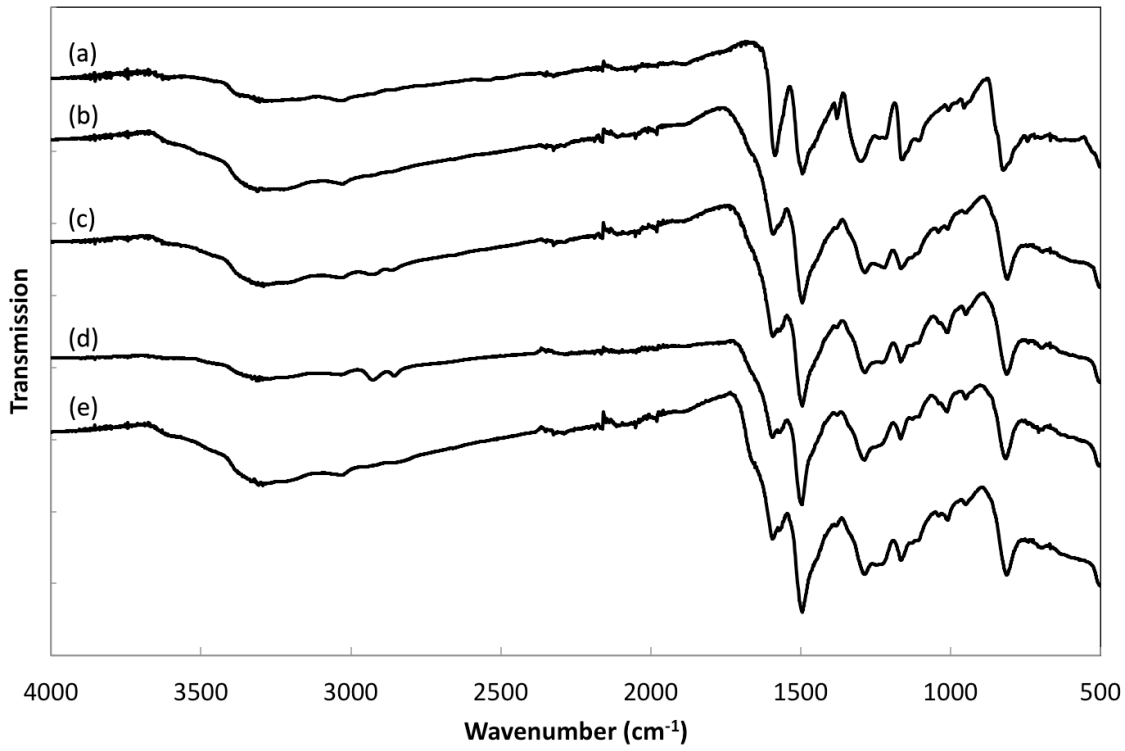

Figure 22. FT-IR-ATR spectra of polyaniline emeraldine base (a) and polyaniline crosslinked with EDA (b), BDA (c), HDA (d) and TRIS (e).

4.3.1.ii. Polyamine Functionalized Polyaniline

Much like the aliphatic monoamine functionalized and covalently cross-linked samples, the polyamine functionalized polyanilines displayed the characteristic C-H stretching peaks around 2900 cm^{-1} (Figure 23). The presence of these peaks confirms addition of the small molecule amines to the backbone, along with the observed reduction in peak intensity for the characteristic quinoid band. Further confirmation of amine attachment is provided by the increasing intensity of the C-H stretching peaks corresponding to the increasing length of the aliphatic chain in the amines. The Q/B peak intensity ratio also provides confirmation of the successful reduction of the polymer backbone (Table 9). The derivatized polyanilines showed a greater degree of reduction in the quinoid peak compared to the parent polyaniline, similar to the cross-linked polyaniline samples (Table 8) although not as extensive. The additional reduction of

quinoid groups likely results from additional reactions carried out by the terminal primary amine groups present, but the more dilute conditions help mitigate some of those additional reactions.

There would also appear to be a slight trend in the Q/B ratios for the aliphatic diamines, indicating differences in reactivity for the different amines. The product undergoes less reduction as the chain length increases for EDA, BDA and HDA which points to a lowering of the degree of substitution as the chain gets longer. The trend breaks down with DDA however, as it shows a degree of reduction similar to that of BDA. There also does not appear to be a consistent trend or pattern of reactivity amongst the aliphatic polyamines, nor does one category of amines seem to be significantly more reactive than the other.

Table 9. Q/B Ratios of FT-IR Peak Intensities for diamine and polyamine substituted polyanilines.

Sample	Q/B Ratio
PAn EB	0.877
PAn PB	0.943
PAn EDA	0.640
PAn BDA	0.653
PAn HDA	0.724
PAn DDA	0.650
PAn DETA	0.706
PAn TETA	0.713
PAn TRIS	0.628

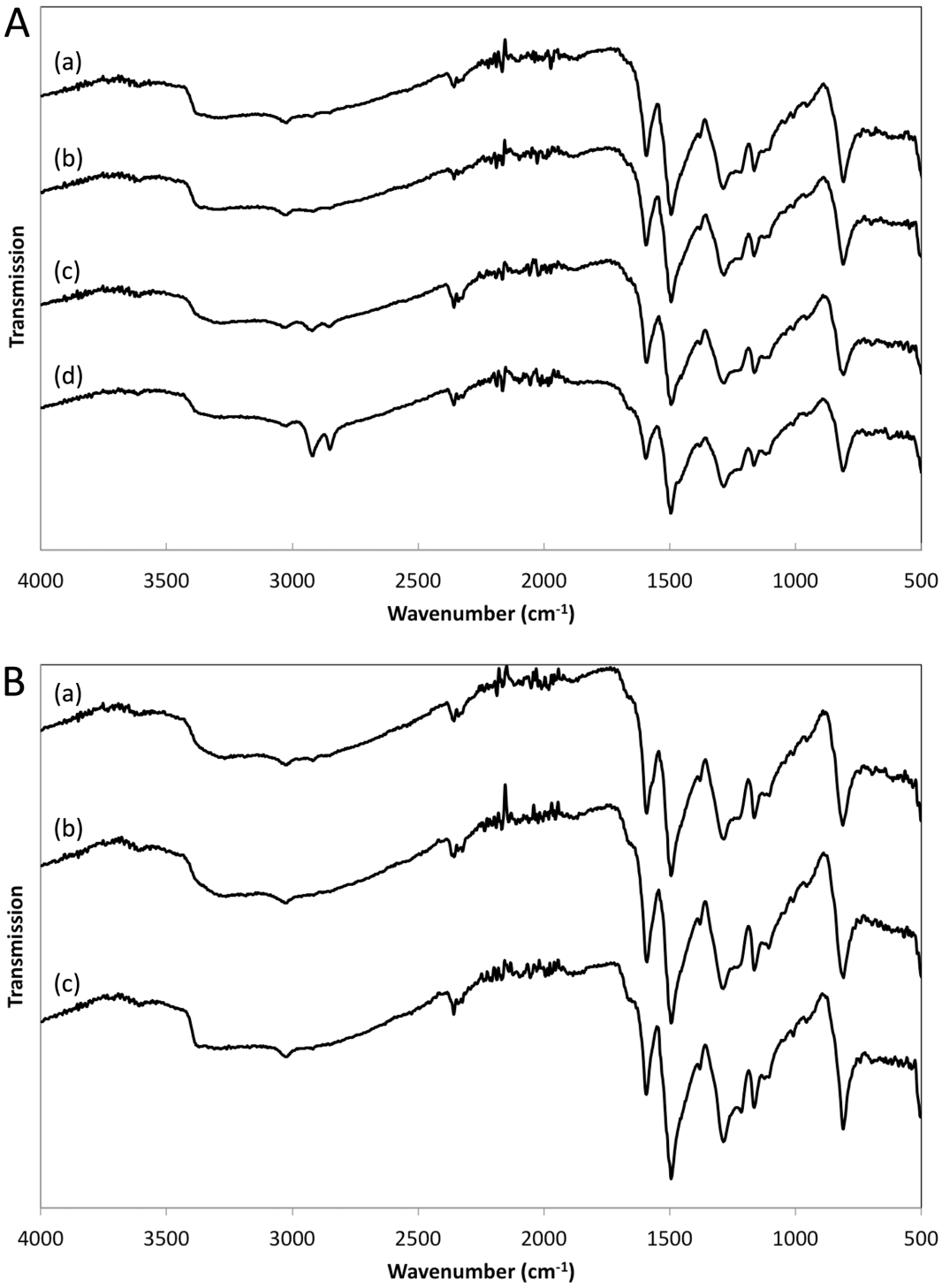

Figure 23. [A] FT-IR-ATR spectra of polyaniline functionalized with the diamine EDA (a), BDA (b), HDA (c) and DDA (d). [B] FT-IR-ATR spectra of polyaniline functionalized with the polyamine DETA (a), TETA (b) and TRIS (c).

4.3.2. Scanning Electron Microscopy

Samples of the cross-linked polyaniline samples demonstrated good retention of the nanofibrillar morphology when polyaniline nanofibers were used as the starting material Figure 24. Despite being a good solvent for polyaniline, the high ratio of polyaniline to NMP leads to swelling of the polymer chains in the sample rather than dissolution and morphology loss. While distinct pores were not obviously visible, channel like openings could be seen between clusters of nanofibers. There did not appear to be a correlation between the size of these channels and the length of the cross linker.

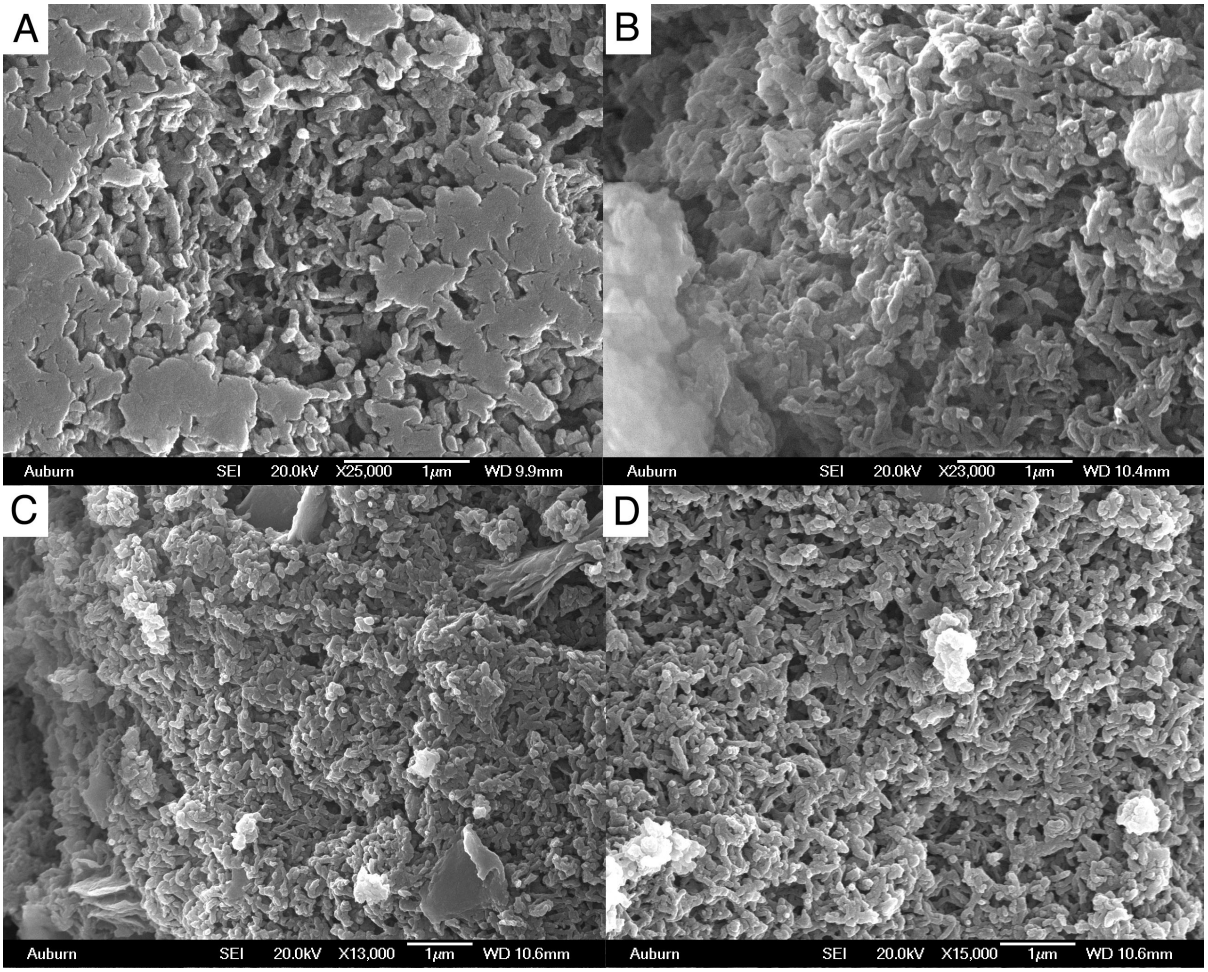

Figure 24. SEM images of polyaniline cross-linked with (a) EDA, (b) BDA, (c) HDA, and (d) TRIS.

4.3.3 Thermogravimetric Analysis

Thermogravimetric analysis (TGA) provides information on the thermal stability of materials by measuring weight loss as a function of temperature. Comparisons of degradation onset and mass retention provide key information on the improvement in thermal stability between materials.

4.3.3.i. Polyamine Cross-linked Polyanilines

Crosslinking of polymers typically leads to an increase in thermal stability as potentially reactive groups are often converted into more stable linkages and there are more intermolecular forces stabilizing the polymer chains.

All of the cross-linked polymer samples showed an improvement in thermal stability compared to pure polyaniline. Not only did the cross-linked samples exhibit a higher temperature for the onset of degradation, but also retained a significant portion of the initial mass (Figure 25), although the residual material was observed to be a grey ash indicating complete degradation of the polymer. It was observed that increasing the distance between active nitrogen atoms led to a decrease in the mass retained. Polyaniline cross-linked with ethylenediamine retained close to 60% of its overall mass at 800 ºC, dropping to 50% for the butanediamine cross-linked, and 40% for hexanediamine cross-linked polyaniline.

The slight decrease in mass at lower temperatures is likely the loss of adsorbed water and solvent from within the interior of the cross-linked sample. TGA of polyaniline films cast from NMP exhibit retention of solvent despite thorough washing and drying procedures, resulting from hydrogen bonding interactions between the solvent and polymer chain[131]. With the thickness of the cross-linked samples prepared here, the presence of residual solvent is highly likely.

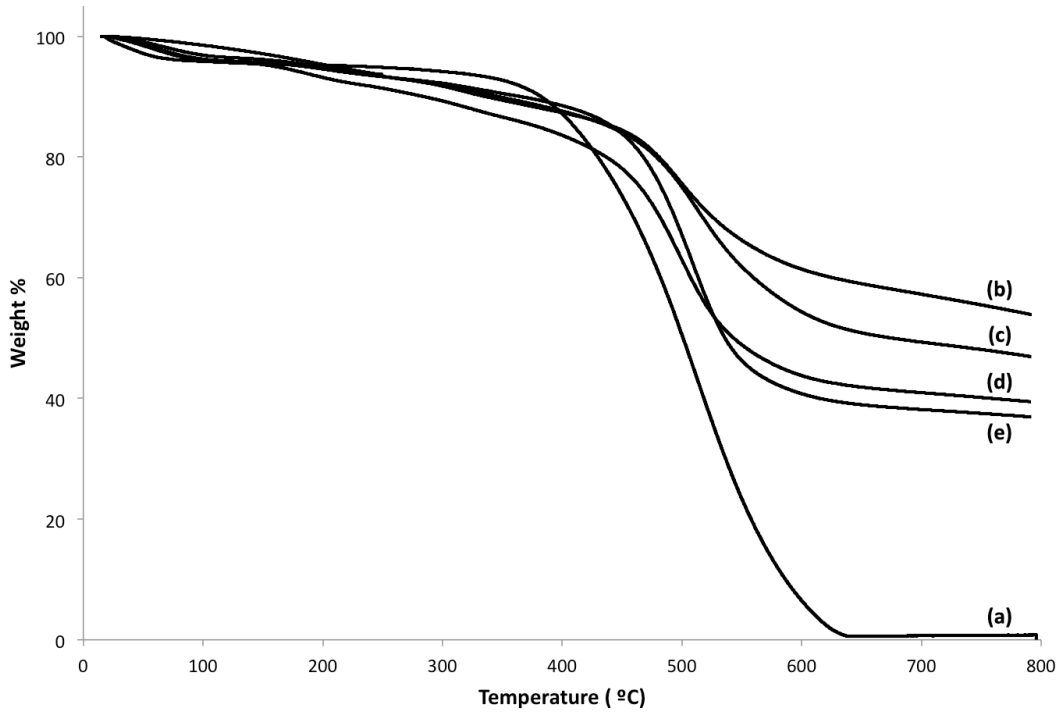

Figure 25. TGA analysis of polyaniline nanofibers (a) cross-linked with EDA (b), BDA (c), HDA (d), and TRIS (e).

The uncrosslinked polyaniline is stable up to 423 ºC, while the cross-linked samples ranged from 446-463 ºC as determined by the onset of degradation and mass loss. The onset values were extrapolated using a method similar to that reported in the literature[193]. Lines tangential to the TGA curve at 200 ºC and the temperature of peak degradation, as determined by the first derivative of the weight loss curve, were extrapolated and their intersection marked as the onset of degradation. This method provides a degree of consistency as the extrapolated onset temperature can vary widely dependent upon the position of the tangent points. Cross-linking of the polymer produced a modest increase in the onset of degradation of 20-40 ºC compared to the uncross-linked polyaniline. The branched amine TRIS produced the smallest improvement, while increases in chain length amongst the linear amines yielded slight increases in the onset temperature.

The mass retention of the cross-linked polymers followed the opposite trend however. As the length of the amine chain increased, the percentage of retained mass decreased despite the increasing degradation onset temperature. Shorter cross-linkers, like EDA, are less likely to bridge distant chains, instead forming crosslinks between adjacent sites. This would lead to clusters of highly cross-linked polymer chains while leaving other areas free or minimally cross-linked. These free sections would then exhibit decomposition similarly to the parent uncross-linked polymer, which is reflected in the lower onset temperature.

Table 10. Thermal stability of cross-linked polyanilines assessed by the onset temperature of degradation.

Sample	Derivative Weight Loss Peak (ºC)	Extrapolated Degradation Onset (ºC)	Mass Retention at 800 ºC (%)
Polyaniline Emeraldine Base	510.75	423.14	0
Polyaniline x-EDA	498.32	454.88	54
Polyaniline x-BDA	513.37	455.75	47
Polyaniline x-HDA	509.18	462.23	37
Polyaniline x-TRIS	498.72	446.17	39

As these sections decompose, the clusters of highly cross-linked polymer chains would remain as evidenced by the higher mass retention. The longer cross-linkers, like HDA, are more likely to join disparate polymer chains than adjacent ones creating a more evenly distributed network structure with fewer uncross-linked sections. A more even cross-linking would account for the lower mass retention as well, since fewer heavily cross-linked sections would be present which are more likely to survive the heating process. The branched amine TRIS also displayed a

low mass retention, and coupled with the lower onset temperature would indicate poorer cross-linking performance compared to the linear diamines.

4.3.4. Dynamic Scanning Calorimetry of Epoxy Resin Cured with Functionalized Polyanilines

Calorimetry measures the flow of heat into or out of a sample, and is useful in measuring the energy associated with chemical reactions, such as crosslinking, and thermal transitions, such as melting and crystallization. The curing of epoxy resins can be easily measured using DSC as the reaction produces a large exothermic peak. By sweeping the temperature and measuring the energy released from the sample, the peak curing temperature of an epoxy-curing agent mixture can be obtained.

Unfunctionalized polyaniline displayed a broad, mildly exothermic peak at 180 ºC when mixed with the neat resin. This can be attributed to the reaction of the secondary amines in the benzoid sections of the polymer, as they have active hydrogens that can assist in facilitating the curing reaction. However, the diamine and polyamine functionalized samples do not display this broad peak, instead exhibiting sharp and well defined exothermic peaks at higher temperatures (Figure 26, Figure 27). The exception to this is the epoxy PAn DDA sample, which exhibited a slightly more defined peak than the emeraldine base but much less prominent than the other amines. This may indicate that there is an upper limit to the beneficial effects of an extended chain, after which it may actively hinder the reaction. The peak curing temperatures are summarized in Table 11, and show a general trend of decreasing curing temperature with increasing chain length. Functionalization with polyamines like TETA further lowered the curing temperature, and the linear polyamines displayed a lower curing temperature than the branched analogue.

Integration of the observed curing peaks in the DSC curves provides the reaction enthalpy for the curing of the resin. The reaction enthalpy is a measure of heat released during curing, primarily generated by the opening of the epoxide rings and the release of energy from the strained bond conformations[194]. The opening of the epoxide by the amine groups of the curing agent leads to the development of the polymer network and curing of the resin system. Thus the number of active amine groups and structure of the curing agent have an observable impact on the curing of the resin[195,196].

In the curing of epoxy resins by amine-functionalized polyanilines, the reaction enthalpy indicated a trend between the amine structure and the heat released in the curing reaction for both aliphatic diamines and aliphatic polyamines (Table 11). For the aliphatic diamines, a steady decrease in reaction enthalpy can be observed as the chain length between the amine centers increases. With the same number of active hydrogen atoms available, the change in enthalpy is a result of the structural differences. As the chain length increases the primary site of reaction is moved further from the polymer backbone, which contains other amine groups that may participate in the curing reaction or facilitate the curing of the resin. This increased separation from other reactive sites would reduce the overall activity of the curing agent and result in the observed decrease in reaction enthalpy.

The polyamine-functionalized samples also displayed variation in the curing enthalpy that can be related to structural differences. The linear polyamines, DETA and TETA, contain primary and secondary amine groups compared to TRIS, which contains primary amine moieties and a tertiary amine at the core. The DETA and TETA functionalized polyanilines displayed the greatest curing enthalpy of all the amine-functionalized samples tested, due to the greater number of reactive sites available. There was not a significant difference in reaction enthalpy between

the two samples however, despite the TETA sample containing an extra reactive amine site. Changing from the linear polyamines to the branched TRIS group resulted in a significant decrease in the enthalpy, on par with the longer diamine functionalized polyanilines. While the branched configuration contains the same number of active hydrogens, the tertiary amine at the core cannot participate in the curing reaction. This results in a larger separation between active amine sites, much like the longer diamines that display similar curing enthalpy values. The linear polyamines have active amine sites along the length of the structure, which is likely the source of their greater curing activity.

Table 11. Peak curing temperatures of epoxy - functionalized polyaniline composites.

Sample	Peak Curing Temperature (ºC)	Curing Enthalpy (J/g)
Polyaniline EB	179	29.75
Polyaniline EDA	218	59.71
Polyaniline BDA	211	48.18
Polyaniline HDA	211	36.01
Polyaniline DDA	174	35.15
Polyaniline DETA	190	71.30
Polyaniline TETA	193	69.86
Polyaniline TRIS	217	39.88

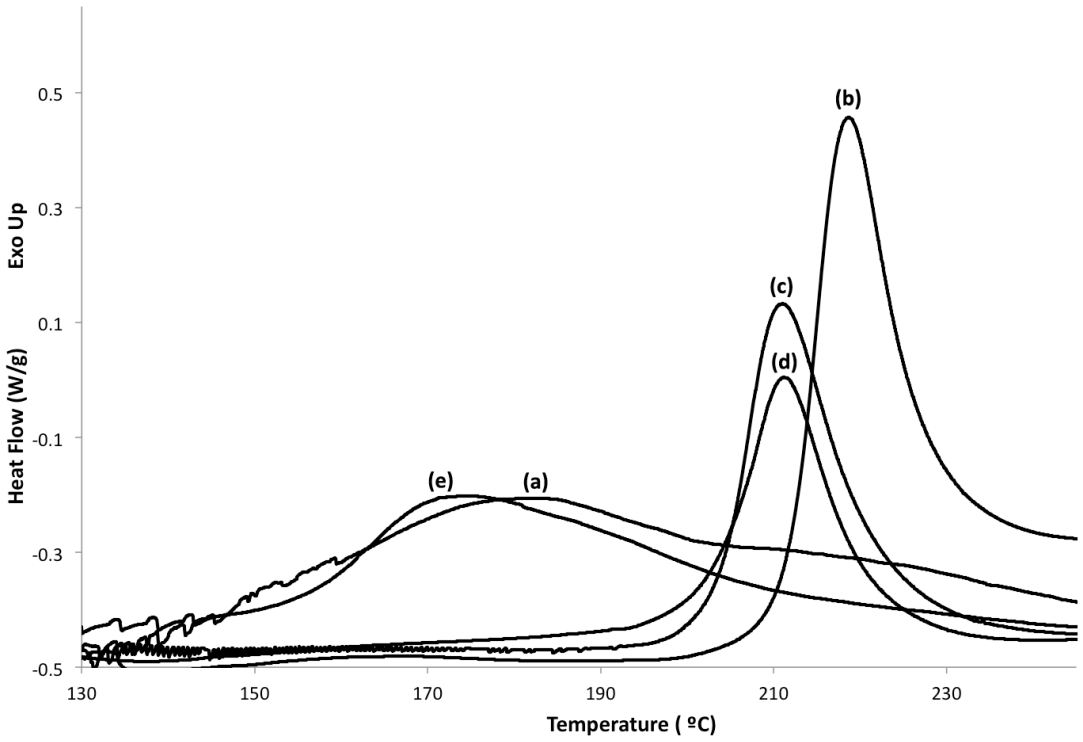

Figure 26. DSC curing curves for epoxy mixed with PAn EB (a), PAn EDA (b), PAn BDA (c), PAn HDA (d) and PAn DDA (e).

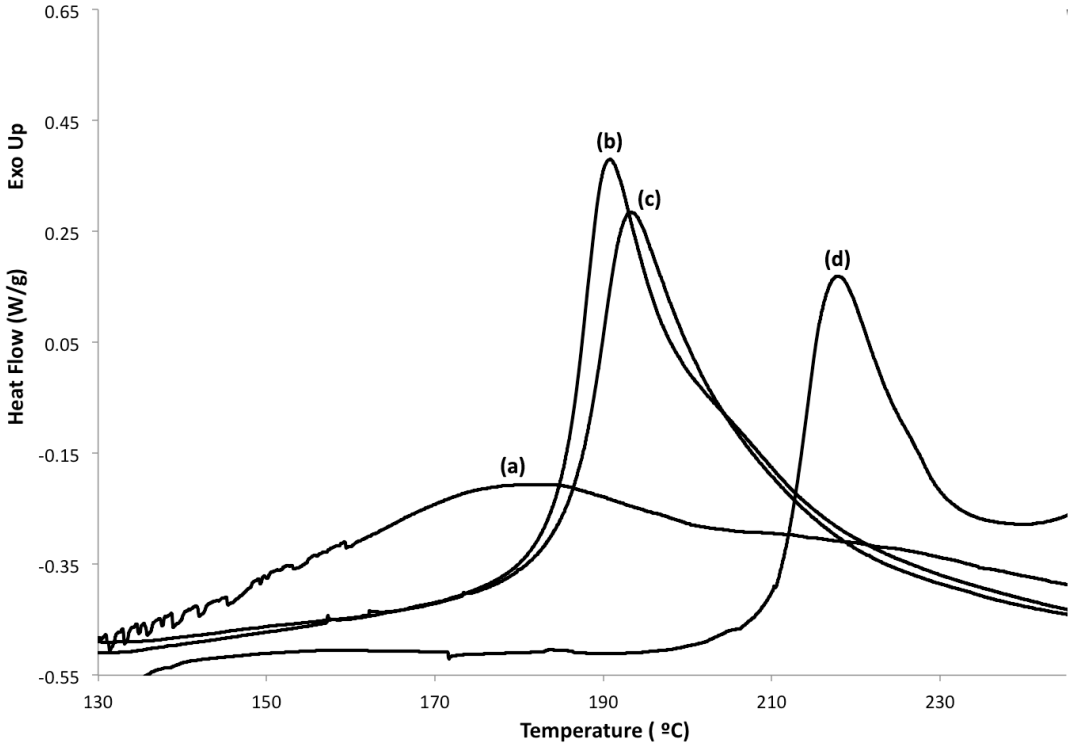

Figure 27. DSC curing curves for epoxy mixed with PAn EB (a), PAn DETA (b), PAn TETA (c), and PAn TRIS (d).

4.4. Summary

Polyaniline pernigraniline base could be successfully cross-linked using small molecule polyamines undergoing reductive addition. Reduction of the polymers and presence of the cross-linker were confirmed by FT-IR spectroscopy. The covalently linked structures showed good retention of the initial polymer morphology and some pore-like channels were observed. However, there was no obvious correlation between the size of these channels and the structure of the crosslinking agent. All cross-linked samples displayed improved thermal stability compared to pure polyaniline emeraldine base, but no trend was observed in regards to crosslinking structure and onset of degradation.

Polyaniline functionalized with various diamines and polyamines were able to successfully cure epoxy resins, albeit at significantly higher temperatures than the small molecule analogues. General trends were observed showing a decrease in curing temperature with increasing aliphatic chain length, as well as a decrease in curing temperature for polyamine derivatives over diamines. This is mainly due to the presence of additional active amines that can participate in the curing reactions.

The reductive addition of amines to polyaniline pernigraniline base provides a new and accessible method for the formation of cross-linked polyaniline networks and provides a promising first step towards the development of conductive curing agents for advanced composite applications. Adaptation of this methodology and exploration of various other amine structures are likely to offer improvement in the thermal stability and curing potential of these cross-linked polyaniline compounds.

5. Summary

Polyaniline is a unique polymeric material with the potential to revolutionize a variety of fields including semiconductors, flexible electronics, chemical sensing and more. As polyaniline continues to gain prominence in advanced technological applications, control and fine-tuning of its chemical properties and surface interactions will become increasingly important. The above work details a facile method for introducing new chemical groups to the polymer backbone and an efficient method for the surface modification of polyanilines.

Investigation of the reaction kinetics allowed for further elucidation and improvement of existing mechanisms. Steric bulk around the nucleophilic nitrogen center did seem to inhibit the reaction but the trends in reaction rate did not match those expected from sterics alone. The reductive addition reaction did exhibit some sensitivity to the electronic nature of substituents and it was found that a slight build up of positive charge occurs during the rate-determining step of the reaction.

Additionally, the utility of amine-functionalized polyanilines was explored through the synthesis of chemically cross-linked polyanilines and polyamine functionalized polyanilines that were used to successfully cure epoxy resins. The methodology introduced in this work provides a robust method for the synthesis of a variety of new polyaniline derivatives and a powerful synthetic tool for expanding the utility of polyaniline.

Section 2: Synthesis of Nanocomposites via the Surface Decoration of Carbon Materials

6. Introduction

As covered in the previous section, intrinsically conducting polymers constitute an important family of materials in the field of organic conductors. While comprised primarily of carbon, the inclusion of hydrogen, heteroatoms and dopants adds a level of structural and chemical complexity. Pure carbon materials, despite their monatomic composition, also contain a surprising diversity of structural complexity arising from the unique bonding abilities of the carbon atom. These materials represent the most fundamental organic conductors, and offer rich opportunities for further development. The projects undertaken in this section aim to further enhance carbon based conductors through the addition of new surface features such as carbon nanotubes or metal oxide nanostructures.

Carbon is a versatile element, forming the basis of all organic compounds and an essential material for advanced applications. The versatility of carbon arises from the variety of chemical bonds it can form with itself as well as other elements. Through high temperature processing, organic compounds can be converted into a variety of pure carbon materials[197-203]. These materials include graphite and graphitic derivatives, carbon fibers, carbon black, diamonds, carbon nanotubes, and fullerenes.

As mentioned before, carbon can engage in several different types of chemical bonding, each providing a distinct geometric conformation of the carbon atom. These chemical bonds are described in terms of the hybrid orbitals of carbon involved in the bonding[204-206]. The hybrid

orbitals are sp^3, sp^2 and sp where the superscript denotes the number of p orbitals being hybridized with the single s orbital. In sp^3 hybrid orbitals, the three p orbitals, p_x, p_y and p_z are equally mixed with the spherical s orbital to produce four identical orbitals in a tetrahedral arrangement about the carbon atom. These orbitals form strong primary bonds with other atoms known as sigma bonds.

If only two of the p orbitals are mixed with the s orbital, then the carbon is said to be sp^2 hybridized. Here three hybrid orbitals are generated with a trigonal planar arrangement, while the unhybridized p orbital is oriented perpendicular to the plane. The hybrid orbitals again form strong σ bonds with other atoms while the p orbital can form a secondary bond with other adjacent p orbitals to form weaker π bonds. The presence of this secondary bond strengthens the overall bond to the other atom while creating a cloud of electrons shared between the two. Adjacent π bonds can interact, sharing electrons and creating large continuous pathways of electron density depending on the number of sp^2 bonded atoms.

The final type of common hybrid orbital is the sp orbital, formed from the mixing of a single p orbital with the s orbital to form two orbitals 180º apart, with the remaining two p orbitals mutually orthogonal. Carbon and other atoms with sp hybrid orbitals form triple bonds comprised of the core σ bond and two π bonds.

It is important to discuss the types of bonds formed by carbon as it helps explain the properties observed in its various allotropes. An allotrope is a distinct structural form of a pure element, and in the case of carbon the two main allotropes are diamond and graphite.

Diamonds are comprised of a network of sp^3 bonded carbons in a tetrahedral arrangement. The crystal structure can either be cubic or hexagonal in structures, with the cubic variety being the most common in both natural and synthetic diamonds[207-209]. The close packing

of the cubic diamond structure coupled with the strong sigma bonds between atoms makes diamonds the most atom dense structure currently known. In addition to their high density, diamonds exhibit incredible hardness and extremely low compressibility[210].

The highly regular structure and symmetry of the lattice is responsible for the properties being isotropic, or independent of direction. Other important properties of diamonds include high thermal conductivity, resulting from lattice vibrations, and low thermal expansion. The range of optical transmission is also quite large, extending from the microwave region to x-ray, and the negligible absorption in the visible spectrum give diamonds their characteristic clarity[211]. At room temperature diamonds are excellent electrical insulators, evidenced by the large electrical band gap brought about by the highly stable carbon-carbon bonds[212,213]. Upon heating however, diamonds display strong semiconducting properties and are able to maintain semi-conduction up to 500 ºC compared to silicon which is semiconducting up to 150 ºC[214].

The excellent hardness of diamonds have led to them being mainly used in grinding and cutting applications in industrial settings, while the optical clarity and refractive properties have made them valuable for jewelry and luxury consumer goods[215]. While an excellent material, diamond is significantly limited by cost and specimen size.

The second major allotrope of carbon is graphite, a material composed of stacked sheets of planar sp^2 bonded carbons atoms. From the trigonal planar arrangement of the sp^2 orbitals, the layers of graphite, known as graphene, take on a hexagonal arrangement while the unhybridized *p* orbitals interact to form a large network of delocalized electrons across the sheet[216]. The stacking of graphene sheets occurs in two main patterns to form the graphite crystal lattice, hexagonal and rhombohedral[217].

Hexagonal graphite is formed from offset sheets in which every other layer is superimposed. This arrangement is the most thermodynamically stable form of graphite and thus the most prevalent crystal structure found in natural and synthetic graphite materials. Rhombohedral graphite is less common due to its lower thermodynamic stability, undergoing conversion to the hexagonal structure at high temperatures[218]. The rhombohedral crystal is formed by offset sheets in which every third sheet is superimposed.

While the properties of diamonds are independent of the direction in which the property is measured, the properties of graphite are anisotropic, or highly dependent on direction[219]. The individual sheets are comprised of carbon atoms held together with σ bonds and reinforced by the additional π bonds formed from the unhybridized *p* orbitals. The inter-sheet bonding however is quite weak, only held together by van der Waals forces[220]. The distance between layers also contributes to the weak interactions, and is a main cause of the anisotropic behavior of the material[221].

Graphite is an excellent thermal conductor in the plane parallel to the graphene sheets, with values around 390 W/m•K but ranging as high as 1180 W/m•K for some materials[222,223]. Perpendicular to the sheets however, the thermal conductivity is approximately 2.0 W/m•K making it an effective thermal insulator[224]. The thermal expansion of graphite shows the opposite trend, with the thermal expansion perpendicular to the planes high enough that delamination of the sheets can occur[225]. The large field of delocalized electrons in the graphene sheets result in good electrical conductivity in the plane of the material while the large spacing between layers inhibits the transfer of electrons between sheets and gives rise to electrical insulation perpendicular to the plane[226,227].

The stability of the carbon-carbon bonds also renders graphite highly inert to chemical reactions, with good resistance to acids, bases and corrosive compounds. Any chemical reactions that do occur are primarily at the edges of planes and defect sites[228]. The lamellar stacking of the graphene sheets also helps limit the reactivity by reducing the surface area exposed to reagents. Some materials such as activated carbon utilize their high surface area to promote reactivity and enhance their ability to filter and purify solutions[229,230].

Graphite and graphitic carbon materials have found myriad applications due to the combination of thermal and electrical conductivity, chemical resistance, and anisotropic dependence of those properties[231,232]. Additionally the variety of processing methods to obtain graphitic carbon materials leads to a diverse array of properties unique to the materials[233]. An in depth discussion on the many types of graphitic carbons and their applications is beyond the scope of this work, but two main types of materials will be discussed further. These are graphene and its derivatives and their application as advanced nanomaterials, and carbon fiber as a reinforcing material for engineering composites.

The focus of the following research projects is the development of new materials using low cost, easily scalable approaches to provide novel and affordable materials for advanced engineering applications. Utilizing microwaves as an energy source for carbonization provides a more energy efficient route to the production of carbon nanomaterials and significantly reduces the time and labor involved to produce these materials.

7. Microwave Synthesis of 1-D Nanostructure Decorated Hollow Carbon Nanospheres.

Microwave energy is finding increasing use in the field of chemical synthesis due to its capability to promote unique reactions and efficiently provide heat to chemical systems[234]. In addition to conventional synthesis, microwave processing techniques have also found use in the production of nanomaterials and novel carbon-based structures[235]. This chapter details the application of microwave processing to the formation of hollow carbon-CNT composite materials.

7.1. Introduction

The versatile bonding abilities of carbon not only produce distinct allotropes but also make possible unique structural features within material types. Of significant interest to researchers are the various nanostructures formed from graphitic carbon, and the unique properties exhibited by these structures. The synthesis of these unique nanomaterials can be accomplished with a variety of techniques, each with advantages and drawbacks. The recent development of microwave assisted processing methods offers a new method for the facile synthesis of complex carbon nanostructures as well as the ability to produce nanocomposites of carbon and metal oxides. A brief survey of some of these carbon nanostructures, as well as an introduction to microwave assisted processing of nanomaterials is presented below.

7.1.1. Carbon Nanomaterials

Graphene

As discussed previously, graphene is a two-dimensional macromolecule formed from hexagonally arranged sp^2 carbons that form the lamellar material graphite. The isolation of individual sheets of graphene from graphite can be accomplished through mechanical exfoliation. This method is facile and low cost but yields only small samples in the range of several micrometers and lacks control over sheet size, shape and orientation[236]. Despite these drawbacks, exfoliation of graphene sheets has allowed further elucidation of the material properties. Graphene displays enhanced thermal and electrical properties compared to graphite, with thermal conductivity as high as 5,000 W/m•K, current carrying capacity up to 10^9 A/cm^2, and carrier mobility above 100,000 cm^2/V•s[237-239].

These extraordinary properties have been achieved under near ideal conditions, and the challenges associated with the incorporation of graphene into devices makes these benchmarks far from attainable in the immediate future. The largest barrier for the inclusion of graphene into current technologies arises from the difficulties in synthesizing samples of adequate size[240-242]. Many synthetic approaches have been investigated including chemical vapor deposition, annealing of carbon doped metals, and graphitization of carbides[243-245]. These methods offer greater control over the quality and orientation of the synthesized graphene as well as greatly increasing the size of samples that can be produced, but require energy intensive processes and highly controlled conditions that contribute to higher material costs.

Carbon Nanotubes

While graphene exists in a planar form, the hexagonal structure of sp^2 carbons can also adopt an additional conformation, that of a tubular structure. These carbon nanotubes (CNTs) display their own unique sets of properties that can be tailored by the angle at which the

hexagonal structure is oriented in regards to the axis of the tube, as well as the diameter of the tube[246-248]. The most common orientations of CNTs are zigzag, armchair and chiral where the extent of chirality can be varied. Carbon nanotubes can also be formed with a single wall (SWNTs) or multiple walls (MWNTs), depending on the synthetic conditions employed, which also offer differences in the thermal, electrical and mechanical properties[249,250].

The synthesis of carbon nanotubes has made significant progress since their discovery, and many methods can be used to control the various dimensions and configurations. The main methods for CNT synthesis are chemical vapor deposition, laser ablation and arc-discharge. Much like the synthesis of graphene, the formation of CNTs by chemical vapor deposition (CVD) utilizes careful control of carbon-rich feed gasses heated in the presence of metal catalysts at high temperature to facilitate controlled carbonization[251,252].

In the arc-discharge method, plasma is generated by the electrical discharge between two carbon electrodes leading to ionization of the carbon atoms followed by their recombination into tubular structures[253,254]. Laser ablation works in a similar manner, using a high-powered laser source to vaporize the carbon source. CVD offers many advantages over arc-discharge and laser ablation, including lower carbonization temperatures and greater control over the quality and orientation of the produced nanofibers[255-257]. The method does however require careful control of the feedstock and catalyst as well as long deposition times.

Hollow Carbon Nanomaterials

The development of new types of carbon-based nanostructures presents an opportunity for their application in a variety of fields to provide improved performance over traditional materials. Carbon nanotubes and graphene are the most dominant of these advanced carbon materials, but recently research interest into hollow carbon spheres (HCSs) and their

incorporation into core-shell nanocomposite materials has developed. Unlike fullerenes, which are hollow spherical shells comprised of a single graphene-like layer, HCSs are thicker shells of graphitic or amorphous carbon ranging in thickness from several nanometers to several tens of nanometers thick, and can contain pores of varying size. The hollow and often porous nature of these novel structures create a low density material that retains the high electrochemical performance associated with nanostructured carbon and offers long-term thermal and mechanical stability. Currently these materials are being evaluated for their performance in catalysis, energy storage, water treatment and electromagnetic shielding applications[259-265].

The term "core-shell structure" is used to describe a two-component material in which the inner "core" material is encapsulated or otherwise surrounded by the second "shell" material. The nomenclature for describing core-shell systems is fairly straightforward and utilizes the @ symbol as an abbreviation for "coated with". Examples of this are metal@polymer, metal oxide@carbon, or carbon@carbon, although the potential types of core-shell systems is vast[262-264,266]. Typically the shell material acts as a barrier to protect the core material from specific environmental conditions or to reduce aggregation of the core materials, which could be detrimental. The rigid shell structures also increase the surface area of the bulk material while simultaneously creating unique nanoscale interstitial spaces that can be utilized in different applications[267,268].

The core-shell nomenclature can also be applied to surface decorated particles where the material being decorated is the core, and the added surface structures would be considered the shell. Core-shell composites of hollow carbon spheres often fall into this definition, using the surface of the sphere as a substrate to introduce a variety of nanomaterials[269-271]. The synthesis of these composites can be achieved by hard or soft templating[272-274] followed by various treatment

methods including carbonization[275], pyrolysis[276], chemical vapor deposition[277] or solvothermal techniques[278]. Intrinsically conducting polymers, predominantly polypyrrole (PPy), are commonly used as the precursor for hollow structures as their morphology can be easily controlled and readily undergo carbonization[279-280].

These decorated HCSs offer advantageous electrochemical performance by combining highly structured carbon and the unique properties of the decorating nanomaterials into a single material. The main drawback has been the larger size of these materials, with the diameter of the hollow sphere frequently in the micron range[281,282]. Larger diameter spheres have a lower specific active surface area compared to spheres in the nanoscale range, which reduces the amount of potential electrochemical interactions for a given amount of material[269,283-285]. To improve the performance of these decorated HCS materials and increase their utility in various applications, the overall diameters of the hollow spheres must be reduced into the nanoscale range through low cost and easily scalable methods.

Towards this end, polypyrrole in combination with various organometallic precursors has been successfully used to prepare nanostructured carbon composite materials with high electrochemical performance[286]. Polypyrrole has attracted significant research interest due to its low cost reagents, facile synthesis and good electrical conductivity[287,288] coupled with the ease of forming variety of nanostructured morphologies ranging from dispersed nanoclusters and nanofibers to complex, self assembled three dimensional structures[264,284,289-294]. Polypyrrole offers the additional advantage of undergoing rapid carbonization under microwave irradiation while maintaining its original morphological features[278].

In addition to focusing on nanostructured carbons, much research has been done on developing other active species based on transition metal oxides[295,296], conducting polymers[297-299]

and heteroatom functional groups for energy storage[300,301]. Iron oxide, specifically Fe_2O_3, stands out from other metal oxides such as MnO_2, V_2O_5, and RuO_2 as a promising anode material in lithium ion batteries due to its low cost, abundance and high theoretical specific capacity (1007 mAh g^{-1})[295,302,303]. It is not without drawbacks though as it exhibits low electrical conductivity and poor cycling stability, two critical properties for any energy storage application. By incorporating Fe_2O_3 with conducting polymers or nanostructured carbon materials, it may be possible to mitigate these issues and develop a material well suited for electrochemical applications.

7.1.2. Microwave assisted growth of CNTs and Metal Oxides

In response to the cost and time involved with the production of CNTs by chemical vapor deposition, microwave energy has been investigated as an alternative approach to the fabrication of CNTs and other nanostructured materials[292,293]. The underlying idea is that a suitable conducting substrate can be used to convert absorbed microwave energy into thermal energy with the speed and intensity necessary to decompose organic precursor materials into reactive carbon species.

Work by the Zhang group developed this approach utilizing conducting polymers, primarily polypyrrole, as the conducting substrate[292]. Under microwave radiation polypyrrole undergoes rapid heating to produce nanostructured graphitic carbon, and the heat generated can be used to convert organometallic precursors such as ferrocene into carbon nanotubes. Other conducting substrates such as indium tin oxide, graphite and milled carbon fibers were also successfully employed in this process, referred to as the "poptube" approach[292].

The poptube growth method produces multiwalled carbon nanotubes (MWNT) with outer diameters ranging from 30-150 nm based upon the substrate. The cyclopentadienyl rings of the

ferrocene precursor naturally lend themselves to the formation of CNTs by virtue of already being sp^2 hybridized and in a ring structures. Upon thermal decomposition of the ferrocene structure, the central iron atom has been shown to produce Fe_2O_3, a common catalyst used in the CVD synthesis of CNTs[304-306].

In addition to the synthesis of carbon-based nanostructures, the poptube approach can also be used to facilitate the formation of other metal oxide nanostructures. Much research has been done on developing other active species based on transition metal oxides[307,308], conducting polymers[309-311] and heteroatom functional groups for energy storage[312,313]. Iron oxide, specifically Fe_2O_3, stands out from other metal oxides such as MnO_2, V_2O_5, and RuO_2 as a promising anode material in lithium ion batteries due to its low cost, abundance and high theoretical specific capacity (1007 mAh g^{-1})[295,314,315]. It is not without drawbacks though as it exhibits low electrical conductivity and poor cycling stability, two critical properties for any energy storage application. By incorporating Fe_2O_3 with conducting polymers or nanostructured carbon materials, it may be possible to mitigate these issues and develop a material well suited for electrochemical applications.

Extending the poptube approach to the synthesis of CNT or metal oxide surface decorated hollow nanocarbons would offer a new, low cost and easily scalable method for the production of complex materials with the utility in high-performance applications.

7.2. Experimental Methods

The following chemicals and reagents, including styrene (99%), ammonium peroxydisulfate (APS, 98% min.), ferrocene (99%) and pyrrole (98+%) were all purchased from Alfa Aesar and used for the synthesis reactions. Sodium dodecyl sulfate (SDS, 99%) was purchased from IBI Scientific. Iron pentacarbonyl (99.5% and 99%-Fe) was purchased from

Strem Chemicals. Ethanol (absolute, 200 proof) was purchased from Electron Microscopy Sciences. Tetrahydrofuran was purchased from BDH. All reagents were used as-received without further treatment unless otherwise specified.

Different characterization techniques were used in order to identify the as-obtained CNT-MONW/HCNS nanocomposites' properties. Both the morphological and compositional features of these nanocomposites were analyzed by JEOL JSM-7000F scanning electron microscope (SEM) equipped with an energy-dispersive X-ray (EDX) detector. Moreover, the in-depth morphological analysis of the as-obtained nanocomposites was performed on a JEOL 2100F transmission electron microscope (TEM) that was operated at 200 kV. The major functional groups exist in these nanocomposites were detected by using a Thermo Nicolet 6700 Fourier Transform Infra-Red (FT-IR) spectroscope. The as-obtained nanocomposites' thermal stability was characterized by using thermal gravimetric analysis (TGA) performed on a TA Q2000 system from room temperature up to 800 °C (at 10 °C/min heating rate, in air). Additionally, the nature of the as-formed MONWs on HCNSs was determined by X-Ray diffractometry (XRD) analysis, which was performed on a Rigaku powder XRD instrument. Microwave irradiation of samples was carried out using a Panasonic Inverter domestic microwave (Model NN-SN936B) at 1250 W.

7.2.1. Synthesis of Polystyrene Templates

The PS NSs were prepared based on a previously reported method[316] by initially adding 4 mL of styrene monomer into a 250 mL round bottom flask containing a magnetic stir bar and 80 mL of 3 mM aq. SDS. A reflux condenser was attached to the reaction medium and the flask was placed in a preheated oil bath at 70 ºC for 20 min under high magnetic stirring. The oxidant, APS (68 mg, 0.298 mmol) was added to 1 mL of deionized H_2O and the solution was slowly added to

the heated monomer solution. The polymerization reaction was allowed to proceed for 4 h at 70 ºC, yielding a milky semi-opaque suspension. The resulting latex solution was removed from the heat and allowed to cool naturally to room temperature before being transferred into a container for storage purposes.

7.2.2. Coating of Templates with Polypyrrole

The polystyrene nanospheres synthesized in the previous step were used as hard templates for the synthesis of polypyrrole nanospheres. Coating of the templates was carried out using the oxidative polymerization of pyrrole with APS under acidic conditions. The general procedure for the synthesis of PPy coated polystyrene nanospheres is as follows. To a 100 mL beaker containing 60 mL 1 M HCl (aq), 10 g of the previously synthesized latex was added and the mixture placed under heavy magnetic stirring. The pyrrole monomer (1 mL, 0.0144 mol) was added to the mixture and left to stir for 10 min to allow distribution of the monomer and mixing with the template. The monomer-template solution was then transferred to an ice bath where it was cooled to 5 ºC and maintained at that temperature. An oxidant solution was prepared by dissolving APS (1.15 g, 0.0050 mol) in 10 ml 1 M HCl (aq) followed by cooling to 5 ºC. The oxidant solution was added dropwise to the monomer solution over 10 min under high magnetic stirring. As the amount of added oxidant increased, the solution took on a pale blue color that darkened with the addition of oxidant until the solution was an opaque black color. Once the oxidant had been completely added the reaction was left under heavy stirring for 1 hr. The resulting black suspension was first filtered and washed with excess 1 M aq. HCl to remove any unreacted monomer and/or oxidant, and eventually it was dried overnight under vacuum at 60 ºC to yield a fine black PPy/PS powder.

7.2.3. Formation of Hollow Spheres through Template Removal

To achieve the desired hollow polypyrrole nanostructures, the PPy coated PS was subjected to a brief microwave treatment followed by extraction of the polystyrene with THF. Generally, 5 g of the PPy coated PS was placed in a 20 mL scintillation vial with a loosely attached cap, and then microwaved at full power for 10 s to minimally carbonize the PPy coating. The brief irradiation carbonizes only a small portion of the conducting polymer and is essential to maintaining the spherical structure during removal of the template core. The short microwaving treatment had no observable effect on the quality of the spheres, other than preventing collapse of the structure upon template removal. The treated powder was then soaked in 50 mL THF for 30 min under high magnetic stirring to dissolve the PS template. The etched nanospheres were collected by several cycles of centrifugation at 5000 rpm for 15 min, decanting the supernatant and replenishing with 35 mL of fresh THF each time. The centrifuge tubes were vortexed after the addition of THF to redisperse the nanospheres. The resulting black solids were allowed to air dry for 2 hrs before vacuum drying at 60 ºC overnight. The dried PPy could easily be broken up with a spatula to form a loose, free flowing powder.

7.2.4. Carbonization and growth of 1-D structures

Carbon nanotube decorated polypyrrole nanospheres were synthesized by mixing 50 mg of partially carbonized PPy hollow nanospheres (PPy HNSs) with ferrocene pre-dissolved in ethanol. The weight ratio of PPy to ferrocene was maintained at 1:1. Ferrocene was added as a solution to improve distribution of the precursor throughout the sample, and to assist in the deposition of ferrocene on the surface of the spheres. The ethanol was allowed to evaporate leaving a characteristic orange residue behind on the sample. The ferrocene-PPy HNS mixture was transferred to a 20 mL glass scintillation vial with the cap loosely fitted, then microwaved at

full power for 30 seconds. After several second of irradiation, intense glowing was observed in the sample along with the evolution of gaseous vapors. The glowing increased in intensity and was accompanied by the appearance of sparks as irradiation continued. The dark PPy powder displayed patches of burning characterized by the intense glow, and the base of the glass vial began to heat rapidly and in some instances melted.

After microwaving the sample was allowed to cool slightly before being removed from the microwave chamber and placed in the fume hood to finish cooling to room temperature. Only free-flowing powder and sample scraped from the interior walls of the vial were collected and transferred to a new container in order to minimize possible contamination from the melted portions of the vial bottoms.

Ferrocene was used as a precursor for the CNT decorated HCNS materials. For the metal oxide decorated HCNSs a similar procedure was followed, using iron pentacarbonyl (0.1 mL) instead of the ferrocene-ethanol solution. Similar vigorous decomposition was observed during microwave irradiation. The reaction vial contained the metal oxide nanowire HCNS composite as well as small clumps of grey, lightweight fibrous decomposition products.

7.3. Results and Discussion

In the synthesis of the polystyrene latex templates, the amount of SDS was varied to determine the size dependency of the formed nanospheres and to explore the effect of varying template size on the formation of HNCSs. The relationship between surfactant concentration and resulting PS nanosphere size can be seen in Figure 28 and Table 12. It was observed that increasing the concentration of surfactant reduced the overall size of the obtained spheres, but was accompanied by greater size distribution. As described in the work by Zhenxing *et al.*[315], the use of surfactants below the critical micelle concentration (CMC) results in the formation of

mixed micelles with the sparingly soluble monomer, which is then polymerized by generated radicals to form the desired nanospheres. The presence of additional surfactant molecules reduces coagulation of the formed polymer chains and thus results in smaller sphere diameters.

Coating of the templates with PPy increased the diameter of the spheres by roughly 20 nm for all template sizes (Table 12). The uniformity of coating thickness and lack of large scale aggregation after coating with PPy was also beneficial. Incorporation of surfactant molecules into the latex spheres facilitates adsorption of the monomer onto the surface of the template, thus aiding in a homogeneous coating. Rapid stirring during polymerization of the polypyrrole also contributes to the reduction of large aggregates. The largest sized PS spheres were used to prepare the PPy HNSs as they exhibited the smallest size distribution, thus offering the most consistent HNSs when coated. It can be seen in Figure 29 that the PPy coating on the templates were uniform and very consistent, comprised of joined granular structures with minimal surface roughness. The partial carbonization of the coated templates had little effect on the overall structure (Figure 29C) when compared to the uncarbonized material (Figure 29B).

Removal of the PS template did produce a consistent defect in the majority of the structures, appearing to be a partial collapse of the sphere (Figure 29D). This collapse likely results from the thin shell wall being unable to maintain the integrity of the spherical shape despite partial carbonization. It may also be caused by removal of the template by centrifuging, as the solubilized core is drawn out of the sphere it could create a slight vacuum effect pulling in one side of the sphere. Template removal is necessary to produce the desired hollow structure, and must be carried out prior to complete carbonization of the shell. If the template remains, the polymer core will also undergo carbonization and the resulting residue cannot be removed from the interior of the structure.

The morphology of the CNT HCNS and MONW HCNS samples were characterized by scanning electron microscopy (Figure 30) and transmission electron microscopy (Figure 31).

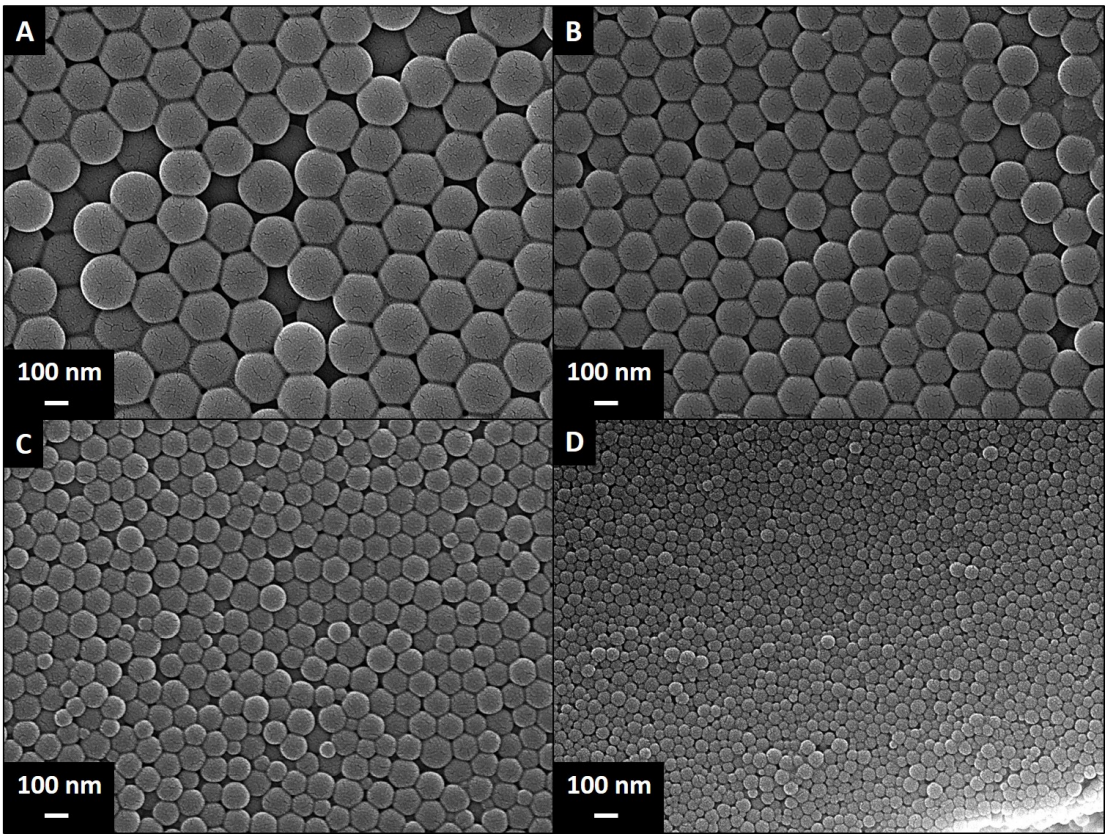

Figure 28. SEM images of the as-synthesized PS NSs with varied concentrations; (A) 1.5 mM, (B) 2 mM, (C) 3 mM, and (D) 6.5 mM of SDS, respectively.

Table 12. Summary of the as-obtained PS NSs' average diameter values with varying SDS concentration.

SDS concentration (mM)	**Average PS NS diameter (nm)**	**PS@PPy NS diameter (nm)**
6.5	60	80
3	110	130
2	180	200
1.5	220	240

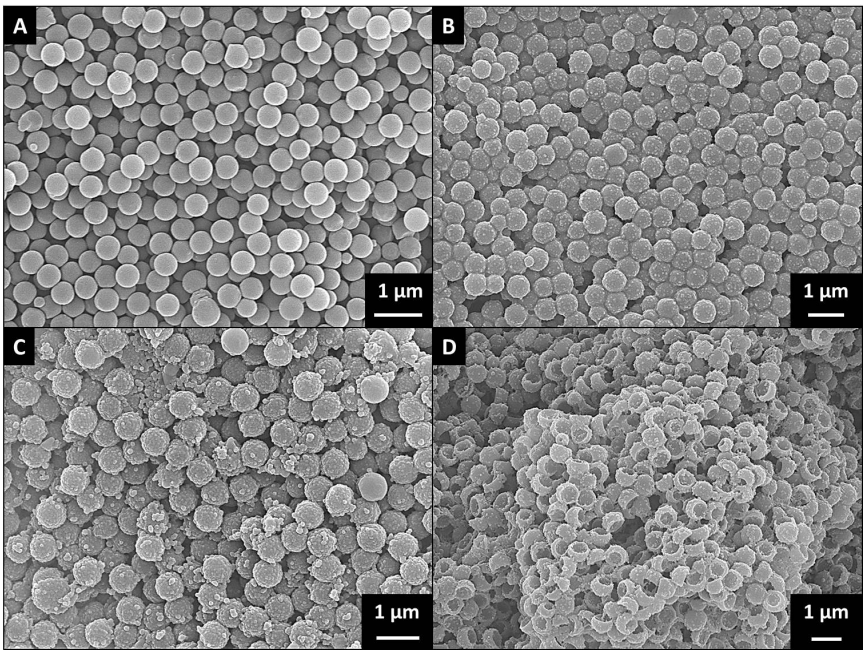

Figure 29. SEM images of the; (A) PS NSs, (B) PPy/PS NSs, (C) partially carbonized PPy/PS NSs, and (D) PPy HNSs after THF extraction.

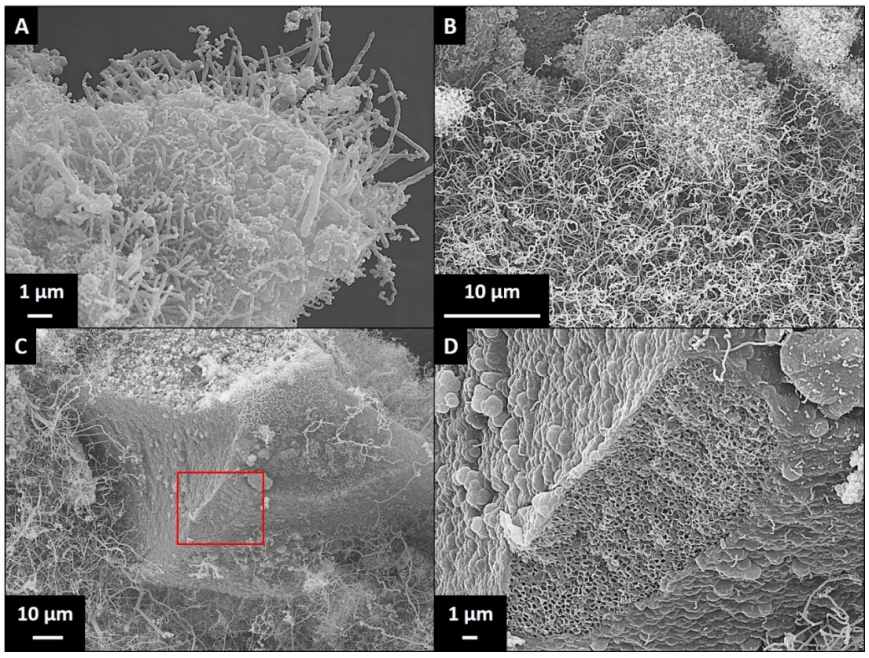

Figure 30. SEM images of the; (A) CNT/HCNSs, (B, C) MONW/HCNSs, and (D) Detailed view of the marked area in Figure 4C.

The successful synthesis of CNTs utilizing the microwave based poptube approach can be observed in Figure 30A. The CNTs formed from the decomposition of ferrocene are several micrometers in length and appear to grow from the surface of the HCNS clusters. During the microwave process the ferrocene-polypyrrole mixture undergoes a series of decomposition reactions that facilitate the formation of CNTs[292,317]. The reaction begins as polypyrrole absorbs the incoming microwave energy, rapidly converting it into heat. The intense heat generated leads to total carbonization of the polymer and decomposition of the ferrocene. Under these conditions the iron center of ferrocene reacts with other nearby iron centers and oxygen present in the atmosphere to generate Fe_2O_3, a metal oxide catalyst commonly used in the synthesis of CNTs by chemical vapor deposition, and frees the cyclopentadienyl anions which act as the pre-structured carbon source for the formation of nanotubes. With catalyst and feedstock now present in a localized environment, the formation of CNTs proceeds rapidly. The coverage of CNTs on the surface of the HCNSs also appears homogeneous, as the application of ferrocene-ethanol solution facilitates even distribution of the precursor.

Formation of the MONW proceeds similarly, rather than acting as a carbon source for nanostructure growth the CO ligands are simply lost leaving behind active iron centers to form the metal oxide nanowires. The MONWs formed in the reaction (Figure 30B,C) are significantly longer than the CNTs formed with more dense coverage on the surface of the HCNSs. A more detailed view of the MONW/HCNS composite (Figure 30D) shows smaller MONWs growing from the surface of the carbonized spheres and the hollow interior of the spheres in the cluster. The hollow spherical carbon structures combined with the dense growth of high aspect ratio metal oxides creates a nanocomposite with an ultra-high specific surface area ideally suited for water treatment or energy storage applications[264].

Further characterization by TEM (Figure 31) confirms the results gathered from SEM imaging of the samples. The spheres display a uniform size distribution, and the coating of PPy on the surface is comprised of connected nanogranules to form a uniform coating. In the CNT/HCNS sample (Figure 31C) the thin carbonized polymer shell can be observed along with some of the CNT structures mixed with the sample. The broken spheres seen in the sample are likely a result of the ultrasonic dispersion used to prepare the sample for TEM, rather than from the microwave processing method. Figure 31D shows one of the CNTs grown in the sample having broken off of a HCNS. The stem of the nanotube is approximately 2 μm long and hollow, with smaller secondary growth branching from it. At the tip is the encapsulated iron oxide nanoparticle responsible for the growth of the nanotube, as demonstrated by previous studies[284,292, 316,318,319].

Unlike the CNT/HCNS samples, the MONW/HCNS composite samples only revealed hollow spheres decorated with small Fe_2O_3 clusters embedded in the outer layer, rather than the long nanowires observed in the SEM images of the same sample. Previous experiments have shown that the nanowires produced from iron carbonyl precursors are not solid, continuous structures but rather a length of connected granules[264,284,293,320,321]. These granules are iron nanoparticles surrounded by thin layers of graphitic carbon, ranging in size from 30-100 nm. These loosely connected structures were unable to survive the sample preparation necessary for TEM, and as such the intact MONW decorated HCNSs could not be directly observed.

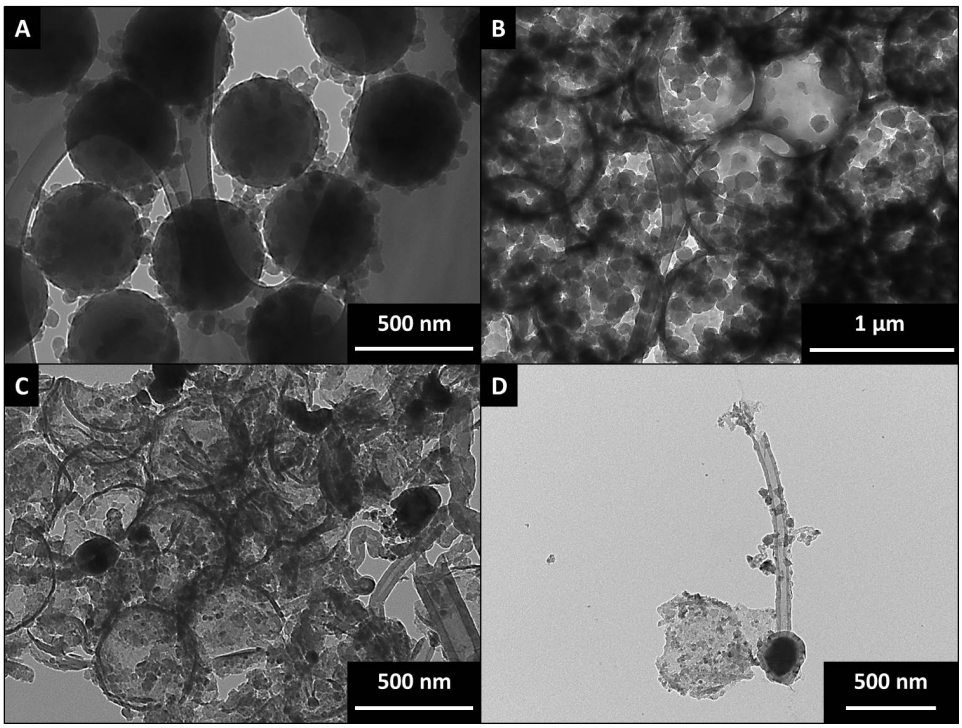

Figure 31. TEM images of the; (A) PPy/PS NSs, (B) PPy HNSs, (C) CNT/HCNS, (D) A broken, tip-grown, single CNT with secondary growths at its hollow stem and the encapsulated Fe NP at its tip, and a broken HCNS with carbonized PPy nanogranules at its surface.

The elemental composition of the metal oxide nanowires was determined through EDX analysis performed during SEM imaging of the samples (Figure 32, Table 13). Analysis of the chains indicates that the structures are comprised entirely of iron and oxygen in ratios close to that of pure Fe_2O_3, offering strong support for the formation of metal oxide nanowires.

Table 13. Summary of the EDX results shown in **Figure 32**.

Spectrum	**Fe (wt%)**	**O (wt%)**	**Total**
1	67.47	32.53	100
2	58.32	41.68	100

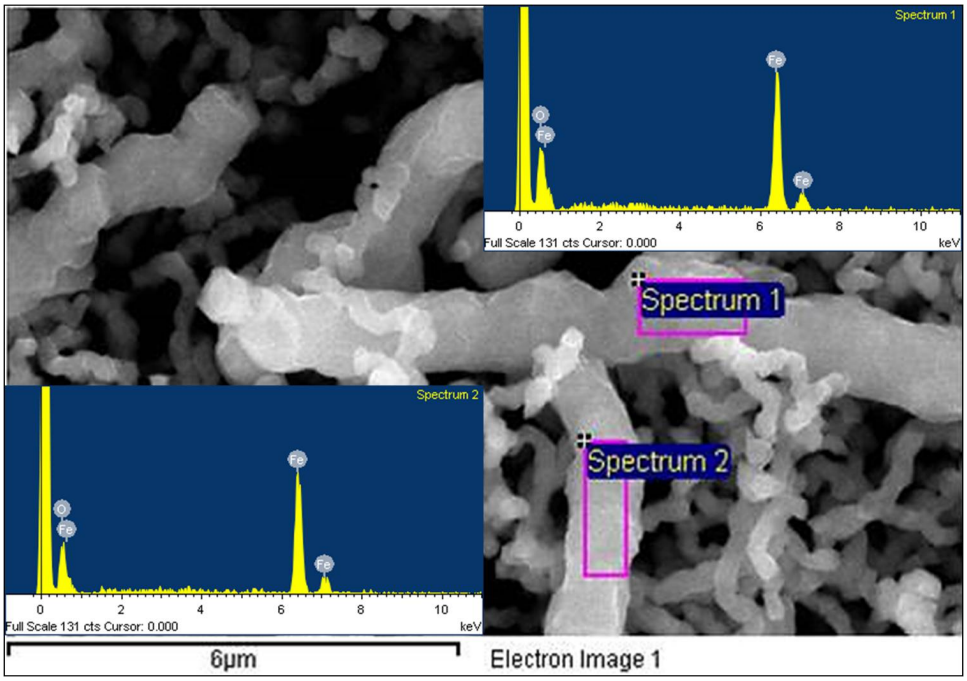

Figure 32. EDX results of the MONWs obtained from $Fe(CO)_5$ system.

X-ray diffraction was also performed on the MONW sample to determine the nature of the iron oxides being formed (Figure 33). The spectrum obtained from the MONW sample displayed peaks characteristic of Fe_2O_3, and not those of Fe_3O_4 or the other iron oxides. This confirmation, coupled with the data obtained from EDX clearly establish the presence of the desired Fe_2O_3 iron oxide, produced through the microwave assisted decomposition of iron carbonyl[264,284].

Additional structural and thermal characterization was carried out on the PS@PPy core shell structures and the hollow PPy nanospheres to confirm successful removal of the template prior to the full carbonization procedure. The results from FT-IR spectroscopy characterization are summarized in Table 14 and displayed in Figure 34. The dried latex templates show the characteristic peaks of polystyrene, including the strong aromatic C=C stretches at 1450 cm^{-1} and 1490 cm^{-1} and sp^2 C-H stretches from 3000-3100 cm^{-1} [127]. When coated with polypyrrole, the

composite material displays characteristic peaks of both materials, and after removal of the template only polypyrrole signals remain[322,323].

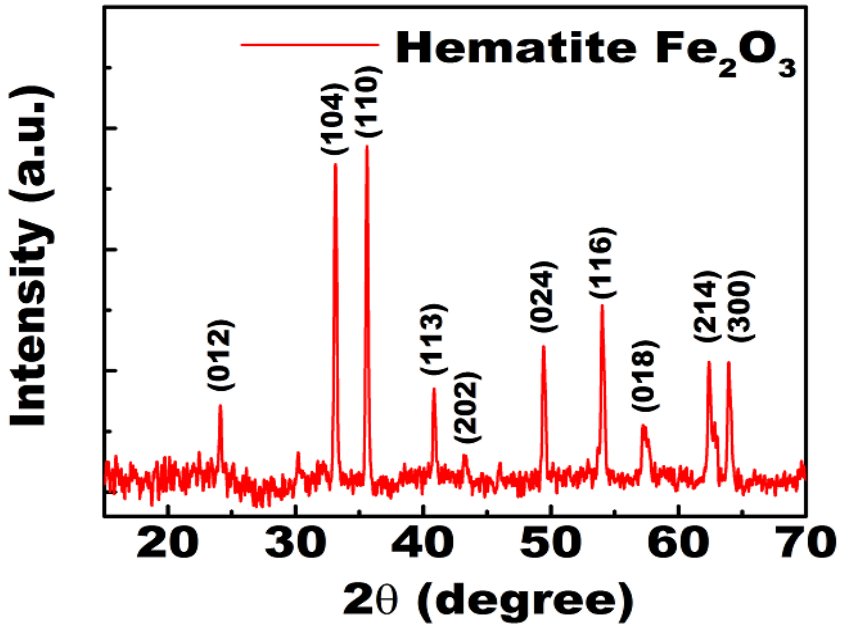

Figure 33. X-Ray diffractogram of the as-grown MONWs in MONW/HCNS sample.

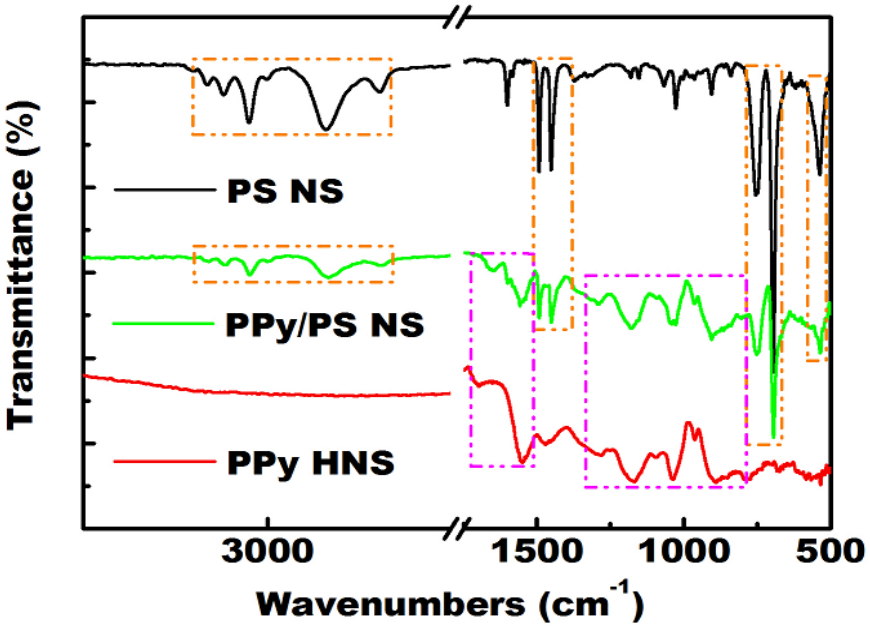

Figure 34. FT-IR spectra of the as-synthesized PS NS, PPy/PS NS and PPy HNS samples.

Table 14. Summary of the common FT-IR spectra peaks detected in PS/PPy NS sample shown in **Figure 34**.

Peak's origin	**Wavenumber (cm^{-1})**	**Definition**
From PS	3080, 3055, 3025	aromatic =C-H stretching vibrations
	2920, 2850	alkyl C-H stretching vibrations
	1490, 1450	aromatic –C=C– stretching vibrations
	755	aromatic =C-H out-of-plane deformation vibrations
	700, 535	out-of-plane ring deformation vibrations
From PPy	1555	secondary amine N-H peak of pyrrole ring
	1470	aromatic C-N stretching of pyrrole ring
	1290	$C\text{-}N^{+}$-H stretching vibrations in pyrrole ring
	1190	C-H in-plane vibrations
	1075	N-H in-plane vibrations (doped state PPy presence)
	905	C-H out-of-plane vibrations

The PPy coated nanospheres also exhibited peaks from both components as seen in Figure 35. The purple circles indicate decomposition peaks shared by the composite and the template free polypyrrole, while the orange indicate decompositions related to polystyrene. The first significant weight loss occurs at 225 ºC as the polypyrrole begins to lose dopant ions and any remaining adsorbed moisture or lower molecular weight components. The next is the onset of polystyrene degradation beginning near 325 ºC and ending near 425 ºC. This is the most significant weight loss for the composite sample as the polystyrene core constitutes the majority of the sample by both weight and volume. The final weight loss occurs between 425 ºC and 600

ºC as the remaining polypyrrole breaks down, with complete loss of material marked by the final purple circle. The steep and significant weight loss at 325 ºC is not observed in the etched sample, further demonstrating thorough removal of the template using THF extraction.

Based upon these results polystyrene latex is able to serve as a suitable template for the coating of polypyrrole and the formation of core-shell nanostructures without the need for pre-treatment or added stabilizing agents. The core can also be easily removed without leaving behind residues and the hollow shell is able to maintain its structure in the absence of the core. These two factors allow for the easy synthesis of large quantities of polypyrrole nanostructures which can subsequently converted into nanostructured hollow carbons through microwave treatment.

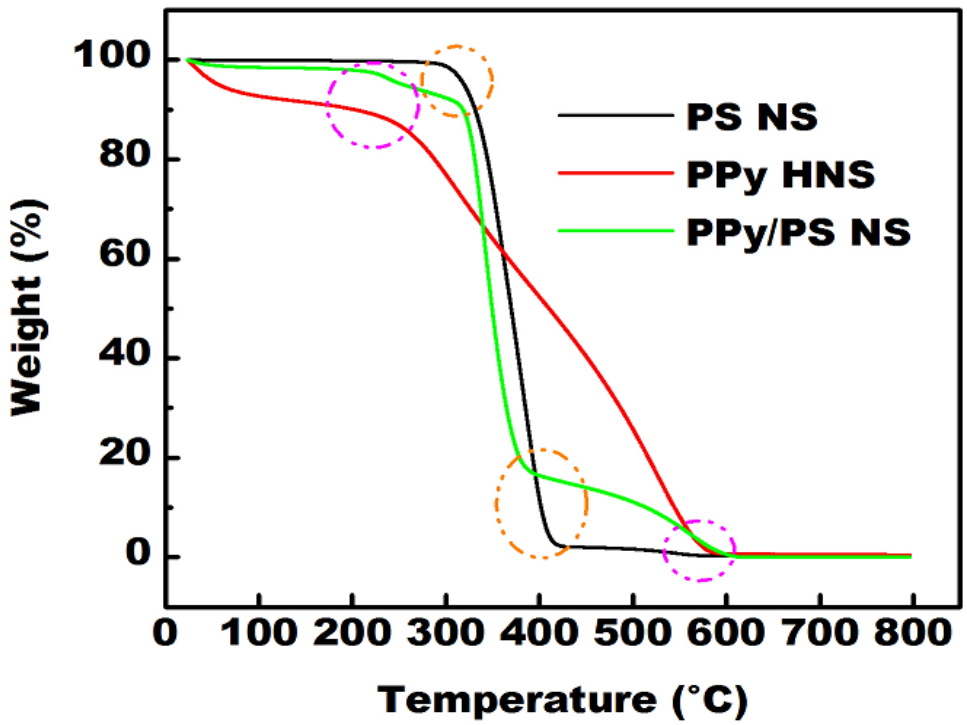

Figure 35. TGA thermograms of the as-synthesized PS NS, PPy/PS NS and PPy HNS samples.

7.4. Summary

This work details a simple, low cost and easily scalable route to the production of novel carbon based nanocomposite materials. By applying more traditional polymer synthesis and templating techniques, hollow conducting polymer structures were produced with a controllable size ranging from 80-240 nm. These hollow structures afford a lightweight, high surface area substrate for the microwave promoted synthesis of carbon nanotube or metal oxide nanowire decorated hollow carbon composites.

A variety of characterization methods elucidated the physical and structural features of these materials, demonstrating their hollow nature and confirming the prevalent growth of the desired nanostructures on the surface of the carbonized material. These nanocomposites offer a new, high performance material with potential for advanced water purification, energy storage, and electrochemical applications.

8. Towards the Development of Carbon Nanotube Decorated Carbon Fiber Fabric

Carbon fiber reinforced composites are becoming increasingly more common in industrial, aerospace and consumer applications as improvements in processing technology and material performance are made. Continued development of carbon fiber based reinforcements for composites will lead to new materials with even greater performance capabilities. To this end, we have undertaken a microwave-based approach to the development of nanomaterial functionalized carbon fibers.

8.1. Introduction

Carbon fibers have gained significant importance in the last several decades as high performance materials for composite and engineering applications[324-326]. Carbon fiber is an attractive material due to its high strength and modulus, low density and chemical stability compared to other reinforcing materials such as glass and ceramics[327-329]. As new production techniques have been developed, the cost of manufacturing carbon fibers has decreased, and the number of available carbon fiber products has increased furthering the number of viable applications

8.1.1. Synthesis of Carbon Fibers

Carbon fibers can be produced from a variety of different precursors but follows the same general procedure. The precursors are generally high carbon containing polymers such as polyacrylonitrile or aromatic rich hydrocarbon mixtures such as pitch that can be processed into

filaments by extrusion[330-332]. Melt extrusion of these materials and subsequent drawing under tension allows for controlled filament diameters and uniform precursor fibers to be produced. These fibers are then carbonized under carefully controlled heating to remove any heteroatoms and to maintain the fiber structure.

The carbonization process produces a filament of smaller diameter than the precursor fiber due to the significant mass loss of H_2O, CO_2, NH_3 and other combustion products. As the precursors decompose, nanoscale ribbons and fibers of sp^2 bonded carbons form and align with the axis of the fiber[333-335]. This preferential orientation is aided by the stretching of the precursors prior to carbonization as it produces greater molecular alignment[336].

It has been shown that the structure of carbon fibers is not entirely graphitic in nature, instead consisting of crystalline graphite regions interspersed with sp^3 bonds[337,338]. While individual crystalline regions display the lamellar stacking seen in graphite, these regions are typically not aligned with neighboring regions on a larger scale. The presence of sp^3 bonds between layers and between larger crystalline sections, coupled with the extended van der Waals interactions along the length of the nano-ribbons are responsible for the cohesion of the fibers and their high tensile properties[339,340].

8.1.2. Properties of Carbon Fibers

Much like graphite, the properties of carbon fibers are highly anisotropic. Individual filaments are rarely used; rather they are combined into fibers made up of several hundred to several thousand filaments or more[341]. These fibers are known as a tow, and the tow size varies depending on the application in which the fibers are used. As a general principle, the larger the diameter of the fiber and the longer the fiber is, the lower the overall strength of the sample[338].

Larger samples have a greater risk of containing structural defects that lower the overall performance of the fiber.

A summary of the mechanical properties of carbon fibers produced from various precursors is shown in Table 15[339]. Additional heat treatments after the carbonization process can be used to increase the graphitic characteristics of the fiber, resulting in improved modulus at the expense of tensile strength. While strong in tension, carbon fibers are generally quite brittle and thus offer little in terms of impact toughness or flexural strength[340,342].

The thermal and electrical conductivity of carbon fibers resemble that of graphite as well, showing high values for both properties along the axis of the fibers. Carbon fibers exhibit both thermal and electrical conductivity greater than that of many metals, including copper and aluminum[343,344].

Table 15. Mechanical properties of carbon fibers from various precursor materials[339].

	PAN	Mesophase Pitch	Rayon
Modulus (GPa)	205-550	380-827	173-520
Tensile Strength (MPa)	1860-6900	1900-2370	1200-2650
Tensile Strain (%)	0.81-2.2	0.25-0.5	
Density (g/cm^3)	1.76-1.87	2.0-2.18	1.40-1.80

8.1.3. Applications of Carbon Fibers and Research Motivation

Carbon fibers are most commonly used as a reinforcement for resin based composite materials due to their high strength and modulus, and low weight compared to metals and other fiber reinforcements like glass[340]. These composites are predominantly used in aerospace applications to replace heavier structural materials like steel and aluminum. Introducing light-

weight materials reduced the force necessary to generate lift and improves the fuel efficiency of the craft[345]. Other industries exploring the use of carbon-reinforced composites are sporting goods and industrial equipment, among others. The main limiting factor for adopting these composites is cost, although continued advancements in production will slowly remove this barrier.

Carbon fibers can be included in composite materials as short staple fibers, as filament yarns, or as woven fabrics, each with its own set of advantages and shortcomings. Staple fibers, fibers a few centimeters or less in length, generally adopt a random orientation when included in the resin matrix. The random orientation mitigates some of the anisotropic nature of the fibers to produce a composite with improved isotropic properties[346,347]. However, the short fiber lengths are unable to take up tensile loads throughout the material and as such their presence can enhance the stiffness of the composite but not the overall strength[348,349].

Composites containing long, continuous fibers offer greater tensile strength, as the fibers become the primary load carrier rather than the matrix[350]. Uniaxially aligned fibers offer high strength in the direction of the fibers but do not provide any support in the transverse direction. Using woven fabrics of carbon fiber allows for improved strength in two directions, as opposed to the single direction when using uniaxial fibers[351,352]. The drawback is that the woven carbon fibers exhibit lower tensile strength in each direction compared to the uniaxial fibers. This is a result of the woven structure putting greater bending stresses on the fiber, leading to breakage.

In any type of composite, there exists an interface between the matrix and the filler, and this interface is typically a weak point in the material[353,354]. In fiber-reinforced composites, one main mode of failure is separation of the fiber from the matrix commonly referred to as fiber pull-out[355,356]. This type of failure results from weak interfacial bonding between the fiber and

the matrix and is particularly common with carbon fiber composites due to the smoothness of the fibers. Increasing the surface roughness of the fibers would improve the strength of the composite interface, thus improving the overall strength of the composite[357].

The decoration of carbon fiber fabrics with carbon nanotube structures would provide an interesting new material for fiber-reinforced composites. The stiffness and extra surface area imparted by the nanotubes would significantly improve the interface between resin and reinforcement while enhancing the overall strength of the composite. Previous work has demonstrated the ability to form carbon nanotube composites from the microwave processing of ferrocene and milled carbon fibers. This work aims to extend that approach to carbon fiber fabric as a substrate, capitalizing on the activity of ferrocene in the presence of organic conductors and microwave irradiation to form carbon nanotube functionalized carbon fiber fabrics.

8.2. Experimental Methods

Unsized carbon fiber fabric was provided by Hexcel, woven in a plain weave pattern, Specimens for processing were cut into 2” x 2” squares, and all chemicals were of reagent grade and used without further purification. Reagents and solvents were supplied by Alfa Aesar with the exception of toluene (BDH), and ammonium persulfate (Fisher Scientific).

Microwave ovens used were Panasonic Inverter 1250 W Model NN-H765BF. SEM characterization was conducted on a JEOL JSM 7000F microscope with samples mounted on aluminum stubs with carbon tape and gold coated for improved resolution.

Saturated solutions of ferrocene were prepared by dissolving portions of ferrocene in 20 mL of the chosen solvent in a glass vial with a foil lined cap, followed by vortexing for several minutes. The ferrocene was allowed to dissolve over the course of 1 hr with periodic agitation to aid in dissolution. This process was repeated until the added ferrocene powder failed to dissolve

further, leaving a small amount of residual crystals in the bottom of the vial. The solutions were allowed to sit over night to ensure complete saturation of the solution before use.

8.3. Results and Discussion

Initial tests involving the microwave treatment of carbon fiber fabrics and ferrocene powder produced some nanostructured growth but the lack nanotubular features prompted the exploration of additional parameters with the goal of achieving growth of carbon nanotubes perpendicular to the surface of the fiber. These parameters include the use of solvents, ferrocene dispersion methods, changes in the microwave processing parameters, and the inclusion of additive components. A general scheme for the microwave processing of the samples can be seen in Figure 36.

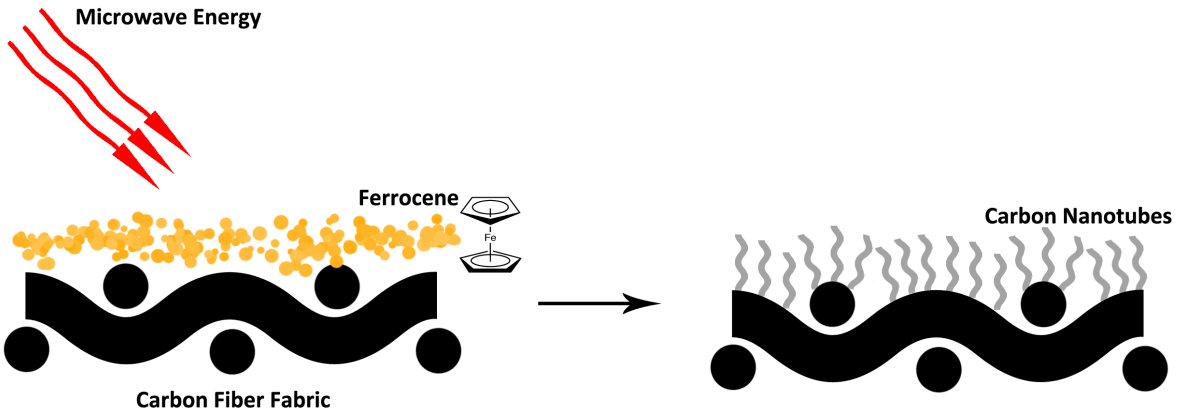

Figure 36. Schematic illustration of the microwave assisted growth of carbon nanotubes on carbon fiber fabric from the decomposition of ferrocene.

8.3.1. Ferrocene Powders and Successive Treatments

The starting point for the growth of CNTs on the fiber surface followed from the general approach to produce other CNT decorated structures. Ferrocene powder (either 25 mg or 50 mg) was dusted across the surface of the fabric using a fine mesh to provide uniform coverage. Samples were then microwaved at full power for 1 min. Successive treatments of ferrocene

addition and microwave processing were conducted to yield samples that had been treated one, two, and three times.

The aim was to determine if surface application of ferrocene to the fabric would be sufficient to produce nanostructure growth, and if the presence of initial growth would promote additional or secondary growth upon repeated treatments.

The first round of treatment showed much greater coverage of nanostructures in the 50 mg samples compared to the 25 mg samples (Figure 37A,D). No CNTs were observed in the deposits on the fabric surface, only amorphous structures and long chains of connected granules dubbed ‘necklaces’. These deposits were not uniformly distributed across the sample, and primarily sat atop the surface fibers or between them. This distribution is consistent with the application of the ferrocene powder as the exact amount of ferrocene dusted in a particular area was highly varied and the powder was unable to penetrate further into the fabric structure

Successive treatments did not yield any improvement in the structure of the deposits formed (Figure 37**)**. Additional treatments lead to larger deposits and greater coverage across the fabric surface, but growth was predominantly necklaces and larger granular structures. These surface deposits were not well adhered to the fiber surface and many were observed to have been broken loose.

The presence of the necklace structures seemed to contribute to the decomposition of additional applications of ferrocene powder. The iron oxides formed from the decomposition of ferrocene acts as an additional microwave absorbing component, but the lack of nanotube growth shows that the additional energy absorbed is still not substantial enough to promote carbon nanotube formation.

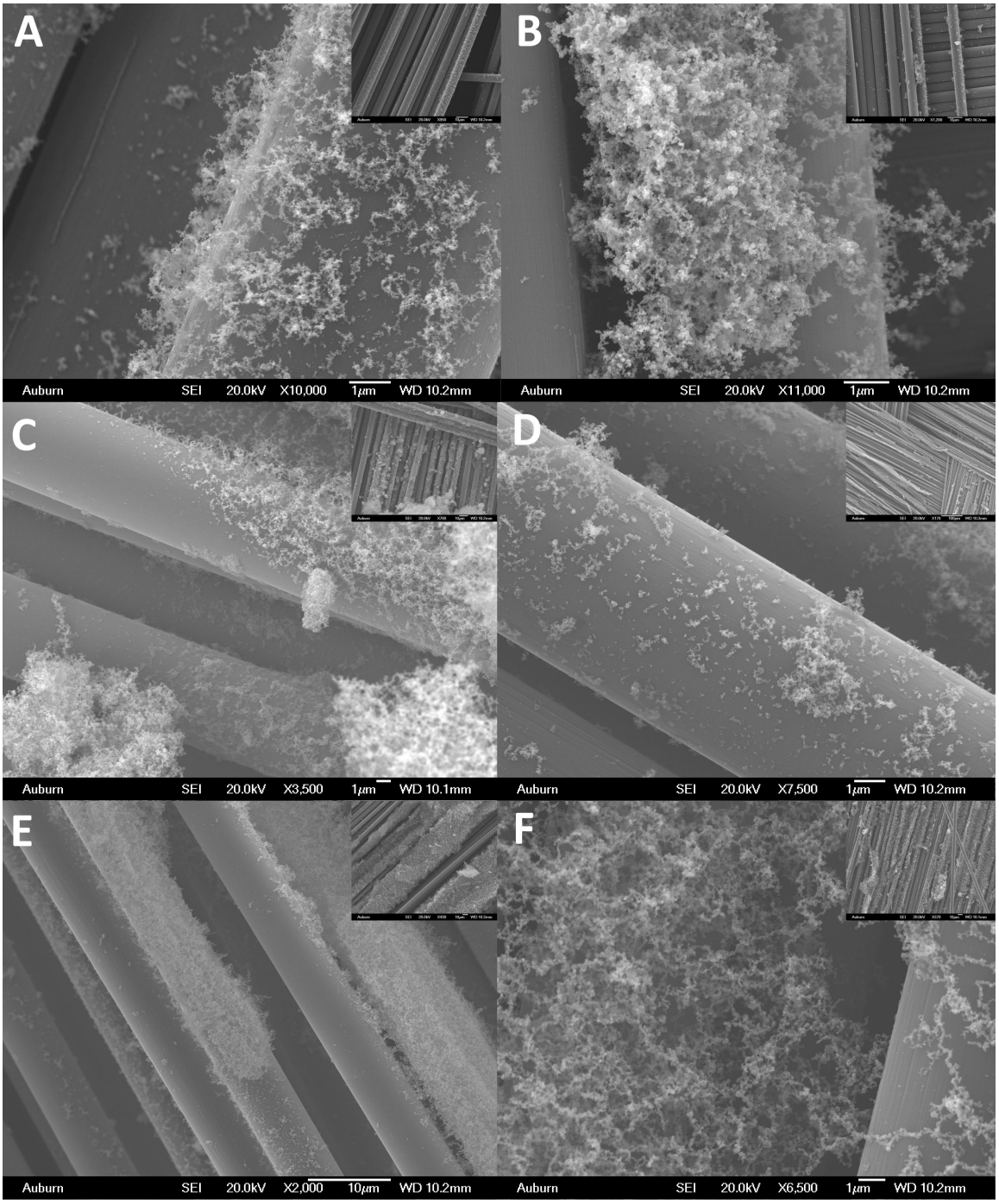

Figure 37. SEM images of carbon fiber fabrics treated with 25 mg (A-C) or 50 mg (D-F) of ferrocene powder after undergoing 1 cycle (A,D), 2 cycles (B, E) or 3 cycles (C, F) of precursor application and microwave processing.

It is also important to note that the orientation of the necklace structures was generally random but none appeared to be anchored to the surface of the fiber. CNT growth perpendicular to the surface of other substrates had been reported, and was the desired orientation for these materials. The deposits of nanostructures on the fibers seemed to encase the fibers rather than grow on them, making them unsuitable for enhancing the interface between the fibers and a matrix material.

The absence of CNT growth and the undesirable orientation of the observed nanostructures may arise from several factors including the distribution of ferrocene on the fabric, the temperature of the substrate, and the retention of active ferrocene species.

8.3.2. Ferrocene Dispersion Methods

In order to achieve uniform growth across the surface of the fabrics several methods for dispersing ferrocene were investigated. These methods were dusting of fixed amounts of ferrocene across the surface, wetting the fabrics with saturated solutions of ferrocene and the spreading of ferrocene-solvent paste mixtures. Solutions and paste mixtures were prepared with either ethanol or toluene. The treated fabrics were allowed to air dry for 5 min before microwave treatment to allow some of the excess solvent to evaporate and to increase the amount of ferrocene retained on the fiber surface. Previous work has shown that the solvents act as a secondary carbon source during the carbonization procedure, facilitating nanotube growth[284,358]. Microwave treatment was carried out at full power for 1 min, leaving the samples uncovered.

Upon microwave treatment, all samples exhibited combustion of the ferrocene precursor along with intense electrical discharge from the edges of the fabric samples. The solution-dispersed samples displayed the most uniform surfaces after microwaving, with no orange residue that would indicate the presence of residual ferrocene. Samples prepared using dry

powders or pastes displayed irregular patches of decomposed material, and in the case of the paste samples, areas of unreacted ferrocene were observed (Figure 38).

SEM images of the fabric samples after treatment (Figure 38) support the initial observations of the microwave processed samples. None of the samples showed CNT growth, only dense formation of the necklace type structures. The samples produced from the ferrocene powders and pastes displayed irregular patches of dense growth, predominantly granular structures with some necklace structures observed as well, mirroring the irregular surface deposits and ferrocene residues visible. The dense patches of growth often surrounded fibers or formed thick mats on the surface of the fabric (Figure 38 A,D,E). Handling of these fabric samples required care as the soot like deposits were easily removed by excessive shifting of the fabric weave or physical contact with the fabric surface.

The solvent dispersed ferrocene samples were much cleaner and produced minimal soot on the fabric surface (Figure 38 B,C). Solvent dispersal yielded better coverage of growth structures across the sample and minimized the build up of large deposits of partially reacted or unreacted precursor. While the coverage seemed to be more uniform, the growth on the fiber surfaces was sparse compared to that of the powder and paste samples. Despite air drying of the samples prior to processing, the use of organic solvents does reduced the amount of ferrocene present on the surface of the fibers and throughout the sample, which would account for the reduced coverage of nanostructured growth.

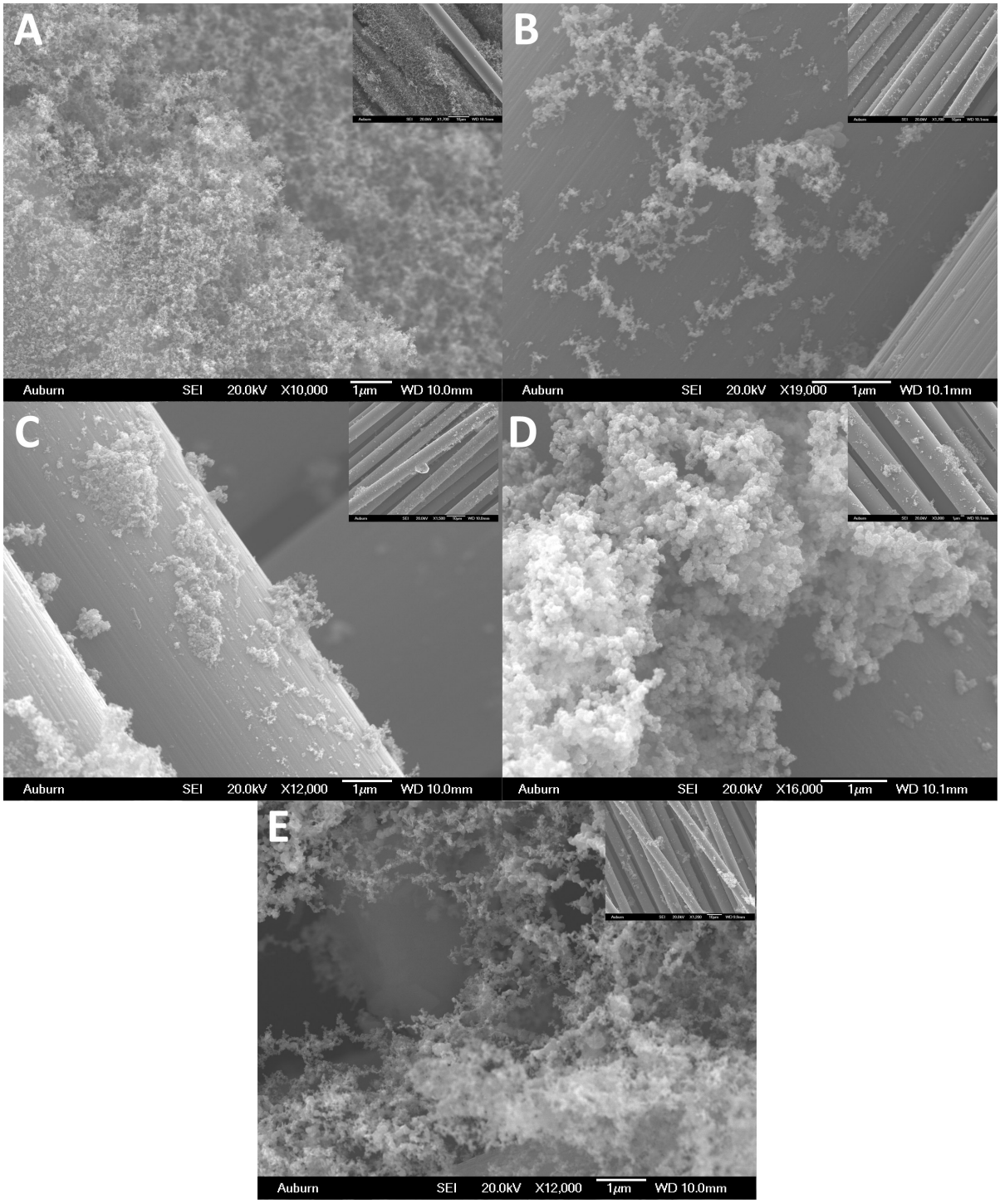

Figure 38. SEM images of carbon fiber fabric treated with different methods of ferrocene dispersion followed by microwave processing. (A) dusting of ferrocene powder, (B) ethanol solution of ferrocene, (C) toluene solution of ferrocene, (D) NMP ferrocene paste, (E) toluene ferrocene paste.

8.3.3. Ferrocene Solutions in Organic Solvents

The dispersal of ferrocene through ethanol and toluene provided improved coverage of growth on the fabric samples. To further investigate the effects of solvent saturated solutions of ferrocene were prepared in ethanol, toluene, ethyl acetate, EG, DEG, NMP, and pyrrolidone. Solvents were chosen based on their various properties including boiling point, dielectric constant, and viscosity (Table 16).

Microwave treatment generates heat, which promotes solvent loss, so solvents with higher boiling points are likely to persist in the reaction environment longer, possibly contributing more significantly as a carbon source during the decomposition of the ferrocene precursor. The dielectric constant of a solvent reflects the susceptibility of the solvent to polarization in an applied electric field. More practically it indicates how a solvent is likely to interact with the applied microwave irradiation, which may be an influencing factor in the excitation and decomposition of ferrocene during processing. Viscosity was also seen as an important solvent property as a more viscous solvent would pass through the fabric sample less readily and thus aid in the even distribution of ferrocene throughout the sample prior to microwave treatment.

Few investigations have been conducted on the solubility of ferrocene in organic solvents, covering many structural variations on alcohols, aliphatic and aromatic hydrocarbons, and some of the more common laboratory solvents[359-361]. While the solubility of ferrocene in some of the chosen solvents has been reported, experimental determination of ferrocene solubilty in ethylene glycol, diethylene glycol, NMP and pyrrolidone have not been reported. Since quantitative transfer of ferrocene to the fabric surface could not be achieved with the chosen application method, only the relative solubility of ferrocene was considered.

Both pyrrolidone and NMP displayed a significant ability to solvate ferrocene, with 20 mL of solution dissolving at least 2.0 g of ferrocene powder, on par with toluene, which had one of the highest solvating capabilities of the solvents recorded in the literature[359,360]. Ethylene glycol and diethylene glycol displayed incredibly low solvation ability, dissolving less than 25 mg of ferrocene in 20 mL. The observed trend in relative ferrocene solubility was toluene ≈ NMP ≈ pyrrolidone > ethyl acetate > ethanol > DEG > EG. Samples were prepared by soaking the fabric in 2 mL of the ferrocene solution, allowing the sample to dry for 5 minutes and then microwaving at full power for 1 min.

Samples prepared with the lower boiling point solvents quickly produced flames as the solvents were vaporized during the initial heating and ignited by the electrical discharge from the fabric. The heat generated during the microwave treatment was enough to dry all of the samples, although the NMP and pyrrolidone solutions left orange ferrocene residues behind on the underside of the fabric sample.

SEM images of the samples showed that in all cases there was no observed CNT growth (Figure 39). The solutions prepared in NMP and pyrrolidone did not yield any necklace type structures, instead forming a thick layer of amorphous deposit around sections of the fiber. The other solvents displayed low to moderate coverage of necklace structures with some visible deposits deeper into the woven structure of the fabric.

Observation of ferrocene residue underneath the fabric samples coupled with an increased presence of nanostructures in between fibers and further below the surface of the fabric indicate that solutions of ferrocene provide significantly greater coverage to the fabric sample as a whole. Additionally, the uniformity of the coverage is greatly enhanced.

Table 16. Properties of solvents used for the dispersal of ferrocene on carbon fiber fabrics.

Solvent	B.P (ºC)	F.P. (ºC)	ε	η (cP)	c_p (J/gK)	μ (D)
Ethanol	78.29	13	25.3	1.074	2.438	1.69
Toluene	110.63	4	2.379	0.56	1.707	0.37
EtOAc	77.11	-4	6.08	0.423	1.937	1.78
EG	197.3	111	41.4	16.1	2.394	2.28
DEG	245.8	124	31.82	30.2	2.307	2.3
NMP	202	96	32.55	1.65	3.105	4.1
pyrrolidone	251	129	28.18	13.3	1.99	3.5

The nature of the solvent does appear to have some influence on the growth of nanostructures on the fabric, although it is unclear what properties of the solvent are responsible for the effect. The electric dipole and dielectric permittivity of the solvent have a significant influence on the heating ability of the solvent under microwave irradiation. Polar molecules, those with greater dipole moments, μ, and dielectric permitivity values, ε, are more easily aligned with the electric field generated by the microwave irradiation. As the field oscillates the molecules attempt to reorient themselves to the new field direction, and this molecular motion is translated into heat. In this application, solvents with high dielectric coefficients would absorb a greater portion of the incoming energy reducing the amount of energy available for the heating of the carbon substrate or the ferrocene precursor. From the SEM results in Figure 39 the higher dielectric solvents (Figure 39 A,D,E,G) did not produce significant nanostructured growth, with the exception of ethanol (Figure 39 A), which has a comparable ε value as pyrrolidone (25.3 and 28.18 respectively) but a substantially lower boiling point. As the ethanol is heated by the

microwave energy it is readily evaporated and subsequently combusted, as evidenced by the flames observed early into the processing. The heat from the flame as well as the early removal of the solvent may contribute to the formation of nanostructures on the fiber surface.

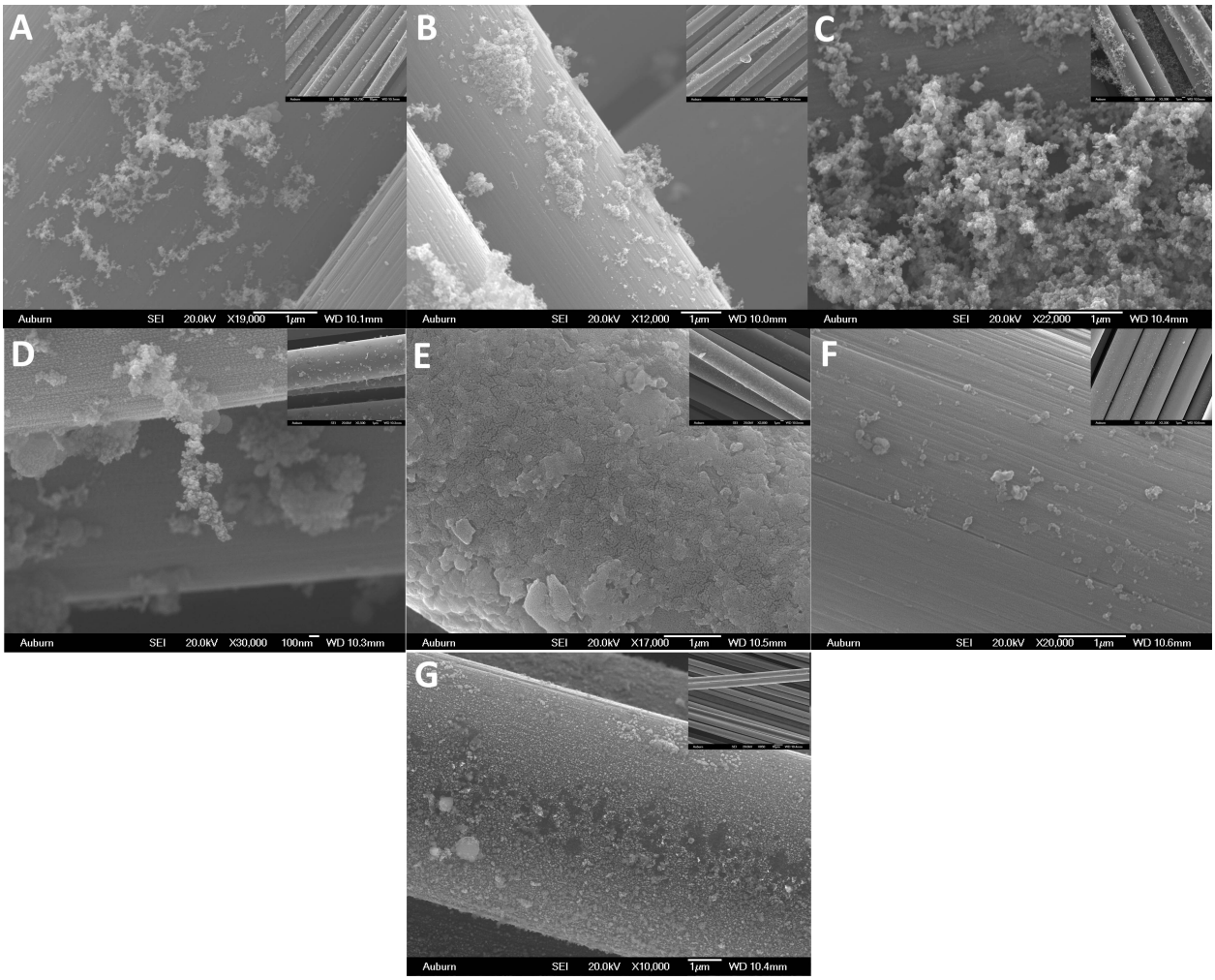

Figure 39. SEM images of carbon fiber fabric treated with saturated solutions of ferrocene in various organic solvents followed by microwave processing. (A) ethanol, (B) toluene, (C) ethyl acetate, (D) NMP, (E) pyrrolidone, (F) EG, (G) DEG.

All of the solvent treated samples were found to be dry after processing indicating that the heating of the sample and solvent is enough to remove even the high boiling point solvents, but fewer and less intense flames were observed. These solvents may be less flammable, and their higher boiling point requires more energy and a longer time to remove from the sample,

which may also influence the growth of nanostructures and decomposition of the ferrocene. These high processing temperatures do not appear to affect the surface of the carbon fibers as no cracking or pitting of the fiber surface was observed.

8.3.4. Ferrocene Suspensions

Although the saturated solutions of ferrocene in ethylene glycol and diethylene glycol did not produce any promising nanostructured growth, the concentration of dissolved ferrocene was quite low, especially in comparison to the other solvents investigated. Additional ferrocene powder was suspended in the saturated solutions to observe whether increasing the amount of precursor with these solvents would lead to improved growth of nanostructures. For these samples, 25-100 mg of finely ground ferrocene powder was suspended in 2 mL of ethylene glycol or diethylene glycol saturated with ferrocene, and the mixture was dispersed on the fabric and allowed to sit for several minutes to thoroughly wet the fibers. The samples were then microwaved at full power for 1 min.

Samples prepared with both solvents displayed the characteristic discharge of energy from the fabric edges as well as the presence of flames on the surface of the fabric. Fine black soot remained on the surfaces and increased in quantity as the amount of ferrocene used increased. Unlike the samples prepared with just the saturated solutions, the ferrocene suspensions produced nanostructured growths on the fiber surface. While primarily necklace type growths, some fibrillar structures were observed intermingled with granular deposits (Figure 40). These fibers appeared to have globular tips, and strongly resembled carbon nanotubes produced in other studies[292,293]. As the amount of ferrocene in the suspension increased so too did the overall growth of nanostructures on the carbon fibers as well as the presence of CNTs.

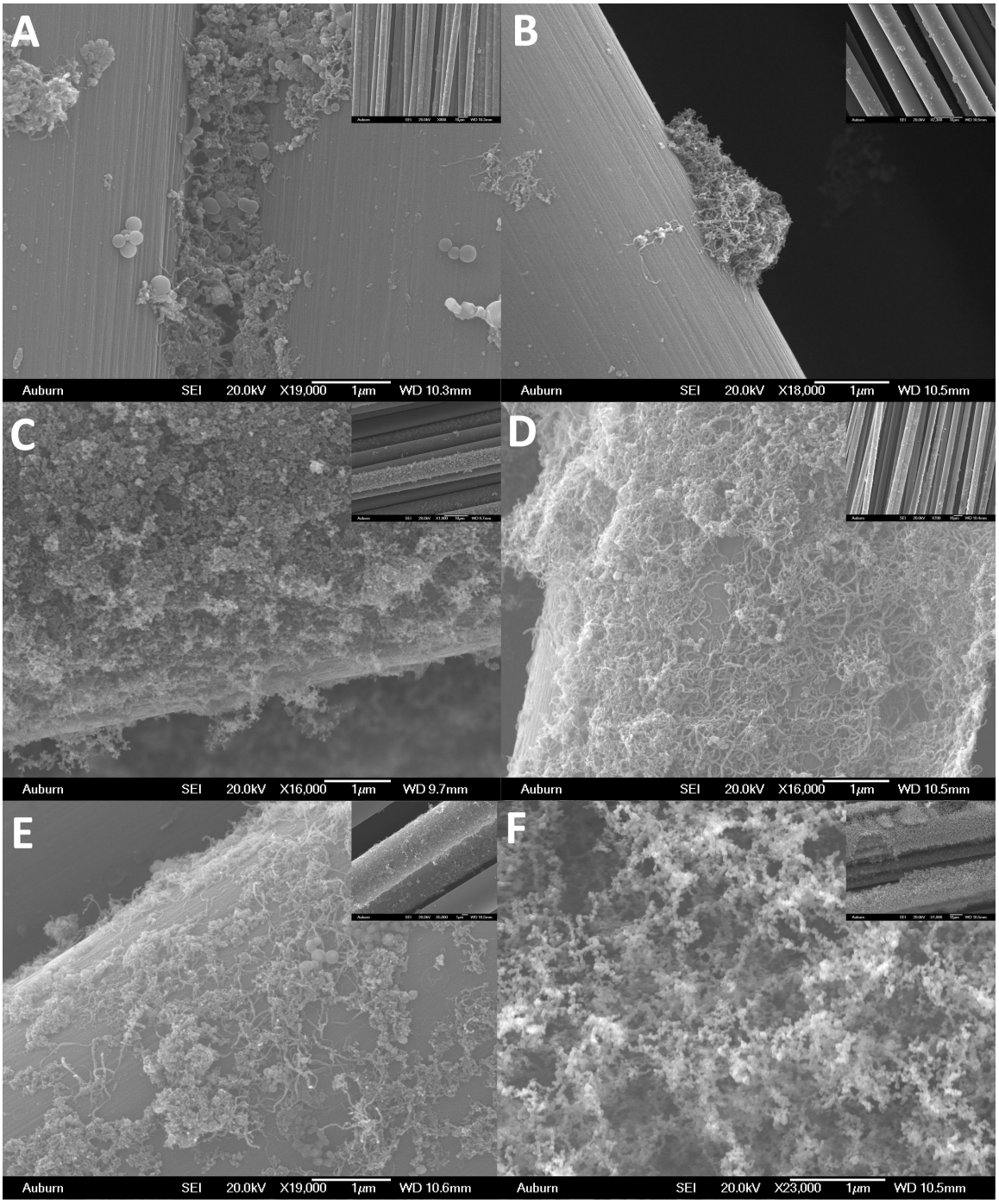

Figure 40. SEM images of carbon fiber fabric treated with saturated solutions of ethylene glycol (A-C) or diethylene glycol (D-F) containing 25 mg (A,D), 50 mg (B,E) or 100 mg (C,F) of suspended ferrocene.

The diethylene glycol suspensions appeared to produce more of the CNT structures than the equivalent ethylene glycol solution, although both did generate CNT growth. It would be

simple to attribute the appearance of CNT structures to the increased presence of ferrocene in the samples, but several of the tested ferrocene solutions contained significant amounts of the organometallic precursor and did not yield the desired nanostructured growth. In light of this, it would seem that solvation of the ferrocene clusters is in fact detrimental to the conversion of ferrocene into CNTs or other nanostructures. The ferrocene suspension results in localized clusters of high precursor concentration while the surrounding solvent minimizes the loss of precursor through sublimation while heating, as well as providing an additional carbon source for growth.

8.4. Further Development.

Following the growth of CNTs on the fabric surface utilizing a combination of applied diethylene glycol solvent containing suspended ferrocene powder, further testing was carried out to try and improve growth characteristics and achieve the desired orientation of CNT growth on the surface of the fibers. Parameters investigated included microwave time, microwave power, the use of an alumina kiln, introduction of polymeric stabilizers, and the implementation of different microwave active heat sources.

8.4.1. Microwave time and power

With CNTs being produced on the fabric samples, changes in microwave time and power were investigated as parameters that could easily influence the decomposition of ferrocene and the growth of CNTs on the sample. Samples were prepared with 50 mg ferrocene suspension in 2 mL DEG and processed at 100, 80, 50 and 20 percent power levels for various times, or 100 mg of ferrocene suspended in 2 mL of DEG and processed at 100 percent power for 1 or 3 minutes.

Samples using the 50 mg suspension were processed at various power levels for 1 minute to determine the effect of the overall power level on the quality or types of growths achieved (Figure 41). One minute at 20 percent power produced dispersed patches of loosely aggregated CNTs on the surface of the fibers, while increasing the power level appeared to increase the number of necklace or granular growths present while the CNTs formed appeared in dense, tightly interwoven clusters on the fibers. This trend runs contrary to the anticipated results as increasing the microwave power should generate more heat to decompose the ferrocene precursor to facilitate CNT formation.

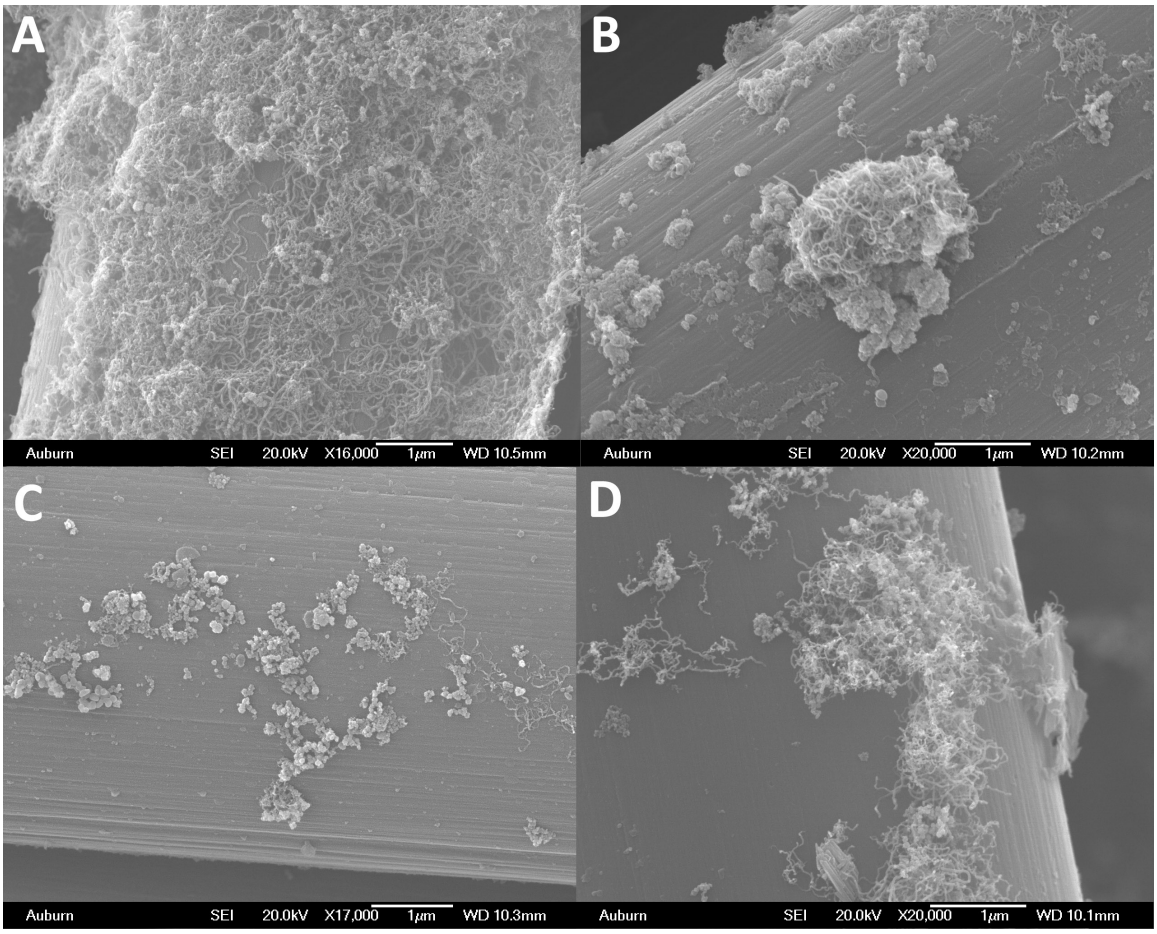

Figure 41. SEM images of carbon fiber fabric treated with saturated solutions of ferrocene in diethylene glycol containing 50 mg of suspended ferrocene. Samples were processed in the microwave for 1 min at 20% (A), 50% (B), 80% (C), and 100% (D) power levels.

Extending the microwave time for the 50 mg ferrocene, 20 percent power samples to 5, 7 and 9 minutes did not improve the growth of CNTs on the samples (Figure 42A-D). Increasing the microwave time actually reduced the overall presence of nanostructured growths on the surface, transitioning from dispersed deposits of CNTs to a prevalence of granular structures before leaving only a thin film on the surface of the fibers with no distinct structural characteristics.

Samples prepared with 100 mg of ferrocene and processed at full power for 1 and 3 minutes demonstrated the opposite behavior in which increasing the microwave time improved the amount of CNTs formed (Figure 42E,F). Treatment of the 100 mg sample at 20 percent power for 7 minutes did not yield any CNT growth, instead producing widespread deposits of granular structures.

From these rather incongruous results it would seem that the growth of CNTs on carbon fiber fabric does display some relationship between microwave power, duration of exposure and concentration of precursor. One issue that complicates the elucidation of this relationship is the way in which the microwave oven implements the gradation of power levels. Rather than modulating the power output of the magnetron, the full power of the microwave is simply switched on and off to supply the desired reduction in power as an average over the time the sample is microwaved. This means that the samples processed at a lower power level were exposed to short bursts of high intensity microwave energy with no exposure in between while the samples prepared at higher power levels received longer periods of exposure.

In samples with lower concentrations of ferrocene, the short bursts of high energy may promote decomposition and activation of the precursor while the intervening time allows for reaction of the active species with solvent or precursor molecules in the vicinity. The decrease in

nanostructured growth with longer times could result from an ablative effect as the formed CNTs conduct the short bursts of microwave energy and are broken apart. Higher concentrations of ferrocene may require more energy to reach the necessary threshold of active species and thus benefit from the higher power level or longer time.

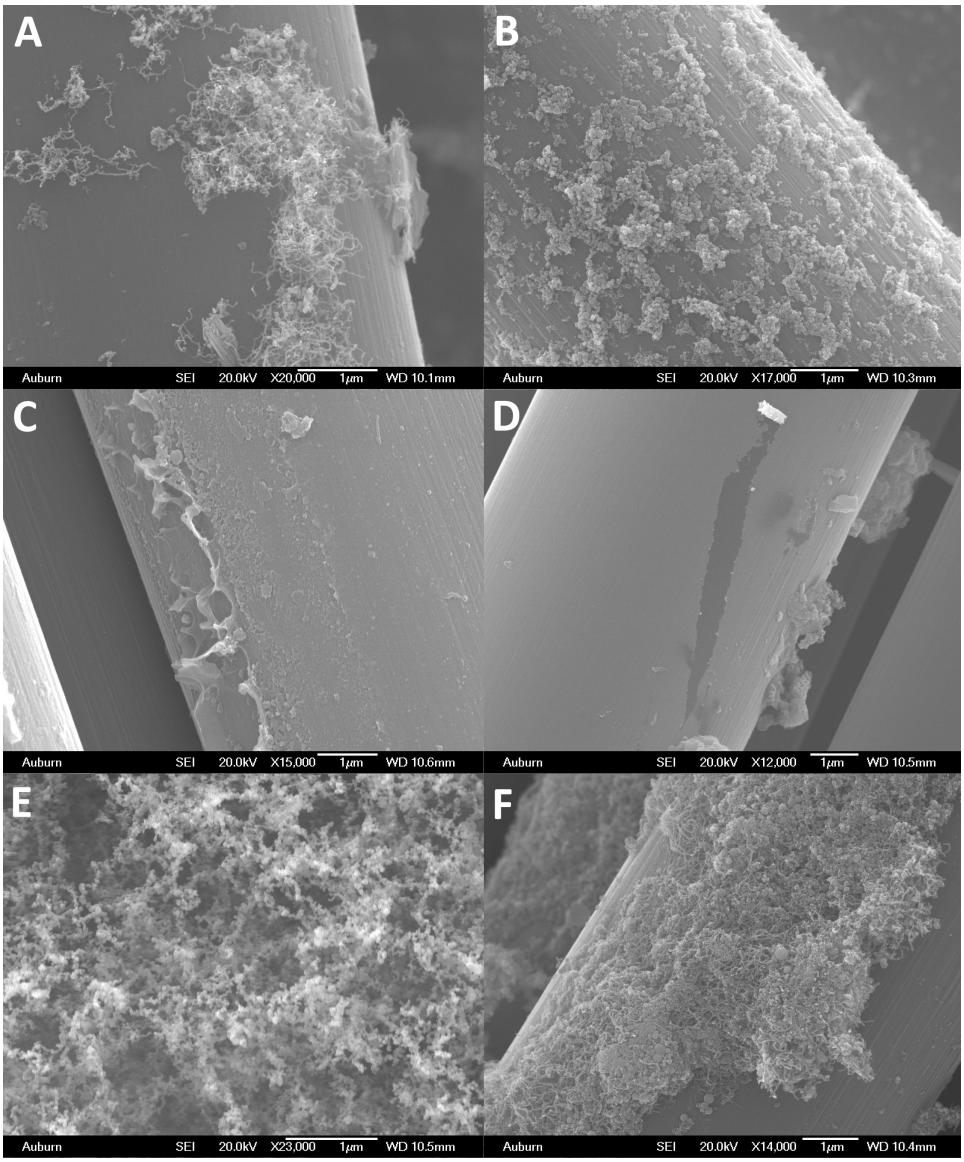

Figure 42. SEM images of carbon fiber fabrics treated with saturated solutions of ferrocene in diethylene glycol containing 50 mg (A-D) or 100 mg (E,F) of suspended ferrocene. Samples containing 50 mg of ferrocene were processed at 20% power for 1 min (A), 5 min (B), 7 min (C) or 9 min (D) while samples containing 100 mg of ferrocene were processed at 100 % power for 1 min (E) or 3 min (F).

8.4.2. Covered vs Uncovered.

The operative idea in implementing the alumina kiln was to create an enclosed environment around the fabric to retain vaporized ferrocene and solvent, which may improve growth by increasing the concentration of active components near the fabric. The kiln had the additional benefit of insulating the microwave oven from the energy discharged by the fabric edges during treatment. Alumina was chosen as a kiln material due to its transparency to microwave radiation, thus minimally affecting the intensity of energy reaching the sample.

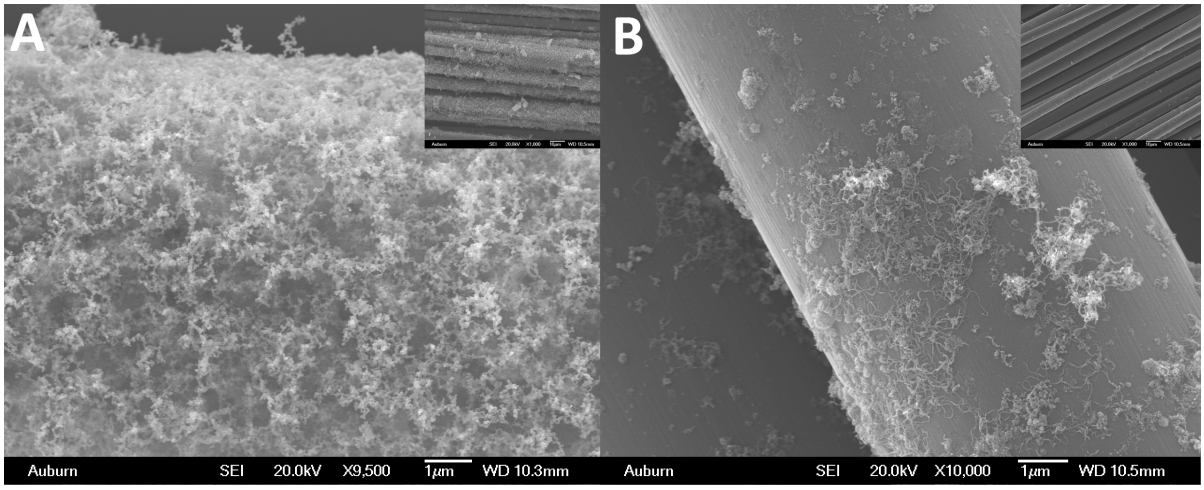

Figure 43. SEM images of carbon fiber fabric treated with a saturated solution of ferrocene in diethylene glycol containing 100 mg suspended ferrocene and processed at 100% power for 1 min uncovered (A) or in an alumina kiln (B).

The samples processed in the alumina kiln displayed less dense coverage of deposits on the surface with CNTs present, while the uncovered samples exhibited high coverage of dense deposits but mainly necklace type growths with some CNTs (Figure 43). Although the alumina used to form the walls of the kiln are microwave transparent, they are effective thermal insulators and retained a significant amount of the heat generated by the interaction of carbon fibers and microwave energy. If samples were removed from the kiln quickly enough after the completion of microwave processing, the fabric could be observed cooling from a red hot state, which is not

observed in the uncovered samples. The excess heat trapped in the kiln facilitates evaporation of the solvent and sublimation of the ferrocene precursor removing both from the surface of the fabric. The higher temperature may also promote the formation of CNTs, evidenced by more visible CNT clusters on the covered sample compared to the uncovered sample.

8.4.3. Polymeric Additives

A variety of long chain polymers were used as a stabilizing agent as well as a potential binder to keep ferrocene closer to the fiber surface to promote the growth of CNTs and possibly achieve the perpendicular growth of nanostructures on the fibers. The polymers chosen were poly(N-vinylpyrrolidone) (PNVP), polyethylene glycol (PEG), and poly(vinyl alcohol) (PVA) and were either mixed dry with ferrocene or mixed into ferrocene-DEG suspensions. The polymer additives were used in a 1:1 weight ratio with ferrocene.

The dry mixed polymer-ferrocene powders were dusted across the surface of the fabric using the same mesh from previous experiments. In all samples the surface layer of fibers was almost entirely covered with dense, uniform growth of nanostructures (Figure 44B,D,F). On closer inspection the nanostructures were revealed to be the necklace-like growths, with no CNTs present. Also in these samples were larger clusters, tens to hundreds of micrometers in size, covered in the necklace structures either in groups or along sections of fibers. They appear to be particles of the polymer that agglomerated during the microwave treatment process. The extensive coverage seems to indicate that the presence of the polymer does facilitate the growth of ferrocene based nanostructures, or at the very least improves the retention of the nanostructures on the fabric. The heavy deposits coupled with the lack of penetration further into the fabric sample produces a dense surface coating that is unlikely to provide any real enhancement to the properties of the fabric sample.

The polymer-ferrocene solutions produced similar results following microwave treatment, although there appeared to be slightly improved coverage of fibers below the uppermost layer (Figure 44A,C,E). The abundance of nanostructured growths was also diminished, with the necklace growth being replaced by granular clusters or larger expanses of agglomerated material.

In both dry and solution based samples, the addition of the polymer inhibited the formation of CNTs but increased amount of material retained on the fabric surface. Dry mixing ferrocene with PVA gave the most necklace-like nanostructures as well as minimal agglomeration of the deposits on the fiber surface. The other two polymers yielded large clusters of material or coverage of the fibers with necklace growth occurring on top of these deposits. For the solvated samples, PVA again produced the most even coverage on the fibers, with individual fibers visible and distinguishable. Both PEG and PNVP created thick solid deposits entirely covering or obscuring the surface fibers.

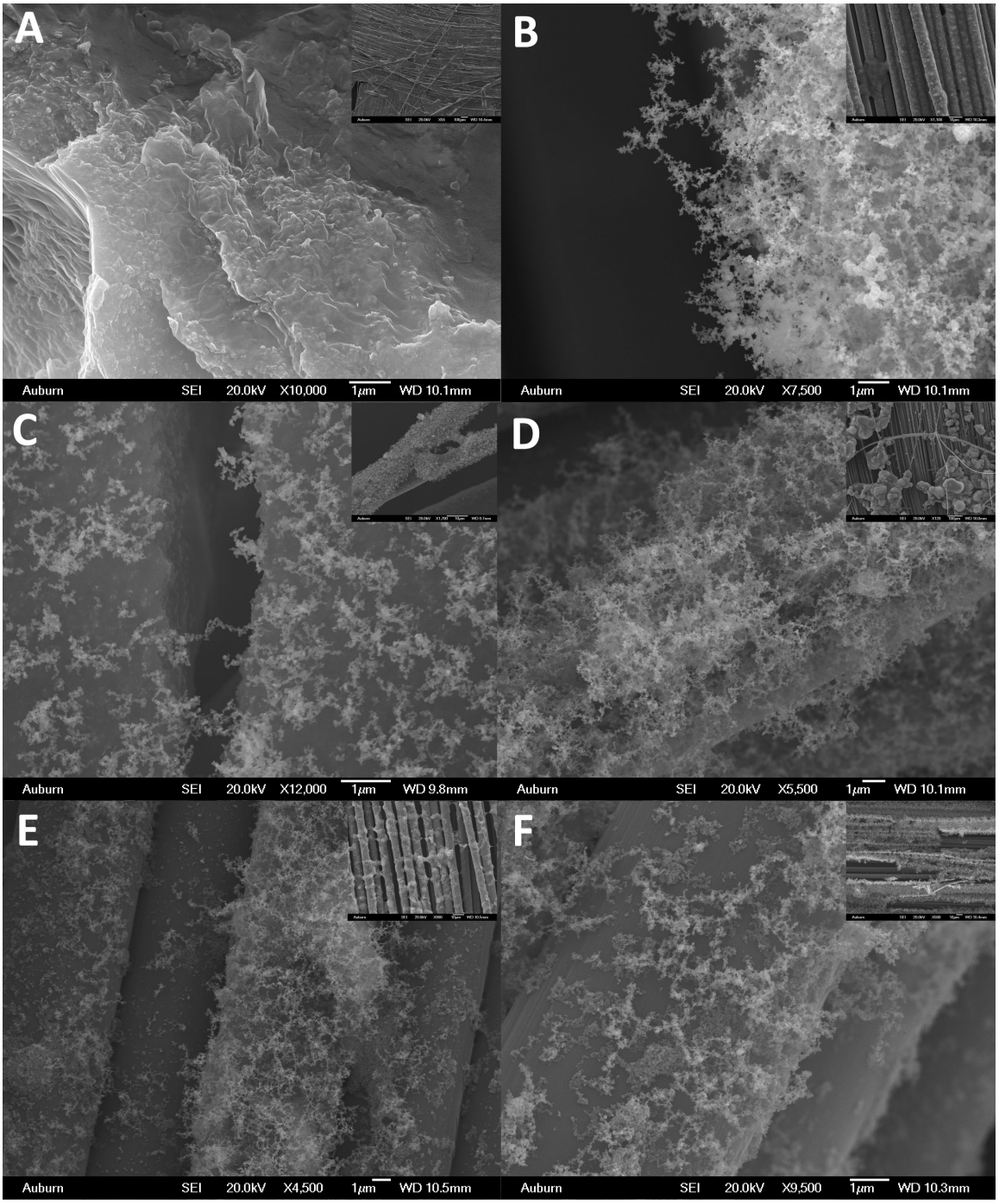

Figure 44. SEM images of carbon fiber fabric treated with 100 mg of ferrocene mixed with 100 mg of poly(ethylene glycol) (A,B), poly(N-vinyl pyrrolidone) (C,D), or poly(vinyl alcohol) (E,F). Mixtures of the dry powders (A,C,E) or suspensions in diethylene glycol (B,D,F) were used.

8.4.4. Ignition Sources

In the hopes of further enhancing the growth of CNTs on the carbon fiber surface, several additional microwave reactive materials were introduced. Polypyrrole nanofibers and granules, and graphene nanoparticles were utilized to help generate favorable conditions for CNT growth in the center of the sample due to the observed discharge of energy from the edges of the samples and the inherent conductivity of the fibers.

Both PPy and graphene nanomaterials have shown to be efficient promoters of CNT growth in microwave treatment, even in small quantities to facilitate growth, 10 mg of PPy, either as nanofibers or granules, or graphene nanoparticles were dispersed in 2 mL of DEG containing 100 mg of ferrocene powder. The solution was then applied to the fabric sample, which was allowed to sit for 5 min before microwaving at full power for 1 min.

The PPy samples displayed more vigorous burning of the solvent-precursor mixture upon irradiation compared to samples prepared without the added conducting polymer. Following treatment, the surface of the fiber was covered in fine black soot with some small deposits visible with the naked eye. Closer investigation revealed some CNT or fiber-like structures on the surface of the carbon fibers as well as the necklace type growths (Figure 45A). However, these structures appeared separate from any necklace growths, unlike growth observed in the ferrocene-EG/DEG suspensions (Figure 41). With the low loading of PPy nanofibers in solution, these small deposits are likely the result of dispersed PPy nanofibers undergoing carbonization during treatment. When PPy granules were used small granular deposits were observed on the surface of the fiber along with necklace structures (Figure 45B). Similar to the PPy nanofibers sample, the smaller granules are the carbonized conducting polymer while the larger necklace structures are the decomposition products from the added solvent/ferrocene mixture.

Samples containing graphene nanoparticles also displayed more intense combustion during the microwave treatment process, and yielded primarily necklace growths although some CNTs could be seen growing from granular nanoparticles, likely the added graphene (Figure 45C). While minor CNT growth was achieved using graphene as an additional heat source, the structures originated from the added nanoparticles, rather than along the fiber.

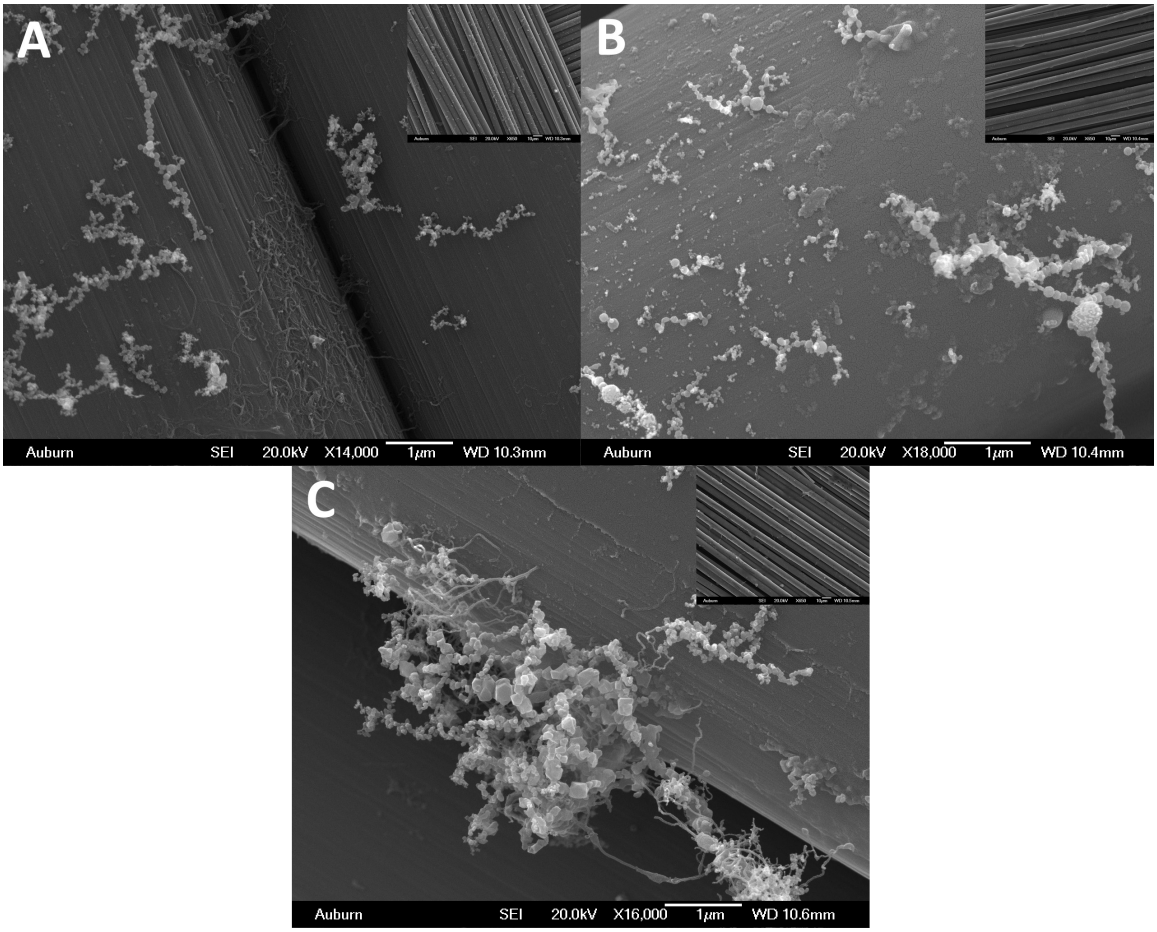

Figure 45. SEM images of carbon fiber fabric treated with a saturated solution of ferrocene in DEG containing 50 mg of suspended ferrocene powder and 1 mg of polypyrrole nanofibers (A), polypyrrole granules (B), or graphite nanoparticles (C) then processed at 100% power for 1 min.

8.5. Summary

The microwave assisted formation of carbon nanotubes from the rapid decomposition of ferrocene has been shown as an effective, low cost synthetic route for a variety of substrates including conducting polymers, indium tin oxide, and milled carbon fibers. Extension of this methodology to carbon fiber fabrics was investigated as a low cost, scalable method to producing a high-performance reinforcement material for advanced composite applications. A variety of parameters were investigated in this pursuit including ferrocene concentrations, methods of ferrocene dispersal, solvent effects, microwave time and power, and the inclusion of polymeric and conducting additives.

Formation of carbon nanotubes on the fiber surfaces proved to be a challenging task, with the bulk of structures produced being iron oxide necklace structures formed around the fibers rather than in the desired perpendicular orientation. Some CNT-like structures were found when ferrocene powders were suspended in ethylene glycol and diethylene glycol solvents, but not in pure solutions of ferrocene in those solvents. One major disadvantage observed in the microwave processing of carbon fiber fabrics was discharging of absorbed energy as plasma from the fiber ends. It seemed that the high conductivity of the fibers directed the energy away from the center of the fibers where growth is desired, thus failing to generate the necessary environment for the decomposition of ferrocene into CNTs across the fabric. However, the growth of CNT-like structures through a combination of solvent and ferrocene dispersion points to potential for future success and a strong link between the nanostructured growth and ferrocene-solvent interactions.

Additional investigation into the surface energy of the carbon fibers and methods for localizing or concentrating the absorbed microwave energy would likely yield significant

improvement in the growth of CNTs on the fabric substrate. From the observed results, elucidation of the relationship between precursor, solvent, and dispersion would also provide tools for optimal growth of nanostructures on the fiber surface.

9. Summary and Future Work

9.1. Dissertation Focus and Findings

Organic conductors present a rich and varied field of study comprised of many facets and unique materials. Two classes of materials from this field, intrinisically conducting polymers and pure carbon materials, are of significant interest due to their rapidly growing application to electronics, devices, and composites with an emphasis placed on the development of nanoscale materials. In order to further expand the utility of these materials, derivatization and modification is essential. This work has focused on the modification of these two classes of materials, although through different routes.

The first section focused on the chemical modification of polyaniline powders using amines via reductive addition to the fully oxidized polyaniline pernigraniline base. Polyaniline is the most widely studied of the intrinsically conducting polymers due to the low cost of reagents, ease of synthesis and unique reversible doping ability. The synthesis of polyaniline derivatives can be achieved through the polymerization of functional monomers or the addition of substituents post-polymerization. The addition of amines follows this second route, with the objective of introducing the substituents without eroding pre-established polymer morphology. The preservation of morphology was important due to the large body of research dedicated to the synthesis of various unique architectures that can be used to tailor the final properties of the polymer, and a relative lack of literature on reestablishing complex morphologies from the solution state. Amines also represent a common functional moiety present in compounds

including proteins, pharmaceuticals, dyes and other industrially or commercially important molecules. By exploring the addition of amines to polyaniline, the potential for new derivatives and applications is greatly expanded.

The addition of aliphatic amines was found to proceed in a several common organic solvents as well as in water, producing low to moderate yields at room temperature over the course of 24 hours. The use of organic solvents led to significant erosion of the polymer morphology, and produced comparable yields to the reaction carried out in water. The exception was the use of NMP as a reaction medium which gave a significantly higher yield as a result of solvation providing greater access of the nucleophile to the polymer. Higher reaction temperatures and increased concentration of amines also improved the reaction yields, but at the cost of the pre-established morphology. Increased substitution about the amine nitrogen also led to lower yields, with diethylamine and triethylamine giving lower yields than hexylamine.

The observed influence of amine structure on the reaction yields prompted investigation of the steric and electronic factors involved. UV-Vis spectrosocopy was used to monitor the decrease in the characteristic absorption of the pernigraniline base as the reductive addition of amines led to the formation of the substituted emeraldine base. Comparison of the observed reaction rates to reported steric values for the substituents indicated that greater steric bulk slowed the reaction, but did not wholly account for the observed trends. A study of the electronics of the reaction was carried out using para-substituted aromatic amines and yielded a linear Hammett relationship with a reaction constant of -0.32, indicating a build up of positive charge in the reaction transition state. The mechanism of the reductive addition of nucleophiles to polyaniline remains largely unexplored in the literature, and no previous reports investigating the steric or electronic properties of nucleophiles for the reaction could be found.

The use of polyamines in the reductive addition to pernigraniline allows for cross-linking and a demonstration of the potential application of adding amines. Under high concentrations the added polyamines are able to link the polyaniline into a solid network of covalently cross-linked polyaniline. Dilute conditions yield polyamine-functionalized polyanilines that can then be used to cross-link epoxy based resins. Thermal characterization showed that increasing the length of the aliphatic chain between amine groups improved the thermal stability of polyaniline networks based upon the extrapolated onset of degradation. Branching of the amine led to a decrease in the thermal stability, but all cross-linked samples showed a significant improvement in stability over the uncross-linked parent polymer. For the curing of epoxy by polyamine-functionalized polyanilines, increasing the length of the added amine led to a decrease in curing enthalpy indicating reduced reactivity. This behavior is explained by greater separation from additional reaction sites that would facilitate cross-linking with the epoxy, since DETA and TETA contain secondary amine groups in the chain and displayed greater curing enthalpies than their diamine counterparts.

This work presents the first comprehensive exploration of the functionalization of polyaniline powders through the reductive-addition of amines, as well as probing the underlying kinetics of the reaction. The data obtained through the Hammett study of the reaction provides new information on the nature of the transition state and further informs previously proposed mechanisms for the addition of amines to the quinoid ring. Furthermore, the introduction of multifunctional amines to polyaniline offers a new method for the formation of cross-linked polyaniline networks and the potential application of amine functionalized polyanilines as a combination filler/curing agent for epoxy resins. Exploring and understanding the reductive-

addition of amines to polyaniline opens a new avenue for advanced conducting materials and broader applications of polyaniline in composites and other applications.

The second section of this work focused on the derivatization of pure carbon materials through surface decoration with carbon nanotubes or metal oxide nanowires. The formation of these nanostructures was accomplished through a microwave assisted processing method that presents a faster, low cost and easily scalable alternative to traditional synthetic approaches such as CVD. This method, also known as the poptube approach, can be used to simultaneously convert conducting polymers into carbon while facilitating the decomposition of ferrocene into carbon nanotubes or organometallic precursors into metal oxides.

The carbonization of conducting polymers allows for unique carbon nanostructures to be produced such as hollow carbon spheres, which have shown potential for electrochemical and energy storage applications. Latexes of polystyrene nanospheres were used as templates for the polymerization of pyrrole, producing core-shell structures of controlled diameter ranging from 80-240 nm. The template could then be removed yielding hollow polypyrrole nanospheres which were then be carbonized under microwave irradiation in the presence of ferrocene or metal carbonyls to produce surface decorated hollow carbon nanospheres in a single step. SEM and TEM confirmed the desired nanoscale features, while spectroscopy and thermal analysis showed complete removal of the polystyrene templates. EDX was effective in confirming the elemental composition of the carbon nanotubes and iron oxide nanowires grown on the surface of the nanospheres.

In addition to utilizing the poptube approach to introduce nanostructures to the surface of hollow carbon nanospheres, an initial investigation was conducted with the aim of growing carbon nanotubes on the surface of carbon fiber fabrics. A variety of parameters were tested

including ferrocene dispersion methods, the use of organic solvents, microwave time and power, as well as the presence of polymeric and conductive additives. While most parameters yielded necklace type growths of iron oxide, samples treated with ethylene glycol or diethylene glycol containing suspended ferrocene particles yielded mats of CNT-like structures around the fibers. While the desired growth would be oriented perpendicular to the fiber surface, the obtained nanostructures represent a promising first step. One challenging aspect in extending the poptupe synthesis approach to long carbon fibers is the conductive nature of the fiber which directs energy away from the center of the fabric sample and discharges as plasma from the fiber ends. Additional exploration of synthesis parameters, as well as treatments to the fiber surface are likely to lead to further developments and at the very least a more comprehensive understanding of the factors that influence the microwave assisted synthesis of carbon nanotubes.

Through these varied projects is the common thread of developing and exploring the derivatization of organic conductors. The chemical functionalization of polyaniline with amines was supported by an exploration of the steric and electronic factors and applied to the synthesis of cross-linked polyaniline networks, while microwave processing of polypyrrole or carbon fibers with ferrocene yielded novel materials comprised of surface decorated carbon structures. Each of these projects further advances the efforts to produce unique materials for the rapidly changing landscape of materials science.

9.2 Future Work and Development

These projects also offer the opportunity for continued development and exploration of their scientific potential. In the case of the amine functionalization of polyaniline continued optimization of the reaction conditions and parameters is necessary to improve the reaction yields, along with more detailed characterization of the products to determine the distribution of

added functional groups along the polymer backbone. Conducting second order kinetic experiments would provide greater detail on the reaction mechanism and elucidate the interaction between nucleophile and polymer in the reductive-addition reaction. Expansion of the substrate scope would serve to further broaden the potential application of amine-derivatized polyaniline as well. Investigation of the mechanical properties of polyaniline-amine cured resins should also be conducted to evaluate the performance and possible advantage of polyaniline based curing agents over traditional systems employing polyaniline fillers and small molecule curing agents.

The surface decoration of carbons also presents avenues for further investigation. The electrochemical and catalytic performance of CNT or MONW decorated hollow carbon nanospheres requires study to determine if the introduction of these surface structures confers new or significant advantages over more traditional materials or even non-decorated carbon nanostructures. The surface modification of carbon fiber fabrics via a microwave-assisted approach also bears further investigating. While some progress was made using ferrocene-solvent suspension, the interaction of variables affecting the decomposition of ferrocene and the growth of CNTs remains unclear. Evaluation and comparison of substrate surface energies may provide insight into why CNT growth can be achieved with some materials and not others, while treatment of the carbon fiber fabrics prior to microwave processing may offer the solution to enhancing CNT growth. If uniform growth can be achieved on the fabric surface then incorporation into lamellar composites for mechanical testing would also be worth investigating.

References

1. Wise, D. L.; Wnek, G. E.; Trantolo, D. J.; Cooper, T. M.; Gresser, J. D. Electrical and optical polymer systems. Marcel Dekker: New York, 1997; 23.

2. Bigg, D. M.; Stutz, D. E. Plastic composites for electromagnetic interference shielding applications. *Polym. Compos*. **2004**, *4* (1), 40-46.

3. King, J. A.; Tucker, K. W.; Vogt, B. D.; Weber, E. H.; Quan, C. Electrically and thermally conductive nylon 6,6. *Polym. Compos.* **1999**, *20* (5), 643-654.

4. Li, J.; Kim, J.-K. Percolation threshold of conducting polymer composites containing 3D randomly distributed graphite nanoplatelets .*Compos. Sci. Technol*. **2007***, 67* (10), 2114-2120.

5. Sichel, E. *Carbon black- polymer composites*. Marcel Dekker: New York, 1982; 53.

6. Chen, P.-W.; Cheng, D. D. L Improving the electrical conductivity of composites comprised of short conducting fibers in a nonconducting matrix: The addition of a nonconducting particulate filler. *J. Electron. Mater.* **1995**, *24* (1), 47-51.

7. Wang, Y.; Chen, K. S.; Mishler, J.; Cho, S. C.; Androher, X. C. A review of polymer electrolyte membrane fuel cells: Technology, applications, and needs on fundamental research. *Appl. Energy* **2011**, *88*, 981-1007.

8. Croce, F.; Appetecchi, G. B.; Rensi, L.; Scrosati, B. Nanocomposite polymer electrolytes for lithium batteries *Nature* **1998**, *394*, 456-458.

9. Meyer. W.H. Polymer Electrolytes for Lithium-Ion Batteries. *Adv. Mater.* **1998**, *10* (6), 439-448.

10. Writon, M. S.; Schrock, R. R. Well-defined redox-active polymers and block copolymers prepared by living ring-opening metathesis polymerization. *J. Am. Chem. Soc.* **1992**, *114* (11), 4150-4158.

11. Shirikawa, H.; Louis, E. J.; MacDiarmid, A. G.; Chiang, C. K.; Heeger, A. G. Synthesis of electrically conducting organic polymers: halogen derivatives of polyacetylene, $(CH)_x$ *J. Chem. Soc. Chem. Commun.* **1977**, *0*, 578-580.

12. Park, S.-M.; Lee, H. J. Recent Advances in Electrochemical Studies of π-Conjugated Polymers. *Bull. Kor. Chem. Soc.* **2005**, *26* (5), 697-706.

13. Saroop, M.; Ghosh, A. K.; Mathur, G.N. Polyaniline based conductive polymers- an overview. *Int J Plast Technol*. **2003**, *7*, 41-61.

14. Ciric-Marjanovic, G. Recent advances in polyaniline research: Polymerization mechanisms, structural aspects, properties and applications. *Synth. Met.* **2013**, *177*, 1-47.

15. Cho, M. S.; Park, S.Y.; Hwang, J. Y.; Choi, J. C. Synthesis and electrical properties of polymer composites with polyaniline nanoparticles. *Mater. Sci. Eng. C.* **2004**, *24*, 15-18.

16. Rao, P. S; Subrahmanya, S.; Sathyanarayana, D. N. Synthesis by inverse emulsion pathway and characterization of conductive polyaniline-poly(ethylene-co-vinyl acetate) blends. *Synth. Met.* **2003**, *139*, 397-404.

17. MacDiarmid, A.G. "Synthetic Metals": A Novel Role for Organic Polymers (Nobel Lecture). *Angew. Chem. Int. Ed.* **2001**, *40*, 2581-2590.

18. Green, A.G.; Woodhead, A.E. CCXLIII- Aniline-black and allied compounds. Part I. *J. Chem. Soc., Trans.* **1910**, *97*, 2388-2403.

19. Masters, J. G.; Sun, Y.; MacDiarmid, A.G.; Epstein, A. J. Polyaniline: Allowed oxidation states. *Synth. Met.* **1991**, *41*, 715-718.

20. Asturias, G. E.; MacDiarmid, A. G.; McCall, R. P., Epstein, A. J. The oxidation state of "emeraldine" base. *Synth*. *Met*. **1989**, *29*, 157-162.

21. Focke, W.W.; Wnek, G.E.; Wei, Y. Influence of oxidation state, pH, and counterion on the conductivity of polyaniline. *J. Phys. Chem.* **1987**, *91* (22), 5813-5818.

22. Ray, A.; Asturias, G.E.; Kershner, D.L.; Richter, A.F.; MacDiarmid, A.G.; Epstein, A.J. Polyaniline: Doping, structure and derivatives. *Synth*. *Met*. **1989**, *29*, l41-l50.

23. Bhadra, S.; Chattopadhyay, S.; Singha, N. K.; Khastgir, D. Improvement of conductivity of electrochemically synthesized polyaniline. *J. Appl. Polym. Sci.* **2008**, *108*, 57-64.

24. Ryu, K. S.; Kim, K. M.; Park, Y. J.; Park, N.-G.; Kang, M. G.; Chang, S. H. Redox supercapacitor using polyaniline doped with Li salt as electrode. *Solid State Ionics* **2002**, *152*, 861-866.

25. Sarno, D. M.; Manohar, S. K.; MacDiarmid, A. G. Controlled interconversion of semiconducting and metallic forms of polyaniline nanofibers. *Synth. Met.* **2005**, *148*, 237-243.

26. Elsenbaumer, R.L.; Jen, K.-Y.; Miller, G. G.; Eckhardt, H.; Shacklette, L. W.; Jow, R. Poly (alkyl thiophenes) and Poly (substituted heteroaromatic vinylenes): Versatile, Highly Conductive, Processible Polymers with Tunable Properties. In *Electronic Properties of Conjugated Polymers;* Kuzmany H., Mehring M., Roth S., Eds.; Springer Series in Solid-State Sciences; Springer: Berlin, Heidelberg, 1987; vol 76, 400-406.

27. Neoh, K. G.; Kang, E. T.; Tan, K. L. A comparative study on the structural changes in leucoemeraldine and emeraldine base upon doping by perchlorate. *J. Polym. Sci. Part A.* **1991**, *29*, 759-766.

28. Cao, Y.; Andreatta, A.; Heeger, A.J.; Smith, P. Influence of chemical polymerization conditions on the properties of polyaniline. *Polymer*. **1989**, *30*, 2305-2311.

29. Abdiryim, T.; Zhang, X.-G.; Ruxangul, J. Comparative studies of solid-state synthesized polyaniline doped with inorganic acids. *Mater. Chem. Phys.* **2005**, *90*, 367-372.

30. Kulkarni, M. V.; Viswanath, A. K.; Marimuth, R.; Seth, T. Synthesis and characterization of polyaniline doped with organic acids. *J. Polym. Sci. A.* **2004**, *42*(8), 2043-2049.

31. Bhadra, S.; Khastgir, D.; Singha, N. K.; Lee, H. H. Progress in preparation, processing and applications of polyaniline. *Prog. Polym. Sci.* **2009**, *34*, 783-810.

32. Huang, W.-S.; Humphrey, B. D.; MacDiarmid, A. G. Polyaniline, A Novel Conducting Polymer. *J. Chem. Soc., Faraday. Trans. 1.* **1986**, *82*, 2385-2400.

33. Guo, Y.; Zhou, Y. Polyaniline nanofibers fabricated by electrochemical polymerization: A mechanistic study. *Eur. Polym. J.* **2007**, *43*, 2292-2297.

34. Wang, Y.-G.; Li, H.-Q.; Xia, Y.-Y. Ordered Whiskerlike Polyaniline Grown on the Surface of Mesoporous Carbon and Its Electrochemical Capacitance Performance. *Adv. Mater.* **2006**, *18*, 2619-2623.

35. Gupta, V.; Miura, N. High performance electrochemical supercapacitor from electrochemically synthesized nanostructured polyaniline. *Mater. Lett.* **2006**, *60*, 1466-1469.

36. Li, G.-R.; Feng, Z.-P.; Zhong, J.-H.; Wong, Z.-L.; Tong, Y.-X. Electrochemical Synthesis of Polyaniline Nanobelts with Predominant Electrochemical Performances. *Macromolecules* **2010**, *43*, 2178-2183.

37. Dinh, H. N.; Vanysek, P.; Birss, V. I. The Effect of Film Thickness and Growth Method on Polyaniline Film Properties. *J. Electrochem. Soc.* **1999**, *146*, 3324-3334.

38. Diaz, A.F.; Logan, J.A. Electroactive polyaniline films. *J. Electroanal. Chem.* **1980**, *111*, 111-114

39. Genies, E.M.; Tsintavis, C. Redox mechanism and electrochemical behavior of polyaniline deposits. *J. Electroanal. Chem*. **1985**, *195*, 109-128.

40. Wang, Y.; Tran, H. D.; Liao, L.; Duan, X.; Kaner, R. B. Nanoscale Morphology, Dimensional Control, and Electrical Properties of Oligoanilines. *J. Am. Chem. Soc.* **2010**, *132*, 10365-10373.

41. Tran, H.D.; D'Arcy, J. M.; Wang, Y.; Beltramo, P. J.; Strong, V. A.; Kaner, R. B The oxidation of aniline to produce "polyaniline": a process yielding many different nanoscale structures. *J. Mater. Chem.* **2011**, *21*, 3534-3550.

42. Li, D.; Huang, J.; Kaner, R. B. Polyaniline Nanofibers: A Unique Polymer Nanostructure for Versatile Applications. *Acc. Chem. Res.* **2009**, *42*, 135-145.

43. Huang, J.; Virji, S.; Weiler, B. H.; Kaner, R. B. Polyaniline Nanofibers: Facile Synthesis and Chemical Sensors. *J. Am. Chem. Soc.* **2003**, *125*, 314-315.

44. Yu, X.; Fan, H.; Wang, H.; Zhao, N.; Zhang, X.; Xu, J. Self-assembly hierarchical micro/nanostructures of leaf-like polyaniline with 1D nanorods on 2D foliage surface. *Mater. Lett.* **2011**, *65*, 2724-2727.

45. Zhang, L.; Long, Y.; Wan, M. The Effect of Hydrogen Bonding on Self-Assembled Polyaniline Nanostructures. *Adv. Funct. Mater.* **2004**, *14*, 693-698.

46. Laslau, C.; Zujovic, Z.; Travas-Sejdic, J. Theories of polyaniline nanostructure self-assembly: Towards an expanded, comprehensive Multi-Layer Theory (MLT). *Prog. Polym. Sci.* **2010**, *35*, 1403-1419.

47. Dhotel, A.; Chen, Z.; Delbreilh, L.; Youssef, B.; Saiter, J.-M.; Tan, L. Molecular Motions in Functional Self-Assembled Nanostructures. *Int. J. Mol. Sci.* **2013**, *14*, 2303-2333.

48. Tao, Y.; Li, J.; Xie, A.; Li, S.; Chen, P.; Ni, L.; Shen, Y. Supramolecular self-assembly of three-dimensional polyaniline and polypyrrole crystals. *Chem. Commun.* **2014**, *50*, 12757-12760.

49. Wei, Z.; Wan, M. Hollow Microspheres of Polyaniline Synthesized with an Aniline Emulsion Template. *Adv. Mater.* **2002**, *14* (18), 1314-1317.

50. Okubo, M.; Fujii, S.; Minami, H. Production of electrically conductive, core/shell polystyrene/polyaniline composite particles by chemical oxidative seeded dispersion polymerization. *Colloid. Polym. Sci.* **2001**, *279* (2), 139-145.

51. Zhu, Y.; Hu, D.; Wan, M. X.; Jiang, L.; Wei, Y. Conducting and Superhydrophobic Rambutan-like Hollow Spheres of Polyaniline. *Adv. Mater.* **2007**, *19* (16), 2092-2097.

52. Zhu, Y.; Li, J.; Wan, M.; Jiang, L. Superhydrophobic 3D Microstructures Assembled From 1D Nanofibers of Polyaniline. *Macromol. Rapid Commun.* **2008**, *29*, 239-243.

53. Chiang, J.-C.; MacDiarmid, A. G. 'Polyaniline': Protonic acid doping of the emeraldine form to the metallic regime. *Synth. Met.* **1986**, *13*, 193 – 205.

54. Monkman, A. P.; Bloor, D.; Stevens, G. C.; Stevens, J. C. H.; Wilson, P. Electronic structure and charge transport mechanisms in polyaniline. *Synth*. *Met*. **1989**, *29*, 277-284.

55. Bhadra, S.; Singha, N.K.; Chattopadhyay, S.; Khastgir, D. Effect of different reaction parameters on the conductivity and dielectric properties of polyaniline synthesized electrochemically and modeling of conductivity against reaction parameters through regression analysis. *J. Polym. Sci., Part B: Polym. Phys.* **2007**, *45*, 2046-2059.

56. Kohlman, R. S.; Zibold, A.; Tanner, B. D.; Ihas, G. G.; Ishiguro, T.; Min, G.; MacDiarmid, A. G.; Epstein, A. J. Limits for Metallic Conductivity in Conducting Polymers. *Phys. Rev. Lett*. **1997**, *78*, 3915-3918.

57. Luthra, V.; Singh, R.; Gupta, S.K.; Mansingh, A. Mechanism of dc conduction in polyaniline doped with sulfuric acid. *Curr. Appl. Phys.* **2003**, *3*, 219-222.

58. Epstein, A. J.; Ginder, J. M.; Zuo, F.; Bigelow, R. W.; Woo, H.-S.; Tanner, D. B.; Richter, A.F.; Huang, W.-S.; MacDiarmid, A. G. Insulator-to-metal transition in polyaniline. *Synth. Met*. **1987**, *18*, 303-309.

59. Medhi, J. Recent progress in chemical modification of polyaniline. *Prog. Polym. Sci.* **2013**, *38*, 1287-1306.

60. Wang, Z. H.; Ray, A.; MacDiarmid, A. G.; Epstein, A. J. Electron localization and charge transport in poly(o-toluidine): A model polyaniline derivative. *Phys. Rev. B.* **1991**, *43* (5), 4373-4384.

61. Wei, Y.; Focke, W. W.; Wnek, G. E.; Ray, A.; MacDiarmid, A.G. Synthesis and electrochemistry of alkyl ring substituted polyanilines. *J. Phys. Chem.* **1989**, *93*, 495-499.

62. Leclerc, M.; D'Aprano, G.; Zotti, G. Structure-property relationships in polyaniline derivatives. *Synth. Met.* **1993**, 55, 1527-1532.

63. Zheng, W.-Y.; Levon, K.; Laakso, J.; Oesterholm, J. E. Characterization and Solid-State Properties of Processable N-Alkylated Polyanilines in the Neutral State. *Macromolecules* **1994**, *27*, 7754-7768.

64. Dao, L. H.; Leclerc, M.; Guay, J.; Chevalier, J. W. Synthesis and characterization of substituted poly(anilines). *Synth. Met.* **1989**, *29*, 37-382.

65. Lindfors, T.; Ivaska, A. pH sensitivity of polyaniline and its substituted derivatives. *J. Electroanal. Chem.* **2002**, *531*, 43-52.

66. Langer, J. J. N-substituted polyanilines: II. Photoacoustic and FT-IR spectra of poly(N-methylaniline) and related copolymers. *Synth. Met.* **1990**, *35*, 301-305.

67. Nabid, M. A.; Entezami, A. A. Comparative study on the enzymatic polymerization of N-substituted aniline derivatives. *Polym. Adv. Technol.* **2005**, *16*, 305-309.

68. Leclerc, M.; Guay, J.; Dao, L. H. Synthesis and characterization of poly(alkylanilines). *Macromolecules*, **1989**, *22* (2), 649-653.

69. Liao, Y.-H.; Angelopoulos, M.; Levon, K. Ring-substituted polyaniline copolymers combining high solubility with high conductivity. *J. Polym. Sci. A.* **1995**, *33* (16), 2725-2729.

70. Bhadra, S.; Singha, N. K.; Khastgir, D. Effect of aromatic substitution in aniline on the properties of polyaniline. *Eur. Polym. J.* ***2008****, 44*, 1763-1770.

71. Langer, J. J. N-substituted polyanilines: I. Poly(N-methylaniline) and related copolymers. *Synth. Met.* **1990**, *35*, 295 - 300.

72. Oka, O.; Kiyohara, O.; Yoshino, K. Preparation of Highly Soluble N-Substituted Polyanilines and Their Novel Solvatochromism. *Jpn. J. Appl. Phys.* **1991**, *30*, 653-656

73. Salavagione, H. J.; Miras, M.; Barbero, C. Chemical Lithography of a Conductive Polymer Using a Traceless Removable Group. *J. Am. Chem. Soc.* **2003**, *125* (18), 5290-5291.

74. Lee, C.-W.; Seo, Y.-H.; Lee, S.-H. A Soluble Polyaniline Substituted with t-BOC: Conducting Patterns and Doping. *Macromolecules*, **2004**, *37* (11), 4070-4074.

75. Wei, Y.; Hariharan, R.; Patel, S. A. Chemical and electrochemical copolymerization of aniline with alkyl ring-substituted anilines. *Macromolecules* **1990**, *23*, 758-764.

76. Yan, H.; Wang, H.-J.; Adisasmito, S.; Toshima, N. Novel Syntheses of Poly(o-aminobenzoic acid) and Copolymers of o-Aminobenzoic Acid and Aniline as Potential Candidates for Precursor of Polyaniline. *Bull. Chem. Soc. Jpn.* **1997**, *69*, 2395-2401.

77. Jiang, X.; Zhang, L.; Dong, S. Assemble of poly(aniline-co-o-aminobenzenesulfonic acid) three-dimensional tubal net-works onto ITO electrode and its application for the direct electrochemistry and electrocatalytic behavior of cytochrome c. *Electrochem. Commun.* **2006**, *8*, 1137-1141.

78. Kwon, A. H.; Conklin, J. A.; Makhinson, M.; Kaner, R. B. Chemical synthesis and characterization of fluoro-substituted polyanilines. *Synth. Met.* **1997**, *84*, 95-96.

79. Cataldo, F.; Maltese, P. Synthesis of alkyl and N-alkyl-substituted polyanilines: A study on their spectral properties and thermal stability. *Eur. Polym. J.* **2002**, *38*, 1791-1803.

80. Neoh, K. G.; Kang, E. T.; Tan; K. L. Chemical copolymerization of aniline with halogen-substituted anilines. *Eur. Polym. J.* **1990**, *26* (4), 403-407.

81. Xu, Y.; Dai, L.; Chen, J.; Gal, J.-Y.; Wu, H. Synthesis and characterization of aniline and aniline-*o*-sulfonic acid copolymers. *Eur. Polym. J.* **2007**, *43*, 2072-2079.

82. Sharma, A. L.; Saxena, V.; Annapoorni, S.; Malhotra, B. D. Synthesis and characterization of a copolymer: Poly(aniline-co-fluoroaniline). *J. Appl. Polym. Sci.* **2001**, *81*, 1460-1466.

83. Zhang, J.; Shan, D.; Mu, S. Chemical synthesis and electric properties of the conducting copolymer of aniline and o-aminophenol. *J. Polym. Sci. Part A.* **2007**, *45,* 5573-5582.

84. Rao, P. S.; Sathyanarayana, D. N. Synthesis of electrically conducting copolymers of aniline with o/m-aminobenzoic acid by an inverse emulsion pathway. *Polymer* **2002**, *43*, 5051-5058.

85. Huang, L.-M.; Wen, T.-C.; Yang, C.-H. Electrochemical copolymerization of aniline and 2,2′-dithiodianiline. *Mater. Chem. Phys.* **2002**, *77*, 434-441.

86. Bergeron, J.-Y.; Chevalier, J.-W.; Dao, L. H. Water-soluble conducting poly(aniline) polymer. *J. Chem. Soc., Chem. Commun.* **1990**, *0*, 180-182.

87. Arsalani, N.; Khavei, M.; Entezami, A. A. Synthesis and Characterization of Novel N-Substituted Polyaniline by Triton X-100. *Iranian Polymer Journal*, **2003**, *12* (3), 237-242.

88. Zhao, B.; Neoh, K. G.; Kang, E. T. Concurrent N-Alkylation and Doping of Polyaniline by Alkyl Halides *Chem. Mater*. **2000**, *12*, 1800-1806.

89. Mikhael, M. G.;Padias, A. B.; Hall Jr., H. K. N-alkylation and N-acylation of polyaniline and its effect on solubility and electrical conductivity. *J. Polym. Sci. A.* **1997**. *35* (9), 1673-1679.

90. Morales, G. M.; Salavagione, H. J.; Grumelli, D. E.; Miras, M. C.; Barbero, C. A Soluble polyanilines obtained by nucleophilic addition of arenesulphinic acids. *Polymer. **2006,** 47*, 8272-8280.

91. Lee, Y.-H.; Park, J.-H.; Jun, Y.-D.; Kim, D.-W.; Lee, J.-J.; Kim, Y. C.; Oh, S.-G. 3-Mercapto-1,2-propanediol-substituted polyaniline/Ag nanocomposites prepared by concurrent reduction and substitution chemistry. *Synth. Met.* **2008**, *158*, 143-149.

92. Chen, S.-A.; Hwang, G.-W. Structure Characterization of Self-Acid-Doped Sulfonic Acid Ring-Substituted Polyaniline in Its Aqueous Solutions and as Solid Film. *Macromolecules*. **1996**, *29*, 3950-3955.

93. Salavagione, H.; Morales, G. M.; Miras, M. C.; Barbero, C. Synthesis of a self-doped polyaniline by nucleophilic addition. *Acta Polym*. **1999**, *50*, 40-44.

94. Acevado, D.F.; Rivarola, C. R.; Miras, M. C.; Barbero, C. A. Effect of chemical functionalization on the electrochemical properties of conducting polymers. Modification of polyaniline by diazonium ion coupling and subsequent reductive degradation. *Electrochim*. *Acta*. **2011**, *56*, 3468-3473.

95. Acevedo, D. F.; Salavagione, H. J.; Miras, M. C.; Barbero, C. A. Synthesis, Properties and Applications of Functionalized Polyanilines. *J. Braz. Chem. Soc.* **2005**, *16* (2), 259-263.

96. Han, C.-C.; Hseih, W.-D.; Yeh, J.-Y.; Hong, S.-D. Combination of Electrochemistry with Concurrent Reduction and Substitution Chemistry To Provide a Facile and Versatile Tool for Preparing Highly Functionalized Polyanilines. *Chem. Mater.* **1999**, *11*, 480 - 486.

97. Han, C.-C.; Hong, S.-P.; Yang, K.-F.; Bai, M.-Y.; Lu, C.-H.; Huang, C.-S. Highly Conductive New Aniline Copolymers Containing Butylthio Substituent. *Macromolecules*, **2001**, *34* (3), 587-591.

98. Stejskal, J.; Trchová, M.; Prokes, J.; Sapurina, I. Brominated Polyaniline. *Chem. Mater*. **2001**, *13* (11), 4083-4086.

99. MacDiarmid, A. G.; Manohar, S. K.; Masters, J. G.; Sun, Y.; Weiss, H.; Epstein, A. J. Polyaniline: Synthesis and properties of pernigraniline base. *Synth Met.* **1991**, 41, 621-626.

100. Han, C.-C.; Jeng, R.-C. Concurrent reduction and modification of polyaniline emeraldine base with pyrrolidine and other nucleophiles. *Chem. Commun.* **1997**, *0*, 553-554.

101. Paike, V. V.; Balakumar, R.; Chen, H.-Y.; Shih, H.-P.; Han, C.-C. A Serendipitous C−C Bond Formation Reaction between Michael Donors and Diiminoquinoid Ring Assisted by Quaternary Ammonium Fluoride. *Org. Lett.*, **2009**, *11* (24), 5586-5589.

102. Barbero, C.; Morales, G. M.; Grumelli, D.; Planes, G.; Salavagione, H.; Marengo, C. R.; Miras, M. C. New methods of polyaniline functionalization. *Synth. Met.* **1999**, *101*, 694-695.

103. Zhang, X.; Goux, W. J.; Manohar, S. K. Synthesis of Polyaniline Nanofibers by "Nanofiber Seeding". *J. Am. Chem. Soc.* **2004**, *126* (14), 4502-4503.

104. Cao, Y. Spectroscopic Studies of Acceptor and Donor Doping of Polyaniline in the Emeraldine Base and Pernigraniline Forms. *Synth. Met.* **1990**, *35*, 319-322.

105. Albuquerque, J. E.; Mattoso, L. H. C.; Faria, R. M.; Masters, J. G.; MacDiarmid, A. G. Study of the interconversion of polyaniline oxidation states by optical absorption spectroscopy. *Synth. Met.* **2004**, *146,* 1-10.

106. Yoon, S.-B.;Yoon, E.-H.; Kim, K.-B. Electrochemical properties of leucoemeraldine, emeraldine, and pernigraniline forms of polyaniline/multi-wall carbon nanotube nanocomposites for supercapacitor applications. *J. Power Sources*. **2011**, *196*, 10791-10797.

107. Albuquerque, J. E.; Mattoso, L. H. C.; Balogh, D. T.; Faria, R. M.; Masters, J. G.; MacDiarmid, A. G. A simple method to estimate the oxidation state of polyanilines. *Synth. Met.* **2000**, *113* (1), 19-22.

108. Chandrakanthi, N.; Careem, M. A. Preparation and characterization of the fully oxidized form of polyaniline. *Polym. Bull.* **2000**, *45*, 113-120.

109. Abraham, M. H.; Grellier, P. L.; Abboud, J.-L. M.; Doherty, R. M.; Taft, R. W. Solvent effects in organic chemistry- recent developments. *Can. J. Chem.* **1988**, *66*, 2673-2686.

110. Parker, A. J. Protic-dipolar aprotic solvent effects on rates of bimolecular reactions. *Chem. Rev.* **1969**, *69* (1), 1-32.

111. Breslow, R. Maitra, U. On the origin of product selectivity in aqueous diels-alder reactions. *Tetrahedron Lett.* **1984**, *25* (12), 1239-1240.

112. Hanggi, P. ; Talkner, P.; Borkovec, M. Reaction-rate theory: fifty years after Kramers. *Rev. Modern Phys.* **1990**, *62*, 251-341.

113. Berne, B. J.; Borkovec, M.; Straub, J. E. Classical and modern methods in reaction rate theory. *J. Phys. Chem.* **1988**, *92*, 3711-3725.

114. Smith, I. W. M. The temperature-dependence of elementary reaction rates: beyond Arrhenius. *Chem. Soc. Rev.* **2008**, *37*, 812-826.

115. Maskill, H., Ed. *The Investigation of Organic Reactions and their Mechanisms;* Blackwell Publishing: Oxford, 2006.

116. Li, D.; Kaner, R. B. Shape and Aggregation Control of Nanoparticles: Not Shaken, Not Stirred. *J. Am. Chem. Soc.* **2006**, *128* (3), 968-975.

117. Cao, Y. Smith, P.; Heeger, A. J. Counter-ion induced processibility of conducting polyaniline and of conducting polyblends of polyaniline in bulk polymers. *Synth. Met.* **1992**, *48*, 91-97.

118. Angelopoulos, M.; Liao, Y.-H.; Furman, B.; Graham, T. O. Solvent and salt effects on the morphological structure of polyaniline. In *Optical and Photonic Applications of Electroactive and Conducting Polymers.* Proceedings of the Society of Phto-Optical Instrumentation Engineers. September 15, 1995.

119. Perkampus, H.-H. *UV-VIS Spectroscopy and its Applications*; Springer-Verlag: Berlin, 1992.

120. Smith, B. C. *Fundamentals of Fourier Transform Infrared Spectroscopy*, 2nd ed.; CRC Press: Boca Raton, 2011.

121. Gunther; H. *NMR Spectroscopy: Basic Principles, Concepts, and Applications in Chemistry*, 3rd ed.; Wiley-VCH: Weinheim, 2013.

122. Bertin, E. P. *Principles and Practices of X-Ray Spectrometric Analysis*; Springer Science & Business Media: Berlin, 2012.

123. Fleming, I. *Molecular Orbitals and Organic Chemical Reactions*, Student Ed.; Wiley: United Kingdom, 2009.

124. Hufner, S. *Photoelectron spectroscopy: principles and applications*; Springer Science & Business Media: Berlin, 2013.

125. Modinos, A. *Field, Thermionic, and Secondary Electron Emmission Spectroscopy*; Springer Science and Business Media: Berlin, 2013.

126. Smith, B. C. *Fundamentals of Fourier Transform Infrared Spectroscopy*, 2nd ed.; CRC Press: Boca Raton, 2011.

127. Quillard, D.; Louran, G.; Lefrant, S.; MacDiarmid, A. G. Vibrational analysis of polyaniline: A comparative study of leucoemeraldine, emeraldine, and pernigraniline bases. *Phys Rev. B.* **1994**, *50* (17), 12496-12508.

128. Socrates, G. *Infrared Characteristic Group Frequencies: Tables and Charts,* Second Edition; Wiley & Sons: Chinchester, 1994; 121-129.

129. Camplbell, D.; Pethrick, R. A.; White, J. R. *Polymer Characterization: Physical Techniques*, 2nd ed.; CRC Press: London, 2000.

130. Akitt, J. W.; Mann, B. E. *NMR and Chemistry: An introduction to modern NMR spectroscopy*, 4th ed.; CRC Press: London, 2000.

131. Keeler, J. *Understanding NMR Spectroscopy*, 2nd ed.; John Wiley & Sons: New Jersey, 2011.

132. Wei, Y.; Jang, G.-W.; Hsueh, K. F.; Scherr, E. M.; MacDiarmid, A. G.; Epstein, A. J. Thermal transitions and mechanical properties of chemically prepared polyaniline. *Polymer* **1992**, *33*, 314-322.

133. Nechtschein, M.; Santier, C.; Travers, J. P.; Chroboczek, J.; Alix, A.; Ripert, M. Water effects in polyaniline: NMR and transport properties. *Synth. Met.* **1987**, *18*, 311-316.

134. Anslyn, E. V.; Dougherty, D. A. *Modern Physical Organic Chemistry*; University Science Books: Sausalito, 2005.

135. Ott, J. B.; Boerio-Goates, J. *Chemical Thermodynamics: Advanced Applications*; Academic PressL London, 2000.

136. Blackmond, D. G. "If Pigs Could Fly" Chemistry: A Tutorial on the Principle of Microscopic Reversibility. *Angew. Chem. Int. Ed.* **2009**, *48*, 2648-2654.

137. House, J. E. *Principles of Chemical Kinetics*, 2nd ed.; Elsevier: Oxford, 2007.

138. Connors, K. A. *Chemical Kinetics: The Study of Reaction Rates in Solution*; VCH Publishers: New York, 1990.

139. Hammett, L. P. Linear free energy relationships in rate and equilibrium phenomena. *J. Chem. Soc., Faraday Trans.* **1938**, *34*, 156-165.

140. Hammett, L. P. The Effect of Structure upon the Reactions of Organic Compounds. Benzene Derivatives. *J. Am. Chem. Soc.* **1937**, *59*, 96-103.

141. Hansch, C.; Leo, A.; Taft, R.W. A survey of Hammett substituent constants and resonance and field parameters. *Chem. Rev.* **1991**, *91*, 165-195.

142. Schreck, J. O. Nonlinear Hammett Relationships. *J. Chem. Edu.* **1971**, *48*, 103-107.

143. Um, I.-H.; Im, L.-R.; Kim, E.-H.; Shin, J. H. Nonlinear Hammett plots in pyridinolysis of 2,4-dinitrophenyl X-substituted benzoates: change in RDS versus resonance contribution. *Org. Biomol. Chem.* **2010**, *8*, 3801-3806.

144. Bergon, M.; Calmon, J.-P. A nonlinear Hammett relationship as evidence for a change-over in mechanism in the alkaline hydrolysis of methyl carbanilates. *Tetrahedron Lett.* **1981**, *22*, 937-940.

145. McGrath, J. M.; Pluth, M. D. Linear Free Energy Relationships Reveal Structural Changes in Hydrogen-Bonded Host-Guest Interactions. *J. Org. Chem.* **2014**, *79*, 11797-11801.

146. Taft, R. W. Polar and Steric Substituent Constants for Aliphatic and o-Benzoate Groups from Rates of Esterification and Hydrolysis of Esters. *J. Am. Chem. Soc.* **1951**, *74*, 3120-3128.

147. Pavelich, W. A.; Taft, R. W. The Evaluation of Inductive and Steric Effects on Reactivity. The Methoxide Ion-catalyzed Rates of Methanolysis of *l*-Menthyl Esters in Methanol. *J. Am. Chem. Soc.* **1957**, 79 (18), 4935-4940.

148. Meyer, A. Y. Molecular Mechanics and Molecular Shape. Part 4. Size, Shape, and Steric Parameters. *J. Chem. Soc., Perkin Trans. 2.* **1986**, 1567-1572.

149. Charton, M. Steric effects. I. Esterification and acid-catalyzed hydrolysis of esters. *J. Am. Chem. Soc.* **1975**, *97* (6), 1552-1556.

150. Charton, M. Nature of the ortho effect. II. Composition of the Taft steric parameters. *J. Am. Chem. Soc.* **1969**, 91 (3), 615-618.

151. Shorter, J. The separation of polar, steric, and resonance effects in organic reactions by the use of linear free energy relationships. *Q. Rev. Chem. Soc.* **1970**, *24*, 433-453.

152. MacPhee, J. A.; Panaye, A.; Dubois, J.-E. Steric effects—I: A critical examination of the taft steric parameter—Es. Definition of a revised, broader and homogeneous scale. Extension to highly congested alkyl groups. *Tetrahedron.* **1978**, *34*, 3553-3562.

153. Hall, H. K.; Bates, R. B. Correlation of alkylamine nucleophilicities with their basicities. *Tetrahedron Lett.* **2012**, *53*, 1830-1832.

154. DeTar, D. F.; Delahunty, C. Ester aminolysis: new reaction series for the quantitative measurement of steric effects. *J. Am. Chem. Soc.* **1983**, *105* (9), 2734-2739.

155. Dienys, G. J.; Kunskaite, L. J. J.; Vaitkevicius, A. K.; Klimavicius, A. V. *Organic Reactivity*. **1975**, *12*, 275-281.

156. Charton, M. Steric effects. 9. Substituents at oxygen in carbonyl compounds. *J . Org. Chem.* **1977**, *42*, 3531-3535.

157. Bunting, J. W.; Mason, J. M.; Heo, C. K. M. Nucleophilicity towards a saturated carbon atom: rate constants for the aminolysis of methyl 4-nitrobenzenesulfonate in aqueous solution. A comparison of the n and N+ parameters for amine nucleophilicity. *J. Chem. Soc. Perkin. Trans. 2.* **1994**, *0*, 2291-2230.

158. White, D. P.; Anthony, J. C.; Oyefeso, A. O. Computational Measurement of Steric Effects: the Size of Organic Substituents Computed by Ligand Repulsive Energies. *J. Org. Chem.* **1999**, *64* (21), 7707-7716.

159. Moon, D.-K.; Ezuka, M.; Maruyama, T.; Osakada, K.; Yamamoto, T. Kinetic study on chemical oxidation of leucoemeraldine base polyaniline to emeraldine base. *Macromolecules.* **1993**, 26, 364-369.

160. Skoog, D. A.; West, D. M.; Holler, J. F.; Crouch, S. R. *Fundamentals of Analytical Chemistry*, 8th ed.; Thompson-Brooks/Cole: Belmont, 2004.

161. Grummt, U.-W.; Pron, A.; Zagorska, M.; Lefrant, S. Polyaniline based optical pH sensor. *Anal. Chim. Acta* **1997**, *357*, 253-259.

162. Jaramillo, P.; Perez, P.; Fuentealba, R. Relationship between basicity and nucleophilicity. *J. Phys. Org. Chem.* **2007**, *20*, 1050-1057.

163. Searles, S.; Tamres, M.; Block, F.; Quarterman, L. A. Hydrogen Bonding and Basicity of Cyclic Imines. *J. Am. Chem. Soc.* **1956**, *78*, 4917-4920.

164. Alder, R. W. Strain Effects on Amine Basicities. *Chem. Rev.* **1989**, *89*, 1215-1223.

165. Graton, J.; Laurence, C.; Berthelot, M.; Le Questel, J.-Y.; Besseau, F.; Raczynska, E. D. Hydrogen-bond basicity pK_{HB} scale of aliphatic primary amines. *J. Chem. Soc., Perkin Trans. 2.* **1999**, 997-1001.

166. Brauman, J. I.; Riveras, J. M.; Blair, L. K. Gas-Phase Basicicties of Amines. *J. Am. Chem. Soc.* **1971**, *94* (16), 3914-3916.

167. Arnett, E. M.; Jones, F. M.; Taagepera, M.; Henderson, W. G.; Beauchamp, J. L.; Hultz, D.; Taft, R. W. Complete thermodynamic analysis of the "anomalous order " of amine basicities in solution. *J. Am. Chem. Soc.* **1972**, *94* (13), 4724-4726.

168. Mayr, H.; Ofial, A. R. Do general nucleophilicity scales exist? *J. Phys. Org. Chem.* **2008**, *21*, 584-595.

169. Kanzian, T. Nigst, T. A.; Maier, A.; Pichl, S.; Mayr, H. Nucleophilic Reactivities of Primary and Secondary Amines. *Eur. J. Org. Chem.* **2009**, *0*, 6379-6385.

170. Yang, D.; Zuccarello, G.; Mattes, B. R. Physical Stabilization or Chemical Degradation of Concentrated Solutions of Polyaniline Emeraldine Base Containing Secondary Amine Additives. *Macromolecules, **2002**, 35*, 5304-5313.

171. Flory, P. J.; Rehner, J. Statistical Mechanics of Cross-Linked Polymer Networks I. Rubberlike Elasticity. *J. Chem. Phys.* **1943**, *11*, 512-520.

172. Krumova, M.; Lopez, D.; Benavente, R.; Mijangos, C.; Pereña, J. M. Effect of crosslinking on the mechanical and thermal properties of poly(vinyl alcohol). *Polymer* **2000**, *41*, 9265-92-72.

173. Safranski, D. L.; Gall, K. Effect of chemical structure and crosslinking density on the thermo-mechanical properties and toughness of (meth)acrylate shape memory polymer networks. *Polymer* **2008**, *49*, 4446-4455.

174. Kaiser, T. Highly crosslinked polymers. *Prog. Polym. Sci.* **1989**, *14*, 373-450.

175. Chen, X.; Dam, M. A.; Ono, K.; Mal, A.; Shen, H.; Nutt, S. R.; Sheran, K.; Wudl, F. A Thermally Re-mendable Cross-Linked Polymeric Material. *Science* **2002**, *295*, 1698-1702.

176. *Handbook of Thermoset Plastics,* 2nd ed.; Goodman, S., H., Ed. Noyes: New Jersey, 1998.

177. Oka O.; Kiyohara, O.; Morita, S.; Yoshino, K. Electrical and mechanical properties of crosslinked polyanilines. *Synth. Met.* **1993**, *55*, 999-1004.

178. MacDiarmid, A. G.; Min, Y.; Wiesinger, J. M.; Oh, E. J.; Scherr, E. M.; Epstein, A. J. Towards optimization of electrical and mechanical properties of polyaniline: Is crosslinking between chains key? *Synth. Met.* **1995**, *55*, 753-760.

179. Germain, J.; Fréchet, J. M. J., Svec, F. Hypercrosslinked polyanilines with nanoporous structure and high surface area: potential adsorbents for hydrogen storage. *J. Mater. Chem*. **2007**, *17*, 4989-4997.

180. Ayad, M.; Zaghlol, S. Nanostructured crosslinked polyaniline with high surface area: Synthesis, characterization and adsorption for organic dye. *Chem. Eng. J.* **2012**, *204*, 79-86.

181. Zhai, D.; Liu, B.; Shi, Y.; Pan, L.; Wang, Y.; Li, W.; Zhang, R.; Yu, G. Highly Sensitive Glucose Sensor Based on Pt Nanoparticle/Polyaniline Hydrogel Heterostructures. *ACS Nano*, **2013**, *7* (4), 3540-3546.

182. Wang, X.; Deng, J.; Duan, X.; Li, D.; Guo, J.; Liu, P. Crosslinked polyaniline nanorods with improved electrochemical performance as electrode material for supercapacitors. *J. Mater. Chem. A*. **2014**, *2*, 12323-12329.

183. Guo, H.; He, W.; Lu, Y.; Zhang, X. Self-crosslinked polyaniline hydrogel electrodes for electrochemical energy storage *Carbon.* **2015**, *92*, 133-141.

184. Wang, X.; Liu, D.; Deng, J.; Duan, X.; Guo, J.; Liu, P. Improving cyclic stability of polyaniline by thermal crosslinking as electrode material for supercapacitors. *RSC Adv*. **2015**, *5*, 78545-78552.

185. Osada, Y.; Kajiwara, K., Tanaka, T.; Ishida, H. *Gels Handbook*; Elsevier Science & Technology: Amsterdam, 2000.

186. Dušek K., *Epoxy Resins and Composites III. Advances in Polymer Science*; vol 78; Springer: Berlin, Heidelberg, 1986.

187. Pan, L.; Yu, G.; Zhai, D.; Lee, H. R.; Zhao, W.; Liu, N.; Wang, H.; Tee, B. C.-K.; Shi, Y.; Cui, Y.; Bao, Z. Hierarchical nanostructured conducting polymer hydrogel with high electrochemical activity. *PNAS* **2012**, *109* (24) 9287-9292.

188. Tanaka, F.; Edwards, S. F. Viscoelastic properties of physically crosslinked networks: Part 1. Non-linear stationary viscoelasticity. *J. Non-Newtonian Fluid Mech.* **1992**, *43*, 247-271.

189. Wang, S.-F.; Jing, X.-B.; Wang, X.-H.; Dong, A.-J. Solution properties of polyaniline and its derivatives. *Synth. Met.* **1995**, *69*, 93-96.

190. Chackos, A. P.; Hardaker, S. S.; Gregory, R. V.; Samules, R. J. Viscoelastic characterization of concentrated polyaniline solutions: New insights into conductive polymer processing. *Synth. Met.* **1997**, *84*, 41-44.

191. Angelopoulos, M.; Liao, Y. H.; Furman, B.; Teresita, G. LiCl Induced Morphological Changes in Polyaniline Base and Their Effect on the Electronic Properties of the Doped Form. *Macromolecules* **1996**, *29*, 3046-3049.

192. Joo, J.; Long, S. M.; Pouget, J. P.; Oh, E. J.; MacDiarmid, A. G.; Epstein, A. J. Charge transport of the mesoscopic metallic state in partially crystalline polyanilines. *Phys. Rev. B*. **1998**, *57*, 9567-9580.

193. Liu, C.; Yu, J.; Sun, X.; Zhang, J.; He, J. Thermal degradation studies of cyclic olefin copolymers. *Polym. Degrad. Stability* **2003**, *81*, 197-205.

194. Rozenberg B.A. Kinetics, thermodynamics and mechanism of reactions of epoxy oligomers with amines. In *Epoxy Resins and Composites II. Advances in Polymer Science*, : Dušek K. Ed.; Springer: Berlin, 1986, vol. 75, 113-165.

195. De Nograro, F. F.; Guerrero, P.; Corcuera, M. A.; Mondragon, I. Effects of chemical structure of hardener on curing evolution and on the dynamic mechanical behavior of epoxy resins. *Appl. Polym. Sci.* **1995**, *56*, 177-192.

196. Swier, S.; Van Mele, B. Reaction Thermodynamics of Amine-Cured Epoxy Systems: Validation of the Enthalpy and Heat Capacity of Reaction As Determined by Modulated Temperature Differential Scanning Calorimetry. *J. Polym. Sci.: Part B.* **2003**, *41*, 594-608.

197. Sevilla, M.; Fuentes, A. B. The production of carbon materials by hydrothermal carbonization of cellulose. *Carbon*, **2009**, *47*(9), 2281-2289.

198. Shinogi, Y.; Kanri, Y. Pyrolysis of plant, animal and human waste: physical and chemical characterization of the pyrolytic products. *Bioresource Technol*. **2003**, *90*(3), 241-247.

199. Wangxi, Z.; Jie, L.; Gang, W. Evolution of structure and properties of PAN precursors during their conversion to carbon fibers. *Carbon*, **2003**, *41*(14), 2805-2812.

200. Davidenko, V.M.; Kidalov, S. V.; Shakhov, F. M.; Yagovkina, M. A.; Yashim, V. A.; Yul, A. Y. Fullerenes as a co-catalyst for high pressure - high temperature synthesis of diamonds. *Diam. Relat. Mater.* **2004**, *13*, 2203-2206.

201. Hunter, J. M.; Fye, J. L.; Roskamp, E. J.; Jarrold, M. F. Annealing Carbon Cluster Ions: A Mechanism for Fullerene Synthesis. *J. Phys. Chem*. **1994**, *98*, 1810-1818.

202. Lee, J.; Kim, J.; Hyeon, T. Recent Progress in the Synthesis of Porous Carbon Materials. *Adv. Mater.* **2006**, *18*, 2073-2094.

203. De Jong, K. P.; Geus, J. W. Carbon Nanofibers: Catalytic Synthesis and Applications. *Catal. Rev.-Scie. Eng.* **2000**, *42* (4), 481-510.

204. Bent, H. A. An appraisal of valence-bond structures and hybridization in compounds of the first row elements. *Chem. Rev.* **1961**, *61*(3), 275-311.

205. Brown, M. G. Atom hybridization and bond properties of some carbon-containing bonds. *Trans. Faraday Soc.* **1959**, *55*, 694-701.

206. Belenkov, E. A.; Greshnyakov, V. A. Classification schemes for carbon phases and nanostructures. *New Carbon Mater.* **2013**, *28*(4), 273-283.

207. Guy, A. G. *Elements of Physcial Metallurgy, 2nd Ed.* Addison-Wesley Publishing: Reading, MA, 1959; pp. 73-85

208. Hornstra, J. Dislocations in the diamond lattice. *Diam. Relat. Mater.* **1992**, *1*, 397-406.

209. Cullity, B. D. *Elements of X-Ray Diffraction*. Addison-Wesley Publishing: Reading, MA, 1956; pp. 42-53.

210. Spear, K. E. Diamond- Ceramic coating of the future. *J. Am. Ceram. Soc.* **1989**, *72*(2), 171-191.

211. Coe, S. E.; Sussmann, R. S. Optical, thermal and mechanical properties of CVD diamond. *Diam. Relat. Mater.* **2000**, *9*, 1726-1729.

212. Ho. K. M.; Chan, C. T.; Soukoulis, C. M. Existence of a photonic gap in periodic dielectric structures. *Phys. Rev. Lett.* **1990**, *65*(25), 3152-3155.

213. Nebel, C. E. Electronic properties of CVD diamonds. *Semicond. Sci. Technol.* **2003**, *18*, S1-S11.

214. Ward, A.; Brodio, D. A.; Stewart, D. A.; Deinzel, G. Ab initio theory of the lattice thermal conductivity in diamond. *Phys. Rev. B.* **2009**, *80*, 125203.

215. *Handbook of Industrial Diamonds and Diamond Films*. Prelas, M. A.; Popovici, G.; Bigelow, L. K. Eds. Marcel Dekker: New York, 1998.

216. Bernal, J. D. The structure of graphite. *Proc. R. Soc. Lond. A.* **1924**, *106*(740), 749-773.

217. Freise, E. J. Structure of Graphite. *Nature* **1962**, *193*, 671-672.

218. Lipson, H. S.; Stokes, A. R. The structure of graphite. *Proc. R. Soc. Lond. A.* **1942**, *181*(984), 101-105.

219. Painter, G. S.; Ellis, D. E. Electronic Band Structure and Optical Properties of Graphite from a Variational Approach. *Phys. Rev. B.* **1970**, *1*, 4747-4752.

220. Charlier, J.-C.; Gonze, X.; Michenaud, J.-P. Graphite Interplanar Bonding: Electronic Delocalization and van der Waals Interaction. *Europhys. Lett.* **1994**, *28*, 403-408.

221. Sengupta, R.; Bhattacharya, M.;Bandyopadhyay, S.; Bhowmick, A. K. A review on the mechanical and electrical properties of graphite and modified graphite reinforced polymer composites. *Prog. Polym. Sci.* **2011**, *36*, 638-670.

222. Klemens, P. G.; Pedraza, D. F. Thermal conductivity of graphite in the basal plane. *Carbon* **1994**, *32*(4), 735-741.

223. Slack, G. A. Anisotropic thermal conductivity of pyrolytic graphite. *Phys. Rev.* **1962**, *127*(3), 694-701.

224. Rasor, N. S.; McClelland, J. D. Thermal properties of graphite, molybdenum and tantalum to their destruction temperatures. *J. Chem. Phys. Solids* **1960**, *15*, 17-26.

225. Nelson, J. B.; Riley, D. P. The thermal expansion of graphite from 15 ºC to 800 ºC: Part I. Experimental. *Proc. Phys. Soc.* **1945**, *57*, 477-486.

226. Krishnan, K. S.; Ganguli, N. Large anisotropy of the electrical conductivity of graphite. *Nature* **1939**, *144*, 667.

227. Celzard, A.; Mareche, J. F.; Furdin, G.; Puricelli, S. Electrical conductivity of anisotropic expanded graphite-based monoliths. *J. Phys. D.: Appl. Phys.* **2000**, *33*, 3094-3101.

228. Hermann, H.; Schubert, T.; Gruner, W.; Mattern, W. Structure and chemical reactivity of ball-milled graphite. *Nanostruct. Mater.* **1997**, *8*(2), 215-229.

229. Sircar, S.; Golden, T. C.; Rao, M. B. Activated carbon for gas separation and storage. *Carbon* **1996**, *34*(1), 1-12.

230. Rivera-Utrilla, J.; Sanchez-Polo, M.; Gomez-Serrano, V.; Alvarez, P. M.; Alvim-Ferraz, M. C. M.; Diaz, J. M. Activated carbon modifications to enhance its water treatment applications. An overview. *J. Hazard. Mater.* **2011**, *187*, 1-23.

231. Wissler, M. Graphite and carbon powders for electrochemical applications. *J. Power Sources* **2006**, *156*, 142-150.

232. Chung, D. D. L. Flexible Graphite for Gasketing, Adsorption, Electromagnetic Interference Shielding, Vibration Damping, Electrochemical Applications, and Stress Sensing. *J. Mater. Eng. Perform.* **2000**, *9*(2), 161-163.

233. Inagaki, M.; Radovic, L. R. Nanocarbons. *Carbon* **2002**, *40*, 2279-2284.

234. Kappe, C. O.; Controlled Microwave Heating in Modern Organic Synthesis. *Angew. Chem. Int. Ed.* **2004**, *43*, 6250-6284.

235. Bilecka, I.; Niederberger, M. Microwave chemistry for inorganic nanomaterials synthesis. *Nanoscale* **2010**, *2*, 1358-1374.

236. Avouris, P.; Dimitrakopoulos, C. Graphene: synthesis and applications. *Mater. Today* **2012**, *15*(3), 86-97.

237. Balandin, A. Thermal properties of graphene and nanostructured carbon materials. *Nat. Mater.* **2011**, *10, 569-581*

238. Du, X.; Skachko, I.; Barker, A.; Andrei, E. Y. Approaching ballistic transport in suspended graphene. *Nat. Nanotechnol.* **2008**, *3*, 491-495

239. Bolotin, K. I.; Sikes, K. J.; Jiang, Z.; Klima, M.; Fundenberg, G.; Hone, J. K.; Kim, P.; Stormer, H. L. Ultrahigh electron mobility in suspended graphene. *Solid State Commun.* **2008**, *146*, 351.

240. Lim, w. S.; Kim, Y. Y.; Kim, H.; Jang, S.; Kwon, N.; Park, B. J.; Ahn, J.-H.;Chung, I.; Hong, B. H.; Yeom, G. Y. Atomic layer etching of graphene for full graphene device fabrication. *Carbon* **2012**, *50*(2), 429-435.

241. Allen, M. J.; Tung, V. C.; Kaner, R. B. Honeycomb Carbon: A Review of Graphene. *Chem. Rev.* **2010**, *110*(1), 132-145.

242. Kim, K. S.; Zhao, Y.; Jang, H.; Lee, S. Y.; Kim, J. M.; Kim, K. S.; Ahn, J.-H.; Kim, P. Choi, J. Y.; Hong, B. H. Large-scale pattern growth of graphene films for stretchable transparent electrodes. *Nature* **2009**, *457*, 706-710.

243. Reina, A.; Jin, X.; Ho, J.; Nezich, D.; Son, H.; Bulovic, V.; Dresselhaus, M. S.; Kong, J. Large area, few-layer graphene films on arbitrary substrates by chemical vapor deposition. *Nano. Lett.* **2009**, *9*(1), 30-35.

244. Zheng, M.; Takei, K.; Hsia, B.; Fang, H.; Zhang, X.; Ferralis, N.; Ko, H.; Chueh, Y.-L.;Zheng, Y.; Maboudian, R.; Javey, A. Metal-catalyzed crystallization of amorphous carbon to graphene. *Appl. Phys. Lett.* **2010**, *96*, 063110.

245. Emstev, K. V.; Bostwick, A.; Horn, K.; Jobst, J.; Kellog, G. L.; Ley. L.; McChesney, J. L.; Ohta, T.; Reshanov, S. A.; Rohnl, J.; Rotenberg, E.; Schmid, A. K.; Waldermann, D.; Weber, H. B.; Seyller, T. Towards wafer-size graphene layers by atmospheric pressure graphitization of silicon carbide. *Nat. Mater.* **2009**, *8*, 203-207.

246. Odom, T. W.; Huang, J.-L.; Kim, P.; Lieber, C. M. Atomic structure and electronic properties of single-walled carbon nanotubes. *Nature* **1998**, *391,* 62-64.

247. Sanchez-Portal, D.; Artacho, E.; Soler, J. M.; Rubio, A.; Ordejon, P. Ab initio structural, elastic, and vibrational properties of carbon nanotubes. *Phys. Rev. B.* **1999**, *59*(19), 12678-12688.

248. Mintmire, J. W.; White, C. T. Electronic and structural properties of carbon nanotubes. *Carbon* **1995**, *33*(7), 893-902.

249. Pantano, A.; Parks, D. M.; Boyce, M. C. Mechanics of deformation of single- and multi-wall carbon nanotubes. *J. Mech. Phys. Solids* **2004**, *52*, 789-821.

250. Thostenson, E. T.; Ren, Z.; Chou, T.-W. Advances in the science and technology of carbon nanotubes and their composites: a review. *Compos. Sci. Technol.* **2001**, *61*, 1899-1912.

251. Qin, L. C. Synthesis of carbon nanotubes. *J. Mater. Sci. Lett.* **1997**, *16*, 457-459.

252. Cassell, A. M.; Raymakers, J. A.; Kong, J.; Dai, H. Large Scale CVD Synthesis of Single-Walled Carbon Nanotubes. *J. Phys. Chem. B* **1999**, *103*(31), 6484-6492.

253. Ebbesen, T. W.; Ajayan, P. M. Large-scale synthesis of carbon nanotubes. *Nature* **1992**, *358, 220-222.*

254. Zhao, X.; Ohkohchi, M.; Wang, M.; Iijima, S.; Ichihashi, T.; Ando, Y. Preparation of high-grade carbon nanotubes by hydrogen arc discharge. *Carbon* **1997**, *35*(6), 775-781.

255. Zhang, Y.; Gu, H.; Iijima, S. Single-wall carbon nanotubes synthesized by laser ablation in a nitrogen atmosphere. *Appl. Phys. Lett.* **1998**, *73*, 3827-3829.

256. Dai, H. Carbon Nanotubes: Synthesis, Integration, and Properties. *Acc. Chem. Res.* **2002**, *35*(12), 1035-1044.

257. Puretzky, A. A.; Geohegan, D. B.; Fan, X.; Pennycook, S. J. Dynamics of single-wall carbon nanotube synthesis by laser vaporization. *Appl. Phys. A* **2000**, *70*(2), 153-160.

258. Lou, X. W.; Archer, L. A.; Yang, Z. C. Hollow Micro-/Nanostructures: Synthesis and Applications. *Adv. Mater.* **2008**, *20*, 3987-4019.

259. Kim, M.; Sohn, K.; Na, H. B.; Heyon, T. Synthesis of Nanorattles Composed of Gold Nanoparticles Encapsulated in Mesoporous Carbon and Polymer Shells. *Nano Lett.* **2002**, *2*, 1383-1387.

260. Kamata, K.; Lu, Y.; Xia, Y. N. Synthesis and Characterization of Monodispersed Core-Shell Spherical Colloids with Movable Cores. *J. Am. Chem. Soc.* **2003**, *125*, 2384-2385.

261. Liu, N.; Wu, H.; McDowell, M. T.; Yao, Y.; Wang, C. M.; Cui, Y. A Yolk-Shell Design for Stabilized and Scalable Li-Ion Battery Alloy Anodes. *Nano Lett.* **2012**, *12*, 3315-3321.

262. Zheng, G. Y.; Zhang, Q. F.; Cha, J. J.; Yang, Y.; Li, W. Y.; Seh, Z. W.; Cui, Y. Amphiphilic Surface Modification of Hollow Carbon Nanofibers for Improved Cycle Life of Lithium Sulfur Batteries. *Nano Lett.* **2013**, *13*, 1265-1270.

263. Ikeda, S.; Ishino, S.; Harada, T.; Okamoto, N.; Sakata, T.; Mori, H.; Kuwabata, S.; Torimoto, T.; Matsumura, M. Ligand-Free Platinum Nanoparticles Encapsulated in a Hollow Porous Carbon Shell as a Highly Active Heterogeneous Hydrogenation Catalyst, *Angew. Chem. Int. Ed.* **2006**, *45*, 7063-7066.

264. Zhang, W. M.; Hu, J. S.; Guo, Y. G.; Zheng, S. F.; Zhong, L. S.; Song, W. G.; Wan, L. J. Tin-Nanoparticles Encapsulated in Elastic Hollow Carbon Spheres for High-Performance Anode Material in Lithium-Ion Batteries. *Advanced Materials* **2008**, *20*, 1160-1165.

265. Liu, Z.; Chen, L.; Zhang, L.; Poyraz, S.; Guo, Z. H.; Zhang, X. Y.; Zhu, J. H. Ultrafast Cr(VI) removal from polluted water by microwave synthesized iron oxide submicron wires. *Chemical Communications* **2014**, *50*, 8036-8039.

266. Fuertes, A. B.; Sevilla, M.; Valdes-Solis, T.; Tartaj, P. Synthetic Route to Nanocomposites Made Up of Inorganic Nanoparticles Confined within a Hollow Mesoporous Carbon Shell. *Chemistry of Materials* **2007**, *19*, 5418-5423.

267. Lu, H. P. Site-specific Raman spectroscopy and chemical dynamics of nanoscale interstitial systems. *J. Phys. Condens. Mater.* **2005**, *17*, R333-R355.

268. Zhu, S.; Xu, G. Single-walled carbon nanohorns and their applications. *Nanoscale* **2010**, *2*, 2538-2549.

269. Jayaprakash, N.; Shen, J.; Moganty, S. S.; Corona, A.; Archer, L. A. Porous Hollow Carbon@Sulfur Composites for High-Power Lithium-Sulfur Batteries. *Angew. Chem. Int. Ed.* **2011**, *50*, 5904-5908.

270. Yang, S. B.; Feng, X. L.; Zhi, L. J.; Cao, Q. A.; Maier, J.; Mullen, K. Nanographene-constructed hollow carbon spheres and their favorable electroactivity with respect to lithium storage. *Advanced Materials* **2010**, *22*, 838-842.

271. Zhang, C. F.; Wu, H. B.; Yuan, C. Z.; Guo, Z. P.; Lou, X. W. Confining Sulfur in Double-Shelled Hollow Carbon Spheres for Lithium-Sulfur Batteries. *Angew. Chem, Int. Ed.* **2012**, *51*, 9592-9595.

272. Caruso, F.; Spasova, M.; Susha, A.; Giersig, M.; Caruso, R. A. Magnetic Nanocomposite Particles and Hollow Spheres Constructed by a Sequential Layering Approach. *Chem. Mater.* **2001**, *13*, 109-116.

273. Jang, J.; Ha, H. Fabrication of Carbon Nanocapsules Using PMMA/PDVB Core/Shell Nanoparticles. *Chem. Mater.* **2003**, *15*, 2109-2111.

274. Qiao, S. Z.; Lin, C. X.; Jin, Y. G.; Li, Z.; Yan, Z. M.; Hao, Z. P.; Huang, Y. N.; Lu, G. Q. Surface-Functionalized Periodic Mesoporous Organosilica Hollow Spheres. *J. Phys. Chem. C* **2009**, *113*, 8673-8682.

275. Lu, A. H.; Li, W. C.; Hao, G. P.; Spliethoff, B.; Bongard, H. J.; Schaack, B. B.; Schuth, F. Easy Synthesis of Hollow Polymer, Carbon, and Graphitized Microspheres. *Angew. Chem. Int. Ed.* **2010**, *49*, 1615-1618.

276. Xu, L. Q.; Zhang, W. Q.; Yang, Q.; Ding, Y. W.; Yu, W. C.; Qian, Y. T. A novel route to hollow and solid carbon spheres. *Carbon* **2005**, *43*, 1090-1092.

277. Katcho, N. A.; Urones-Garrote, E.; Avila-Brande, D.; Gomez-Herrero, A.; Urbonaite, S.; Csillag, S.; Lomba, E.; Agullo-Rueda, F.; Landa-Canovas, A. R.; Otero-Diaz, L. C. Carbon Hollow Nanospheres from Chlorination of Ferrocene. *Chem. Mater.* **2007**, *19*, 2304-2309.

278. Wang, Z. F.; Mao, P. F.; He, N. Y. Synthesis and characteristics of carbon encapsulated magnetic nanoparticles produced by a hydrothermal reaction. *Carbon* **2006**, *44*, 3277-3284.

279. Zhang, X. Y.; Manohar, S. K. Microwave synthesis of nanocarbons from conducting polymers. *Chem. Commun.* **2006**, *23*, 2477-2479.

280. Fujii, S.; Matsuzawa, S.; Nakamura, Y. One-pot synthesis of conducting polymer-coated latex particles: ammonium persulfate as free radical initiator and chemical oxidant. *Chem. Commun.* **2010**, *46*, 7217-7219.

281. Zhang, J. R.; Qiu, T.; Ren, S. S.; Yuan, H. F.; He, L. F.; Li, X. Y. Simple synthesis of polypyrrole-polystyrene hybrid hollow spheres. *Mater. Chem. Phys.* **2012**, *134*, 1072-1078.

282. Chang, C. H.; Son, P. S.; Yoon, J. A.; Choi, S. H. Synthesis of Hollow Conductive Polypyrrole Balls by the Functionalized Polystyrene as Template. *J. Nanomater.* **2010**, *168025*, 1-6.

283. Fu, J. W.; Xu, Q.; Chen, J. F.; Chen, Z. M.; Huang, X. B.; Tang, X. Z. Controlled fabrication of uniform hollow core porous shell carbon spheres by the pyrolysis of core/shell polystyrene/cross-linked polyphosphazene composites. *Chemical Communications* **2010**, *46*, 6563-6565.

284. Fang, B.; Kim, J. H.; Kim, M. S.; Bonakdarpour, A.; Lam, A.; Wilkinson, D. P.; Yu, J. S. Fabrication of hollow core carbon spheres with hierarchical nanoarchitecture for ultrahigh electrical charge storage. *J. Mater. Chem.* **2012**, *22*, 19031-19038.

285. Liu, Z.; Zhang, L.; Poyraz, S.; Smith, J.; Kushvaha, V.; Tippur, H.; Zhang, X. Y. An ultrafast microwave approach towards multi-component and multi-dimensional nanomaterials. *RSC Adv.* **2014**, *4*, 9308-9313.

286. Fujii, S.; Matsuzawa, S.; Nakamura, Y.; Ohtaka, A.; Teratani, T.; Akamatsu, K.; Tsuruoka, T.; Nawafune, H. Synthesis and Characterization of Polypyrrole−Palladium Nanocomposite-Coated Latex Particles and Their Use as a Catalyst for Suzuki Coupling Reaction in Aqueous Media. *Langmuir* **2010**, *26*, 6230-6239.

287. Malinauskas, A. Chemical deposition of conducting polymers. *Polymer* **2001**, *42*, 3957-3972.

288. Cho, S. H.; Kim, W. Y.; Jeong, G. K.; Lee, Y. S. Synthesis of nano-sized polypyrrole-coated polystyrene latexes. *Colloid. Surface. A* **2005**, *255*, 79-83.

289. Liu, Z.; Liu, Y.; Poyraz, S.; Zhang, X. Y. Green-nano approach to nanostructured polypyrrole. *Chem. Commun.* **2011**, *47*, 4421-4423.

290. Zhang, X. Y.; Manohar, S. K. Bulk Synthesis of Polypyrrole Nanofibers by a Seeding Approach. *J. Am. Chem Soc.* **2004**, *126*, 12714-12715.

291. Zhang, X. Y.; Manohar, S. K. Narrow Pore-Diameter Polypyrrole Nanotubes. *J. Am. Chem. Soc.* **2005**, *127*, 14156-14157.

292. Liu, Z.; Zhang, X. Y.; Poyraz, S.; Surwade, S. P.; Manohar, S. K. Oxidative Template for Conducting Polymer Nanoclips. *J. Am. Chem. Soc.* **2010**, *132*, 13158-13159.

293. Liu, Z.; Wang, J. L.; Kushvaha, V.; Poyraz, S.; Tippur, H.; Park, S.; Kim, M.; Liu, Y.; Bar, J.; Chen, H.; Zhang, X. Y. Poptube approach for ultrafast carbon nanotube growth. *Chem. Commun.* **2011**, *47*, 9912-9914.

294. Zhang, X. Y.; Liu, Z. Recent advances in microwave initiated synthesis of nanocarbon materials. *Nanoscale* **2012**, *4*, 707-714.

295. Hu, C. C.; Chang, K. H.; Lin, M. C.; Wu, Y. T. Design and Tailoring of the Nanotubular Arrayed Architecture of Hydrous RuO2 for Next Generation Supercapacitors. *Nano Letters* **2006**, *6*, 2690-2695.

296. Zhang, L. L.; Li, S.; Zhang, J. T.; Guo, P. Z.; Zheng, J. T.; Zhao, X. S. Enhancement of Electrochemical Performance of Macroporous Carbon by Surface Coating of Polyaniline. *Chem. Mater.* **2010**, *22*, 1195-1202.

297. Kelly, T. L.; Yano, K.; Wolf, M. O. Supercapacitive Properties of PEDOT and Carbon Colloidal Microspheres *ACS Appl. Mater. Interfaces* **2009**, *1*, 2536-2543.

298. Lei, Z. B.; Chen, Z. W.; Zhao, X. S. Growth of Polyaniline on Hollow Carbon Spheres for Enhancing Electrocapacitance. *J. Phys. Chem. C* **2010**, *114*, 19867-19874.

299. Chen, Z.; Qin, Y. C.; Weng, D.; Xiao, Q. F.; Peng, Y. T.; Wang, X. L.; Li, H. X.; Wei, F.; Lu, Y. F. Design and Synthesis of Hierarchical Nanowire Composites for Electrochemical Energy Storage *Adv. Funct. Mater.* **2009**, *19*, 3420-3426.

300. Hulicova, D.; Kodama, M.; Hatori, H. Electrochemical Performance of Nitrogen-Enriched Carbons in Aqueous and Non-Aqueous Supercapacitors. *Chem. Mater.* **2006**, *18*, 2318-2326.

301. Liu, Z.; Zhang, L.; Poyraz, S.; Zhang, X. Y. Conducting Polymer - Metal Nanocomposites Synthesis and Their Sensory Applications. *Curr. Org. Chem.* **2013**, *17*, 2256-2267.

302. Yang, S. B.; Feng, X. L.; Ivanovici, S.; Mullen, K. Fabrication of Graphene‐Encapsulated Oxide Nanoparticles: Towards High-Performance Anode Materials for Lithium Storage. *Angew. Chem. Int. Ed.* **2010**, *49*, 8408-8411.

303. Lai, X. Y.; Halpert, J. E.; Wang, D. Recent advances in micro-/nano-structured hollow spheres for energy applications: From simple to complex systems. *Energy Environ. Sci.* **2012**, *5*, 5604-5618.

304. Fan, S.; Chapline, M. G.; Franklin, N. R.; Tombler, T. W.; Cassell, A. M.; Dai, H. Self-Oriented Regular Arrays of Carbon Nanotubes and Their Field Emission Properties. *Science* **1999**, *283*, 512-514.

305. Moisala, A.; Nasibulin, A. G.; Kauppinea, E. I. The role of metal nanoparticles in the catalytic production of single-walled carbon nanotubes-a review. *J. Phys.: Condens. Mater.* **2003**, *15*, S3011-S3035.

306. Emmenegger, L.; Bonard, J.-M.; Mauron, P.; Sudan, P.; Lepora, A.; Grobety, B.; Zuttel, A.; Schlapbach, L. Synthesis of carbon nanotubes over Fe catalyst on aluminium and suggested growth mechanism. *Carbon* **2003**, *41*(3), 539-547.

307. Hu, C. C.; Chang, K. H.; Lin, M. C.; Wu, Y. T. Design and Tailoring of the Nanotubular Arrayed Architecture of Hydrous RuO2 for Next Generation Supercapacitors. *Nano Letters* **2006**, *6*, 2690-2695.

308. Zhang, L. L.; Li, S.; Zhang, J. T.; Guo, P. Z.; Zheng, J. T.; Zhao, X. S. Enhancement of Electrochemical Performance of Macroporous Carbon by Surface Coating of Polyaniline. *Chem. Mater.* **2010**, *22*, 1195-1202.

309. Kelly, T. L.; Yano, K.; Wolf, M. O. Supercapacitive Properties of PEDOT and Carbon Colloidal Microspheres *ACS Appl. Mater. Interfaces* **2009**, *1*, 2536-2543.

310. Lei, Z. B.; Chen, Z. W.; Zhao, X. S. Growth of Polyaniline on Hollow Carbon Spheres for Enhancing Electrocapacitance. *J. Phys. Chem. C* **2010**, *114*, 19867-19874.

311. Chen, Z.; Qin, Y. C.; Weng, D.; Xiao, Q. F.; Peng, Y. T.; Wang, X. L.; Li, H. X.; Wei, F.; Lu, Y. F. Design and Synthesis of Hierarchical Nanowire Composites for Electrochemical Energy Storage *Adv. Funct. Mater.* **2009**, *19*, 3420-3426.

312. Hulicova, D.; Kodama, M.; Hatori, H. Electrochemical Performance of Nitrogen-Enriched Carbons in Aqueous and Non-Aqueous Supercapacitors. *Chem. Mater.* **2006**, *18*, 2318-2326.

313. Liu, Z.; Zhang, L.; Poyraz, S.; Zhang, X. Y. Conducting Polymer - Metal Nanocomposites Synthesis and Their Sensory Applications. *Curr. Org. Chem.* **2013**, *17*, 2256-2267.

314. Yang, S. B.; Feng, X. L.; Ivanovici, S.; Mullen, K. Fabrication of Graphene‐Encapsulated Oxide Nanoparticles: Towards High-Performance Anode Materials for Lithium Storage. *Angew. Chem. Int. Ed.* **2010**, *49*, 8408-8411.

315. Lai, X. Y.; Halpert, J. E.; Wang, D. Recent advances in micro-/nano-structured hollow spheres for energy applications: From simple to complex systems. *Energy Environ. Sci.* **2012**, *5*, 5604-5618.

316. Zhenxing, H., Xiaowei, Y., Junliang, L., Yuping, Y., Ling, W., Yanwei, Z. An investigation of the effect of sodium dodecyl sulfate on quasi-emulsifier-free emulsion polymerization for highly monodisperse polystyrene nanospheres. *Eur. Polym. J.* **2011**, *47*, 24-30.

317. Poyraz, S.; Zhang, L.; Schroder, A.; Zhang, X. Y. Ultrafast Microwave Welding/Reinforcing Approach at the Interface of Thermoplastic Materials. *ACS Appl. Mater. Interfaces* **2015**, *7*, 22469-22477.

318. Poyraz, S.; Liu, Z.; Liu, Y.; Zhang, X. Y. Devulcanization of Scrap Ground Tire Rubber and Successive Carbon Nanotube Growth by Microwave Irradiation. *Curr. Org. Chem.* **2013**, *17*, 2243-2248.

319. Xie, H.; Poyraz, S.; Thu, M.; Liu, Y.; Snyder, E. Y.; Smith, J. W.; Zhang, X. Y. Microwave-assisted fabrication of carbon nanotubes decorated polymeric nano-medical platforms for simultaneous drug delivery and magnetic resonance imaging. *RSC Adv.* **2014**, *4*, 5649-5652.

320. Liu, Z.; Zhang, L.; Wang, R. G.; Poyraz, S.; Cook, J.; Bozack, M. J.; Das, S.; Zhang, X. Y.; Hu, L. B. Ultrafast Microwave Nano-manufacturing of Fullerene-Like Metal Chalcogenides. *Sci. Rep.* **2016**, *6*, 22503-22510.

321. Schwenke, A. M.; Hoeppener, S.; Schubert, U. S. Synthesis and Modification of Carbon Nanomaterials utilizing Microwave Heating. *Adv. Mater.* **2015**, *27*, 4113-4141.

322. Zhang, J. R.; Qiu, T.; Ren, S. S.; Yuan, H. F.; He, L. F.; Li, X. Y. Simple synthesis of polypyrrole-polystyrene hybrid hollow spheres. *Mater. Chem. Phys.* **2012**, *134*, 1072-1078.

323. Cho, S. H.; Kim, W. Y.; Jeong, G. K.; Lee, Y. S. Synthesis of nano-sized polypyrrole-coated polystyrene latexes. *Colloids Surf. A* **2005**, *255*, 79-83.

324. Chand, S. Carbon fibers for composites. *J. Mater. Sci.* **2000**, *35*, 1303-1313.

325. Minus, M. L.; Kumar, S. The processing, properties, and structure of carbon fibers. *J.O.M.* **2005**, *57*, 52-58.

326. Hammel, E.; Tang, X.; Trampert, M.; Schmitt, T.; Mauthner, K.; Eder, A.; Potschke, P. Carbon nanofibers for composite applications. *Carbon* **2004**, *42*, 1153-1158.

327. Christensen, R. M. Properties of carbon fibers. *J. Mech. Phys. Solids.* **1994**, *42*, 681-695.

328. Edie, D. D.; The effect of processing on the structure and properties of carbon fibers. *Carbon* **1998**, *36*, 345-362.

329. Huang, X. Fabrication and properties of carbon fibers. *Materials* **2009**, *2*(4), 2369-2403.

330. Rahaman, M. S. A.; Ismail, A. F.; Mustafa, A. A review of heat treatment on polyacrylonitrile fiber. *Polym. Degrad. Stabil.* **2007**, *92*, 1421-1432.

331. Derbyshire, F.; Andrews, R.; Jacques, D.; Jagtoyen, M.; Kimber, G.; Rantell, T. *Fuel*, **2001**, *80*, 345-362.

332. Thwaits, M. W.; Stewart, M. L.; McNeese, B. E.; Sumner, M. B. Synthesis and characterization of activated pitch-based carbon fibers. *Fuel Process. Technol.* **1993**, *34*, 137-145.

333. Machida, I.; Yoon, S.-H.; Takano, N.; Fortin, F.; Korai, Y.; Yokogawa, K. Microstructure of mesophasepitch-based carbon fiberand its control. *Carbon* **1996**, *34*, 941-956.

334. Bacon, R.; Silvaggi, A. F. Electron microscope study of the microstructure of carbon and graphite fibers from a rayon precursor. *Carbon*, **1971**, *9*, 321-325.

335. Frank, E.; Steudle, L.M.; Ingildeev, D.; Sporl, J. M.; Buchmeiser, M. R. Carbon Fibers: Precursor Systems, Processing, Structure, and Properties. *Angew. Chem. Int. Ed.* **2014**, *53*, 5262-5298.

336. Zaldivar, R. J.; Rellick, G. S. Some observations on stress graphitization in carbon-carbon composites. *Carbon*, **1991**, *29*, 1155-1163.

337. Vasquez-Santos, M. B.; Geissler, E.; Laszlo, K.; Rouzaud, J.-N.; Martinez-Alonso, A.; Tascon, J. M. D. Comparative XRD, Raman, and TEM Study on Graphitization of PBO-Derived Carbon Fibers. *J. Phys. Chem. C* **2012**, *116*, 257-268.

338. Dobiasovaa, L.; Staryb, V.; Golgarc, P.; Valvodaa, V. Analysis of carbon fibers and carbon composites by asymmetric X-ray diffraction technique. *Carbon* **1999**, *37*, 421-425.

339. Donnet, J. B.; Bansal, R. C. *Carbon Fibers*, 3rd Ed; Marcel Dekker: New York, 1998.

340. Pierson, H. O. *Handbook of Carbon, Graphite, Diamond and Fullerenes: Properties, Processing and Applications*. Noyes: New Jersey, 1993.

341. Oberlin, A.; Guigon, M. in *Fiber Reinforcements for Composite Materials*; Bunsell, A. R. Ed.; Elsevier: New York, 1988.

342. Fitzer, E. PAN-based carbon fibers-present state and trend of the technology from the viewpoint of possibilities and limits to influence and to control the fiber properties by the process parameters. *Carbon*, **1989**, *27*, 621-645.

343. Zhang, X.; Fujiwara, S.; Fujii, M. Measurements of Thermal Conductivity and Electrical Conductivity of a Single Carbon Fiber. *Int. J. Thermophys.* **2000**, *21*, 965-980.

344. Heremans, J.; Rahim, I.; Dresselhaus, M. S. Thermal conductivity and Raman spectra of carbon fibers. *Phys. Rev. B* **1985**, *32*, 6742-6747.

345. Soutis, C. Carbon fiber reinforced plastics in aircraft construction. *Mater. Sci. Eng. A* **2005**, *412*, 171-176.

346. Fu. S.-Y.; Lauke, B.; Mader, E.; Yue, C.-Y.; Hu, X. Tensile properties of short-glass-fiber- and short-carbon-fiber-reinforced polypropylene composites. *Compos. Part A: Appl. S.* **2000**, *31*, 1117-1125.

347. Rezaei, F.; Yunus, R.; Ibrahim, N. A. Effect of fiber length on thermomechanical properties of short carbon fiber reinforced polypropylene composites *Mater. Des.* **2009**, *30*, 260-263.

348. Karsli, N. G.; Aytac; A. Tensile and thermomechanical properties of short carbon fiber reinforced polyamide 6 composites. *Compos. Part B: Eng.* **2013**, *51*, 270-275.

349. Zhang, H.; Zhong, Z.; Friedrich, K. Effect of fiber length on the wear resistance of short carbon fiber reinforced epoxy composites. *Compos. Sci. Technol.* **2007**, *67*, 222-230.

350. Wisnom, M. R.; Kahn, B.; Hallett, S. R. Size effects in unnotched tensile strength of unidirectional and quasi-isotropic carbon/epoxy composites. *Compos. Sctruct.* **2008**, *84*, 21-28.

351. Manocha, L. M.; Bahl, O. P. Influence of carbon fiber type and weave pattern on the development of 2D carbon-carbon composites. *Carbon* **1988**, *26,* 13-21.

352. Lee, B.; Leong, K. H.; Herszberg, I. Effect of Weaving on the Tensile Properties of Carbon Fibre Tows and Woven Composites. *J. Reing. Plast. Compos.* **2001**, *20*, 652-670.

353. Achenbach, J. D.; Zhu, H. Effect of interfacial zone on mechanical behavior and failure of fiber-reinforced composites. *J. Mech. Phys. Solids* **1989**, *37*, 381-393.

354. Totry, E.; Molina-Aldareguia, J. M.; Gonzalez, C.; Llorca, J. Effect of fiber, matrix and interface properties on the in-plane shear deformation of carbon-fiber reinforced composites. *Compos Sci. Technol.* **2010**, *70*, 970-980.

355. Hsueh, C.-H. Interfacial debonding and fiber pull-out stresses of fiber-reinforced composites. *Mater. Sci. Eng.* **1990**, *123*, 1-11.

356. Sakai, M.; Matsuyama, R.; Miyajima, T. The pull-out and failure of a fiber bundle in a carbon fiber reinforced carbon matrix composite. *Carbon* **2000**, *38*, 2123-2131.

357. Soutis, C. Fiber reinforced composites in aircraft construction. *Prog. Aerospace Sci.* **2005**, *41*, 143-151.

358. Zhu, H. W.; Xu, C. L.; Wu, D. H.; Wei, B. Q.; Vajtai, R.; Ajanyan, P. M. Direct Synthesis of Long Single-Walled Carbon Nanotube Strands. *Science* **2002**, *296*, 884-886.

359. Yousefinejad, S.; Honarasa, F.; Solhjoo, A. On the Solubility of Ferrocene in Nonaqueous Solvents. *J. Chem. Eng. Data* **2016**, *61*, 614-621.

360. De Fina, K. M.; Ezell, C.; Acree Jr.; W. E. Solubility of Ferrocene in Organic Nonelectrolyte Solvents. Comparison of Observed Versus Predicted Values Based Upon Mobile Order Theory. *Phys. Chem. Liquids* **2001**, *39*, 699-710.

361. Joens, O.; Gjaldbaek, J. Chr.; The Solubility of Ferrocene in Non-Polar Solvents. *Acta. Chem. Scand. A*. **1974**, *28*, 528-530.